Function of the Spir actin nucleators in intracellular vesicle transport processes

Sabine Weiß

This thesis is submitted to obtain the academic degree of Doctor rerum naturalium (Dr. rer. nat.) from the Julius-Maximilians-University of Würzburg.

Place of birth Suhl

Würzburg, 2011

Eingereicht am: 15.04.2011

Mitglieder der Promotionskommission:

Vorsitzender: Prof. Dr. Wolfgang Rössler
Gutachter: Prof. Dr. Eugen Kerkhoff
Gutachter: Prof. Dr. Thomas Raabe

Tag des öffentlichen Promotionskolloquiums: 06.07.2011

Doktorurkunde ausgehändigt am:

Erklärung:

Hiermit erkläre ich an Eides statt, dass ich die Dissertation "Funktion der Spir Aktin Nukleatoren in intrazellulären Vesikeltransportprozessen" selbständig angefertigt und keine anderen als die von mir angegebenen Hilfsmittel und Quellen verwendet habe.

Ich erkläre außerdem, dass diese Dissertation weder in gleicher oder anderer Form bereits in einem anderen Prüfungsverfahren vorgelegen hat.

Ich habe früher außer den mit dem Zulassungsgesuch urkundlich vorgelegten Graden keine weiteren akademischen Grade erworben oder zu erwerben versucht.

Regensburg, den 13.04.2011

Sabine Weiß

Abstract

Spir proteins are the founding members of the novel class of WH2-actin nucleators. A C-terminal modified FYVE zinc finger motif is necessary to target Spir proteins towards intracellular membranes. The function and regulation of the Spir actin organizers at vesicular membranes is almost unknown. Live cell imaging analyses performed in this study show that Spir-2 is localized at tubular vesicles. Cytoplasmic Spir-2-associated vesicles branch and form protrusions, which can make contacts to the microtubule network, where the Spir-2 vesicles stretch and slide along the microtubule filaments. The analysis of living HeLa cells expressing eGFP-tagged Spir-2, Spir-2-ΔKIND and Spir-2-ΔKW (lacking the 4 WH2 domains and the KIND domain) showed Spir-2-associated tubular structures which differ in their length and motility. Throughout the course of that study it could be shown that the tail domain of the actin motor protein myosin Vb, as a force-generating molecule, is colocalizing and co-immunoprecipitating with Spir-2-ΔKW. By using the tail domain of myosin Vb as a dominant negative mutant for myosin Vb-dependent vesicle transport processes it could be shown that Spir-2-ΔKW/MyoVb-cc-tail- associated vesicles exhibit an increased elongation. Moreover, using the microtubule depolymerizing drug nocodazole it could be shown that the elongation and the motility of Spir-2-ΔKW-associated vesicles depends on an intact microtubule cytoskeleton. Motility and morphological dynamics of Spir-2-associated vesicles is therefore dependent on actin, actin motorproteins and microtubule filaments. These results propose a model in which myosin/F-actin forces mediate vesicle branching, allowing the vesicles to move to and in between the microtubule filaments and thereby providing a new degree of freedom in vesicular motility. To determine the exact subcellular localization of Spir-2, colocalization studies were performed. It could be shown that Spir-2 shows a partial colocalization to Rab11a-positive compartments. Furthermore, Spir-2 exhibits an almost identical localization to Arf1 and the Arf1 small G protein but not Rab11a could be immunoprecipitated with Spir-2-ΔKW. This suggests, that Arf1 recruits Spir-2 to Arf1/Rab11a-positive membranes. Another important function of the Spir-2 C-terminus is the membrane targeting by the FYVE domain. By performing a protein-lipid overlay assay, it has been shown that purified GST- and 6xHis-tagged Spir-2-ΔKW bind phosphatidic acid suggesting a mechanism in which Spir-2 is recruited to phosphatidic acid-enriched membranes. To further elucidate the mechanism in which Spir-2 membrane-targeting could be regulated, interaction studies of C-terminal parts

of Spir-2 revealed that the Spir-2 proteins interact directly.

Zusammenfassung

Spir Proteine sind die ersten beschriebenen Mitglieder der neuen Klasse der WH2-Aktin Nukleatoren. Ein C-terminaler modifizierter FYVE Zinkfinger ist notwendig um Spir Proteine an intrazelluläre Membranen zu bringen. Die Funktion und die Regulation dieser Aktin Nukleatoren an vesikulären Membranen ist bis jetzt noch nahezu unbekannt.

In dieser Studie durchgeführte "*Live-cell-Imaging*" Experimente zeigten, dass Spir-2 an tubulären Vesikeln lokalisiert ist. Zytoplasmatische Spir-2-assoziierte Vesikel formen Ausläufer, die Kontakte zum Mikrotubuli Netzwerk bilden. Spir-2 Vesikel haben die Fähigkeit sich entlang des Mikrotubuli Zytoskeletts auszudehnen und daran entlang zu gleiten. Die Analyse von lebenden HeLa Zellen, welche eGFP-Spir-2, eGFP-Spir-2-ΔKIND und eGFP-Spir-2-ΔKW (Deletion der 4 WH2 Domänen sowie der KIND Domäne) Fusionsproteine exprimieren, zeigen Spir-2-assoziierte tubuläre Vesikel, die sich in Länge und Beweglichkeit unterscheiden.

Während dieser Studie konnte außerdem gezeigt werden, dass die "*tail*" Domäne des Aktinmotors myosin Vb mit Spir-2-ΔKW kolokalisiert und koimmunopräzipitiert. Die Verwendung der "*tail*" Domäne als dominant negative Mutante für myosin Vb-abhängigen Vesikeltransport zeigte, dass Spir-2-ΔKW/MyoVb-cc-tail-assoziierte Vesikel eine stark erhöhte Elongation aufweisen. Desweiteren konnte duch die Verwendung von Nocodazol, welches spezifisch Mikrotubulifilamente depolymerisiert, gezeigt werden, dass die Elongation und die Motilität der Spir-2-ΔKW-assoziierten Vesikel von einem intakten Mikrotubuli Zytoskelett abhängig ist. Motilität und morphologische Dynamik der Spir-2-ΔKW-assoziierten Vesikel ist daher abhängig von Aktinfilamenten, Aktin Motorproteinen und Mikrotubulifilamenten. Anhand dieser Ergebnisse lässt sich ein Modell erstellen, in welchem eine Myosin/F-actin induzierte Bewegung eine Verzweigung der Vesikel bewirkt. Dadurch ist eine Bewegung der Vesikel zu Mikrotubulifilamenten aber auch zwischen verschiedenen Mikrotubulifilamenten möglich, welches einen ganz neuen Freiheitsgrad in der vesikulären Bewegung eröffnet. Um die genaue zelluläre Lokalisation von Spir-2 zu analysieren wurden Kolokalisationsstudien durchgeführt. Hierbei konnte gezeigt werden, dass Spir-2 eine partielle Kolokalisation mit Rab11a-positiven Kompartimenten zeigt. Außerdem weist Spir-2 eine nahezu identische Lokalisation zu Arf1 auf. Arf1, aber nicht Rab11a, konnte mit Spir-2-ΔKW koimmunpräzipitiert werden. Arf1 könnte

daher für die Rekrutierung von Spir-2 an Arf1/Rab11a-positive Membranen ausschlaggebend sein.

Eine weitere wichtige Funktion des Spir-2 C-Terminus ist die Membranlokalisation, welche durch die FYVE Domäne vermittelt wird. Mittels Protein-Lipid Bindungsstudien konnte gezeigt werden, dass aufgereinigte GST- bzw. 6xHis-Spir-2-ΔKW-Fusionsproteine an Phosphatidylsäure binden. Dies deutet darauf hin, dass Spir-2 spezifisch zu Phosphatidylsäure-positiven Membranen rekrutiert wird. Um die weitere Regulation der Spir-2 Membranlokalisation aufzuklären, wurden Protein-Protein-Interaktionsstudien durchgeführt, welche eine direkte Interaktion von Spir-2 Proteinen anhand ihrer C-Termini ergaben.

Contents

Danksagungen

Ich möchte mich bei folgenden Personen recht herzlich bedanken:

Bei Prof. Dr. Eugen Kerkhoff für die Aufnahme in seine Arbeitsgruppe, für die hervorragende Betreuung und für die vielen hilfreichen Tipps. Besonders möchte ich mich für die Freiheit bedanken, die er mir während des gesamten Forschungsprojektes gewährte.

Mein besonderer Dank gilt Prof. Dr. Thomas Raabe für die überaus freundliche Übernahme der Zweitbetreuung.

Desweiteren möchte ich meinen Arbeitskollegen und nun Freunden, Dr. Agnes Pawelec, Sandra Pleiser und Annette Samol danken. Danke für die zahlreichen konstruktiven und motivierenden Gespräche, sowie das überaus harmonische Arbeitsklima. Mit Ihrer Ausdauer, Ruhe und Geduld standen Sie mir auch in schwierigen Situationen stets beiseite.

Ein weiterer Dank gilt Martin Beusch, der mich durch seine liebenswerte, kollegiale und immer hilfsbereite Art stets aufgemuntert hat.

Im Besonderen möchte ich meinen Eltern danken, ohne deren Förderung und finanzielle Unterstützung mir dieses Studium nicht möglich gewesen wäre. Ganz besonderen Dank dafür, dass Sie mir auch während dem Erstellen dieser Doktorarbeit immer unterstützend und liebevoll zur Seite standen. Ein herzliches Dankeschön an meine gesamte Familie für jedwede Unterstützung und Ihren Beistand.

Meiner beßten Freundin Nicole Geringswald danke ich aus ganzem Herzen für alles.

1 *INTRODUCTION*

1.1 Regulation of actin filament assembly

The assembly of actin monomers into filaments is a tightly regulated basic cellular function. The dynamic assembly and disassembly of actin filaments is crucial for many cellular processes, like migration, endocytosis, and cytokinesis. Eukaryotic cells use actin polymerization to form contractile structures, to internalize extracellular materials, and to coordinate changes in morphology (Welch and Mullins, 2002, Chesarone and Goode, 2009). Regulation is essential, because cells contain high concentrations of actin monomers, which have the ability to polymerize. The actin monomer consist of two major domains each containing two subdomains referred as subdomains 1-4 (Kabsch et al., 1990, Dominguez and Holmes, 2010). Two large clefts are formed between the two major domains (Dominguez and Holmes, 2010). The lower cleft mediates the binding to several actin-binding proteins (Dominguez, 2004, Oda et al., 2009, Fujii et al., 2010), whereas the upper cleft provides the binding site for the nucleotide and the associated Mg^{2+} (Otterbein et al., 2001). Each actin filament consists of two α-helical protofilaments with a fast-growing "barbed" end (+end) and a "pointed" end (-end). Details of the actin filament structure have been obtained from X-ray fiber diagrams (Holmes et al., 1990, Oda et al., 2009, Oda and Maeda, 2010) and from electron cryo-microscopy (Fujii et al., 2010, Holmes et al., 2003) but there is still no structure of ATP F-actin. The dissociation equilibrium (ratio of the rate constants for dissociation and association of subunits) also known as the critical concentration is lower at the "barbed" end (0.1 µm) than at the "pointed" end (0.7 µm) (Pollard and Borisy, 2003) resulting in an asymmetric actin filament. ATP-bound actin monomers associate to the "barbed" end, whereas ADP-actin monomers dissociate from the "pointed" end, a process known as actin filament treadmilling (Pollard, 2007). Globular actin (G-actin) is not an efficient ATPase in comparison to filamentous actin (F-actin). The two major domains of an actin monomer undergo a propeller-twist upon polymerization, re-

sulting in the stimulation of the ATPase activity (Oda and Maeda, 2010). ATP hydrolysis by polymerized actin is irreversible (Carlier et al., 1988) and fast (with a half time of 2 seconds) (Blanchoin and Pollard, 2002), whereas the dissociation of the γ-phosphate is slow (with a half time of 6 minutes) (Blanchoin and Pollard, 1999). The property of the ADP-Pi-actin intermediate is identical to ATP-actin. ADP-actin dissociates from the actin filament more rapidly than ATP-actin, suggesting that ATP hydrolyzation and dissociation of γ-phosphate could trigger actin filament disassembly in cells.

De novo assembly of filaments by pure actin monomers is unfavorable due to the fact that actin dimers and trimers are unstable (Pollard and Borisy, 2003, Sept and McCammon, 2001). Otherwise, elongation of existing actin filaments is favorable and depends on the concentration of ATP-actin monomers. There are several actin-binding proteins, which control actin filament assembly (Dominguez, 2004). ADF/cofilins have been proposed to increase the rate of treadmilling by promoting severing and dissociation of ADP-actin subunits from filament ends (Carlier et al., 1997, Blanchoin et al., 2000, Yeoh et al., 2002). The actin binding protein thymosin ß4 inhibits nucleotide exchange, whereas profilin, as the nucleotide exchange factor, promotes nucleotide exchange and blocks actin nucleation at both ends of the filament (Dominguez, 2007). Gelsolin is a F-actin capping and severing protein (McGough et al., 2003).

It has been shown that profilin binds actin-monomers more tightly than thymosin ß4. This maintains a pool of association-competent actin-profilin, whereas a smaller fraction of actin monomers bound to thymosin ß4 is kept in reserve.

Due to the fact, that *de novo* actin filament assembly is unfavorable, cells require actin nucleators to overcome the kinetic barrier to filament nucleation. Furthermore, the expression of different actin nucleation and elongation factors enables the cell to construct actin networks with specialized architectures and function.

1.2 Actin nucleation factors

1.2.1 The Arp2/3 complex

The Arp2/3 complex is an important cellular actin nucleator (Machesky et al., 1994), which together with its multiple nucleation promoting factors (NPFs) nucleates actin filaments of various cellular structures (Welch and Mullins, 2002).

The Arp2/3 complex consists of 7 subunits: two actin-related proteins, Arp2 and Arp3 within a complex with five other subunits: ARPC1 (for the 40-kDa subunit), ARPC2 (35-kDa subunit), ARPC3 (21-kDa subunit), ARPC4 (20-kDa subunit), and ARPC5 (16-kDa subunit). According to the "dendritic nucleation model" activated Arp2/3 complex nucleates new actin branches in a 70^{o} angle on the sides of existing actin mother filaments. The pointed end of the daughter filament is anchord to the mother filament whereas the free barbed end grows away from the Arp2/3 - F-actin complex. In the branch model Arp2 und Arp3 form an actin-like dimer template for nucleation (Mullins et al., 1998, Pollard, 2007).

The Arp2/3 complex is active at the leading edge of motile cells, organizing actin filaments during lamellipodia protrusion. Corresponding to the "dendritic nucleation model" lamellipodial actin networks are generated through the branching of new filaments from the sides of existing filaments, producing a dendritic array (Mullins et al., 1998). Recent results, using electron tomography, show that actin filaments do not form dendritic arrays *in vivo* (Urban et al., 2010), challenging the "dendritic nucleation model". Therefore, if the branched network is just an artefact of the 2-dimensional projections of densely packed 3-dimensional filament networks, remains an open question.

The Arp2/3 complex is intrinsically inactive but is strongly activated by proteins called nucleation promoting factors (NPFs), actin monomers and by pre-existing actin filaments. In the crystal structure of the inactive bovine Arp2/3 complex, Arp2 and Arp3 are not in this dimer-like conformation. This leads to the hypothesis that activation of the Arp2/3 complex involves a conformational change that brings Arp2 and Arp3 together. Binding of an actin monomer than creates the actin-trimer, which is then followed by rapid actin filament polymerization (Mullins et al., 1998, Robinson et al., 2001).

Major activators of the Arp2/3 complex are the Wiskott-Aldrich syndrome protein (WASP) family of nucleation promoting factors. WASP, neuronal WASP (N-WASP) and SCAR/WAVE1-3 (suppressor of cAMP receptor/WASP family verprolin homologous protein 1-3) were the first identified members of Arp2/3 NPFs (Veltman and Insall, 2010). New members; WHAMM, JMY and WASH, were recently discovered (Campellone et al., 2008, Linardopoulou et al., 2007, Zuchero et al., 2009).

All proteins of the WASP-family contain a carboxy-terminal activation domain consisting of one or two WH2 (WASP-homology) domains (also called verprolin homology domain, V-

domain), the acidic (A) domain, which mediates the binding to the Arp2/3 complex, and an intermediate conserved sequence (C) named cofilin homology domain (Veltman and Insall, 2010). The WH2 domain (Paunola et al., 2002, Chereau et al., 2005, Dominguez, 2007) binds an actin monomer and is therefore crucial for the nucleation of a new actin filament (by contributing an actin monomer for the actin trimer).

1.2.2 Formins

Formins are large multidomain proteins that form homodimers. All proteins of the formin-family contain the highly conserved formin homology 2 (FH2) domain and a neighboring proline rich FH1 domain. Phylogenetic analysis of FH2 domains show that metazoan formins fall into eight groups, named: Dia (diaphanous); DAAM (dishevelled-associated activator of morphogenesis); FRL (formin-related gene in leukocytes); FHOD (formin homology domain-containing protein); INF1 (inverted formin); WHIF1 (also referred to as INF2); FMN (formin) and delphilin (Schonichen and Geyer, 2010). Most eukaryotes have multiple formin isoforms.

FH2 domains have been shown to alter actin polymerization dynamics by accelerating *de novo* filament nucleation, altering filament elongation and/or depolymerization rate and by preventing filament barbed-end capping by capping proteins. It has been shown that the crystal structure of the FH2 domain from budding yeast formin Bni1 is dimeric (Xu et al., 2004). Other mammalian formin FH2 domains were also found to be dimeric (Harris et al., 2004, Li and Higgs, 2005). Two FH2 domains form a head-to-tail doughnut-shaped dimer that encircles the barbed end of the actin filament (Xu et al., 2004, Lu et al., 2007, Yamashita et al., 2007, Otomo et al., 2005b).

Furthermore, FH2 domains have the ability to move processively with an elongating actin filament "barbed" end (Shimada et al., 2004, Romero et al., 2004, Xu et al., 2004, Lu et al., 2007, Romero et al., 2007). Each functional half of the FH2 dimer is called a hemi-dimer and contains two F-actin binding sites (Xu et al., 2004). One side could dissociate to promote incorporation of an additional actin monomer while the other side of the FH2 dimer remain bound. In this way the FH2 dimer could move processively with the growing barbed end, protecting it from capping proteins. By solving the crystal structure of the yeast Bni1p FH2 domain in complex with tetramethylrhodamine-actin it has been proposed that the FH2 dimer exists in two different states: an open state, that allows actin subunit association or a closed

state, that prevents polymerization. Interconversion between these states allows processive "barbed" end polymerization and depolymerization in the presence of bound FH2 domain. The addition of one actin subunit shifts the position of the open-closed equilibrium by one unit forward along the filament (Otomo et al., 2005a).

The main feature of the N-terminal located FH1 domain is their high proline content. FH1 is a binding site for the actin monomer binding protein profilin (Kovar et al., 2003, Sagot et al., 2002). Profilin-bound actin monomers cannot nucleate spontaneously, and they cannot add to pointed ends but add to barbed ends (Pollard and Cooper, 1984, Pring et al., 1992, Pantaloni and Carlier, 1993, Pollard et al., 2000). Thus, profilin inhibits spontaneous nucleation and only when filaments are nucleated, they can use the profilin-bound actin monomers to elongate at their barbed ends. FH1 domains can also mediate protein-protein interactions to SH3 or WW domain-containing signaling proteins (Wallar and Alberts, 2003). Interactions between profilin and the FH1 domain are crucial for the recruitment of actin monomers to the elongating actin filament.

A common regulation mechanism of the formin protein family is autoinhibition. The C-terminus of several formins includes a diaphanous autoregulatory domain (DAD), which can mediate autoinhibition through binding to the N-terminus, a domain called diaphanous inhibitory domain (DID). DAD-DID interactions inhibit the ability of the FH2 domain to nucleate actin filaments (Li and Higgs, 2003). One mechanism to release formins from autoinhibition is the binding of Rho small G proteins to a N-terminal Rho-binding domain (Lammers et al., 2005).

1.2.3 The WH2 domain containing nucleation factor Spir

The first informations about Spir function have been obtained from a *Drosophila* screen for female sterile mutants (Manseau and Schupbach, 1989). The *Drosophila spire* and *cappuccino* mutant phenotypes were found to be identical. The Cappuccino (Capu) protein is an actin nucleation factor of the formin family. Mutation of *spire* and *cappuccino* affects both the dorsal-ventral and the anterior-posterior axes of the *Drosophila* egg and embryo (Emmons et al., 1995). The major phenotype of *spire* and *cappuccino* mutant *Drosophila* oocytes is a premature microtubule-dependent fast streaming at stage 8, before the polarity axes have been established (Theurkauf, 1994). Premature fast streaming has also been observed in *chickadee*

mutants (the *Drosophila* actin monomer-binding protein profilin) and after treatment with actin-depolymerizing drugs, like cytochalasin D (Manseau et al., 1996). These data suggest that Spir, Cappuccino and profilin are required to nucleate actin filaments, which repress premature microtubule-based cytoplasmic streaming. A current model has been proposed in which Spire and Capu assemble a dynamic actin mesh in the oocyte cytoplasm (Dahlgaard et al., 2007). During stages 5-10A, the mesh inhibits kinesin-dependent motility. When the actin mesh is present, the oocyte microtubules always form an anterior-posterior gradient, whereas they form cortical arrays when the mesh is absent. Once polarization factors a correctly targeted the actin mesh is disassembled at stage 10B. This relieves the inhibition of kinesin-dependent movement and switches on fast ooplasmic streaming. A similar actin mesh that is important for spindle positioning during asymmetric partitioning of the cytoplasm was also found in vertebrate oocytes (Azoury et al., 2008, Li et al., 2008, Schuh and Ellenberg, 2008).

1.2.3.1 Domain structure of Spir-family proteins

All known Spir proteins share a common domain architecture. The N-terminus contains the kinase non-catalytic C-lobe domain (KIND), which is a protein-protein interaction module. The Spir KIND domain represents the isolated C-lobe of kinases and is catalytically inactive (Ciccarelli et al., 2003). Regarding that the C-lobe of kinases mediates interaction with upstream activator proteins and downstream targets, a possible function of the Spir KIND domain could be the interaction with, or the recruitment of signaling proteins. A cluster of 4 WH2 domains is located in the central region of all Spir proteins. Spir proteins nucleate actin polymerization by the binding of four actin monomers to the four WH2 domains (WH2-A - WH2-D). Maximal nucleation activity requires all four WH2 domains and also the linker regions between the WH2 domains, especially the third linker region (L-3) between WH2-C and WH2-D. The deletion of WH2-C and WH2-D results in a nearly abolished nucleation activity, suggesting a model for Spir-induced actin polymerization, in which WH2-C and WH2-D each bind one actin monomer and L-3 might promote actin dimer formation by stabilizing the interaction of those two actin monomers. WH2-B and WH2-A than add two further actin monomers to the initial dimer. It is supposed that Spir mediates the formation of the initial dimer to nucleate one strand of the long-pitch filament helix (Quinlan et al., 2005).

The C-terminus of Spir proteins consists of the Spir-box and the modified FYVE domain. The Spir-box is highly conserved between the different Spir proteins. It shares sequence similarity with a helical region of the Rab3A effector rabphilin-3A, which mediates the interaction with the small G protein Rab3A (Kerkhoff et al., 2001, Ostermeier and Brunger, 1999). This suggests, that the Spir-box could mediate binding to Rab small G proteins. The modified FYVE domain is located adjacent to the Spir-box, at the C-terminus. FYVE zinc fingers contain 8 cysteine residues, which bind two zinc ions (Misra and Hurley, 1999). FYVE domains are membrane binding modules, forming a hydrophobic "turret loop", which penetrates the membrane (Kutateladze and Overduin, 2001, Psachoulia and Sansom, 2009). It has been shown that mutation of the FYVE domain and deletion of the Spir-box of *Drosophila* p150 Spir disrupts the membranous localization of Spir (Kerkhoff et al., 2001). A common feature of FYVE domains is a cluster of basic amino acids between cysteines 2 and 3, which is crucial for the binding to phosphatidylinositol 3-phosphate (PtdIns(3)P). The modified Spir FYVE domain lacks the basic cluster and has a loop insertion between cysteines 6 and 7. This suggests that Spir exhibits different phospholipid binding properties in comparison to other FYVE domain containing proteins.

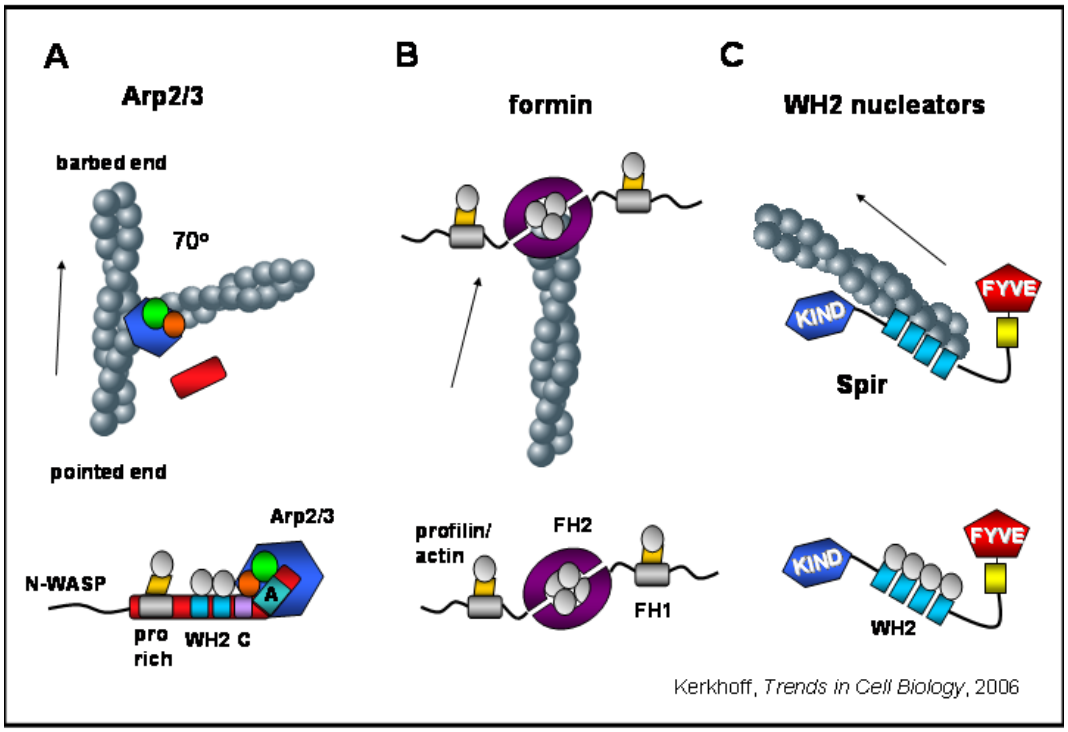

Figure 1.1: **Actin nucleation factors**
Actin nucleation factors like the Arp2/3 complex, formins and the WH2-domain containing actin nucleator Spir are required for the polymerization of free actin monomers. The Arp2/3 complex **A**, which is activated by binding to nucleation promoting factors, like N-WASP. **B** Formins mediate actin nucleation and polymerization by forming a ring-like dimer structure in which each FH2 domain binds two actins. The proline-rich FH1 domain binds profilin-actin. **C** Spir proteins are the founding members of a class of WH2-domain containing actin nucleation factors. Four WH2-domains in the central region of the protein bind 4 actin monomers. Formin and Spir proteins nucleate unbranched filaments, whereas the Arp2/3 complex nucleates branched filaments.
Figure adapted from Kerkhoff, 2006.

1.2.3.2 Spir-formin cooperation

According to the identical phenotypes of *cappuccino* and *spire* mutants in *Drosophila* oocytes it has been shown that Spir and Capu interact (Rosales-Nieves et al., 2006, Quinlan et al., 2007). Quinlan et al. found that the KIND domain of Spir binds to the Capu FH2 domain. Furthermore the KIND domain inhibits actin nucleation by the Capu FH2 domain whereas Capu FH2 leads to an increased actin nucleation of Spir KIND WH2 but not Spir WH2 (Quinlan et al., 2007).

Vertebrate genomes encode two *spir* genes, *spir-1* and *spir-2* (Schumacher et al., 2004, Pleiser et al., 2010), which show a high similarity. There are two Capu homologs in mammals, formin-1 (FMN-1) (Zhou et al., 2006, Dettenhofer et al., 2008, Kobielak et al., 2004) and formin-2 (FMN-2) (Leader and Leder, 2000, Leader et al., 2002). It has been shown that *spir-1* and *formin-2* show a similar expression pattern during mouse embryogenesis and in the adult mouse brain (Schumacher et al., 2004). Mouse *spir-2* was detected in epithelial cells of the digestive tract and in neuronal cells of the nervous system (Pleiser et al., 2010). Analogous to Spir and Cappuccino, the mammalian homologs Spir-1 and formin-2 show a regulatory interaction. The interaction is mediated by a Spir-binding site at the very C-terminus of formin-2 (formin-Spir-interaction site; FSI) adjacent to its core FH2 domain (Pechlivanis et al., 2009). It has been shown that both mammalian Spir proteins, Spir-1 and Spir-2, interact with each of the two formin proteins, formin-1 and formin-2 (Pechlivanis et al., 2009).

1.2.4 Other WH2-domain containing actin nucleation factors

Regulation of the actin cytoskeleton is mediated by the action of a vast number of actin-binding proteins. A limited number of folding motifs mediate the interaction of actin-binding proteins and actin, among which the β-thymosin/WH2 fold plays a prominent role (Paunola et al., 2002, Dominguez, 2007, Dominguez and Holmes, 2010). WH2 domains are small actin binding modules including 17-27 amino acids (Chereau et al., 2005, Paunola et al., 2002). They contain the consensus motif L++V/T (+ representing basic amino acids) and a conserved N-terminal amphiphilic helix, which mediates the binding to the hydrophobic pocket of actin. Tβ4, a short 43 amino acid polypeptide is the best-known member of the β-thymosin family. It contains a long C-terminal extension, which extends along the nucleotide binding cleft of actin and is important for the actin sequestration activity of Tβ4 (Dominguez, 2007). WH2

domains lack that C-terminal extension. If the β-thymosin and WH2 domains are evolutionary related or evolved independently is still a matter of debate (Edwards, 2004, Dominguez, 2007). Several WH2-domain containing actin nucleation factors were recently discovered, which have the ability to nucleate actin filaments without the Arp2/3 complex.

The actin nucleation factor Cordon-bleu (Cobl) is a three-WH2-domain protein involved in neural tube formation (Gasca et al., 1995, Carroll et al., 2003). Neuronal expression of the C-terminal region, which contains the three WH2-domains, induces branches of the axons and increases the number of dendrites (Ahuja et al., 2007).

Leiomodin-2 (Lmod-2) is another recently identified WH2-domain-containing actin nucleator in muscle cells. Leiomodin nucleates unbranched actin filaments *in vitro* (Chereau et al., 2008).

Moreover, two type-III secretion virulence factors of the pathogens *Vibrio cholerae* and *Vibrio parahaemolyticus*, called VopF (Tam et al., 2007) and VopL (Liverman et al., 2007) seem to use a Spir-like mechanism to nucleate actin. VopL and VopF, which are found to be associated to actin structures *in vivo*, contain three WH2 domains and three copies of a proline rich motif. Both factors alter the eukaryotic actin cytoskeleton. VopL induces stress fibers (Liverman et al., 2007), whereas VopF induces aberrant actin-rich protrusions (Tam et al., 2007). Otherwise, the type-III secretion factor TARP (translocated actin recruiting phosphoprotein) from *Chlamydia trachomatis,* which also promoted actin nucleation *in vitro*, contains only a single WH2 domain. It has been proposed that TARP oligomerizes to nucleate actin (Jewett et al., 2006). These observations suggest that pathogens have adopted a Spir-like actin nucleation mechanism to manipulate the host cytoskeleton.

1.3 Cellular vesicle transport

1.3.1 Spir function in vesicle transport processes

Targeting of cytosolic proteins to specific intracellular membranes is regulated by the specific localization of different phospholipids. Several lipid binding domains are described which are crucial for that lipid-mediated protein targeting (Lemmon, 2003).

DNA sequence comparisons of Spir-proteins revealed that the Spir C-terminus contains a FYVE domain (named after the initial letters of four proteins containing a FYVE fin-

ger: **F**ab1p, **Y**OTB, **V**ac1p, **E**EA1) (Stenmark et al., 1996). FYVE domains are membrane binding modules, consisting of a hydrophobic "turret loop", which penetrates the membrane (Kutateladze and Overduin, 2001, Psachoulia and Sansom, 2009). They have eight conserved cysteines, which coordinate two Zn^{2+}ions (Stenmark et al., 1996). FYVE domains are known phospholipid interaction modules, which were subsequently identified as phosphatidylinositol 3-phosphat (PtdIns(3)P) binding domains (Gaullier et al., 1998, Patki et al., 1998, Burd and Emr, 1998). The R(R/K)HHCRxCG motif between cysteine 2 and 3 is crucial for the binding to PtdIns (3)P. Several proteins, like Rabphilin-3A have FYVE-related domains that lack several conserved residues of FYVE fingers. Spir also contains a modified FYVE domain, lacking the basic cluster between cysteines 2 and 3 and furthermore has a loop insertion between cysteines 6 and 7.

The *Drosophila* Spire protein and Spir-1 show colocalization to Rab11 in transiently transfected NIH3T3 mouse fibroblasts. Rab11 is implicated in the endocytic (Ullrich et al., 1996, Goldenring et al., 1996, Calhoun et al., 1998) and the exocytic secretory pathway (Chen et al., 1998, Wilcke et al., 2000, Urbe et al., 1993, Deretic, 1997). Furthermore, the localization of Spir to membranes is dependent on the integrity of the FYVE domain and the Spir-box (Kerkhoff et al., 2001). The expression of a truncated version of Spir-1 (Spir-1-CT), which lacks the KIND domain and the 4 WH2 domains and therefore the ability to nucleate actin filaments, inhibits the transport of vesicular stomatitis virus G protein (VSV-G) to the plasma membrane (Kerkhoff et al., 2001), suggesting a role for Spir-1 in the secretory pathway.

Another study showed a possible role for Spir-1 in the endocytic pathway (Morel et al., 2009). It has been shown, that the nucleation of actin patches on early endosomes is dependent on annexin A2 and Spir-1, suggesting that actin nucleation is crucial for endosome biogenesis.

1.3.2 Regulation of vesicle transport processes

1.3.2.1 The Rab family of small G proteins (Ras-related in brain)

Rab small guanine nucleotide-binding proteins (G proteins) belong to the protein family of Ras small G proteins. They serve as organizers of almost all membrane transport processes in eukaryotic cells (Stenmark, 2009). Rab proteins and their effectors or regulators are highly compartmentalized in organelle membranes, which is crucial for membrane identity. Like other small G proteins, also Rab proteins circle between a GTP-bound "active" and a GDP-

bound "inactive" conformation. However, there are a lot of other regulation factors identified coordinating Rab activity (Ullrich et al., 1993, Alexandrov et al., 1994, Pfeffer et al., 1995, Sivars et al., 2005, Dirac-Svejstrup et al., 1997, Soldati et al., 1994). Rab proteins are reversibly associated with membranes by geranylgeranyl groups that are attached to one or two cysteine residues at the C-terminus (Chavrier et al., 1991). The enzyme catalyzing this reaction is Rab geranylgeranyltransferase (GGTase) (Casey and Seabra, 1996). A Rab Escort Protein (REP) binds nonprenylated precursors directly after translation and presents them to the GGTase (Alexandrov et al., 1994). Rab proteins are maintained in the GDP-bound inactive conformation by GDP-dissociation inhibitors (GDIs) (Ullrich et al., 1993, Soldati et al., 1994).

Although, there are examples of Rab effectors that prefer the GDP-bound conformation most effectors are activated only by the GTP-bound Rab protein (Seabra, 1996, Eathiraj et al., 2005). Exchange of GDP with GTP is catalyzed by guanine nucleotide exchange factors (GEFs) after displacement of the GDI, which is catalyzed by a GDI-displacement factor (GDF) (Sivars et al., 2005). Rab proteins have an intrinsic GTPase activity but there are also GTPase-activating proteins (GAPs), which could catalyze GTP hydrolysis to inactivate the GTPase (Barr and Lambright, 2010, Bos et al., 2007). Together, GAPs, GDIs and REPs ensure that Rab proteins are maintained in the inactive state in the cytosol so that activation occurs only at the target membrane.

Rab11 There are three Rab11 isoforms: Rab11a, Rab11b and Rab11c/Rab25 (Bhartur et al., 2000). Rab11a (Goldenring et al., 1996) and Rab11b (Lai et al., 1994) are ubiquitously expressed, whereas Rab25 has an epithelial restricted expression profile (Goldenring et al., 1993). Rab11 has been detected on several subcellular membranes. It is associated with the pericentrosomal recycling system in nonpolarized (Ullrich et al., 1996, Ren et al., 1998) and polarized cells (Goldenring et al., 1996, Lapierre et al., 2007, Calhoun et al., 1998). The recycling endosome has a tubular morphology and its organization is dependent on the microtubule cytoskeleton. Internalized receptors, like the transferrin receptor, first enter the early endosome (also called sorting endosome) then are transported to the recycling endosome (slow cycle) or directly to the plasma membrane (fast cycle). It has also been shown that Rab11 mutants modify the morphology of the recycling endosome and effect transferrin receptor transport (Ullrich et al., 1996).

Rab11 is also localized to Golgi membranes (Urbe et al., 1993, Deretic, 1997, Chen et al.,

1998). Expression of the dominant negative Rab11S25N mutant protein led to a significant inhibition of the transport from the *trans*-Golgi network (TGN) to the plasma membrane of the VSV-G protein, resulting in an accumulation of the VSV-G protein in the Golgi (Chen et al., 1998). This suggests that functional Rab11 is required for efficient export of VSV-G protein from the Golgi. GDI proteins are frequently be used to alter the membrane association of Rab proteins. Overexpressing of GDIs leads to a release of Rab11-GDP from membranes. It has been shown that an excess of GDI proteins causes an inhibition in membrane transport from the *trans*-Golgi network to the plasma membrane (Chen et al., 1998). Furthermore, a role for Rab11a in retrograde traffic has also been observed, where it regulates the exit of membranes from the recycling endosome (Wilcke et al., 2000).

Small G proteins of the Rab11 family, including Rab11a and Rab25 have an effect of migration and invasion of tumor cells. It has been shown that Rab11a and Rab25 control recycling of internalized α5ß1 integrin (Roberts et al., 2001, Caswell et al., 2007, 2008). Elevated levels of Rab25 in ovarian and breast cancer cell lines participate in tumor progression by increasing tumor growth and aggressiveness of already transformed tumor cells (Cheng et al., 2004, Agarwal et al., 2009). Rab11 family-mediated recycling of multiple factors could therefore collectively contribute to tumor pathogenesis.

Rab11a/myosin Vb cooperation The motorprotein myosin V has been implicated in organelle trafficking along actin filaments. To ensure the correct targeting of the motorprotein to specific vesicles or organelles, Rab G proteins have been identified as important regulators of myosin V recruitment. Rab27a recruits myosin Va to melanosomes via the adaptor protein melanophilin (Wu et al., 2001). Mutations in the Rab27a, melanophilin or the myosin Va gene result in a disease called Griscelli syndrome (Fukuda, 2005). Griscelli syndrome is defined by the characteristic hypopigmentation (albinism) and variable immunodeficiencies due to defects in the transport of melanosomes in melanocytes and lytic granules in cytotoxic T-lymphocytes (Griscelli and Prunieras, 1978). Another important cooperation between a Rab G protein and a myosin V motor is the recruitment of myosin Vb to recycling endosomes by Rab11 (Volpicelli et al., 2002, Fan et al., 2004, Hales et al., 2002, Swiatecka-Urban et al., 2007). Overexpression of the tail domain of myosin Vb leads to an accumulation of Rab11a in recycling endosomes (Lapierre et al., 2001). Furthermore, it has been shown, that the Rab11-binding protein FIP2 is involved in the recruitment of myosin Vb by binding to its tail domain (Hales et al.,

2002, Lapierre et al., 2001). Myosin Vb is enriched in the hippocampus (Zhao et al., 1996) and it has been shown that myosin Vb together with Rab11/Rab11-FIP2 mediates Ca^{2+}-dependent, actin-based transport of AMPA receptor containing recycling endosomes during (LTP). Myosin Vb motor activity and myosin Vb-binding to Rab11/Rab11-FIP2 is required for AMPA receptor insertion and spine growth and thus synaptic potentiation (Wang et al., 2008).

Rab11 FIP family proteins Consistent with the role of Rab11 in several membrane traffic pathways, many Rab11-interacting proteins have been identified (Wallace et al., 2002). There are six novel Rab11-interacting proteins belonging to a family of proteins called family of Rab11-interacting proteins (FIPs). All FIPs contain a highly conserved Rab binding domain (RBD) at their C-termini. Another feature of all FIPs is their α-helical coiled coil domain at the C-terminus, which is crucial for their homo- and hetero-interacting abilities (Wallace et al., 2002). Based on sequence homology, all FIPs can be divided into three classes. Rip11, FIP2 and RCP (Rab coupling protein) are class I FIPs. They all contain a C2 domain at the N-terminus. FIP3/Eferin and FIP4 (Wallace et al., 2002), which are containing EF-hands, belong to class II. The only member of class III is FIP1. FIP1 is the only Rab11-interacting protein, which lacks any N-terminal structural domains (Fig. 1.2).

FIP proteins do not require Rab11 for membrane binding (Meyers and Prekeris, 2002). Overexpression of the dominant negative mutant Rab11S25N had no effect on the localization of endogenous FIP2, Rip11 and FIP3 (Meyers and Prekeris, 2002). This raises the possibility that FIPs may target Rab11 to defined membrane structures in the cell. In this way Rab11-FIPs could play a role as Rab11 scaffolding proteins. Rab11/FIP complexes at specific membrane compartments could than recruit other proteins, such as motor proteins or Arf proteins (Shin et al., 1999, 2001, Shiba et al., 2006, Hales et al., 2002, Lapierre et al., 2001).

FIP2, a member of class I FIPs, contains a N-terminally located C2 domain. C2 domains are implicated in phospholipid binding and protein-protein interaction. It has been shown, that the C2 domain of FIP2 binds preferentially to phosphatidylinositol 3,4,5-trisphosphate ($PtdIns(3,4,5)P_3$) and phosphatidic acid (PA), suggesting that the C2 domain targets FIP2 to $PtdIns(3,4,5)P_3$ and PA-enriched membranes (Lindsay and McCaffrey, 2004). Expression of truncation mutants of FIP2 that lack their C2 domains leads to inhibition of endsomal recycling traffic and causes tubulation of the transferrin receptor (TfR)-positive endosomal

compartments (Lindsay et al., 2002, Lindsay and McCaffrey, 2002, Prekeris et al., 2000).

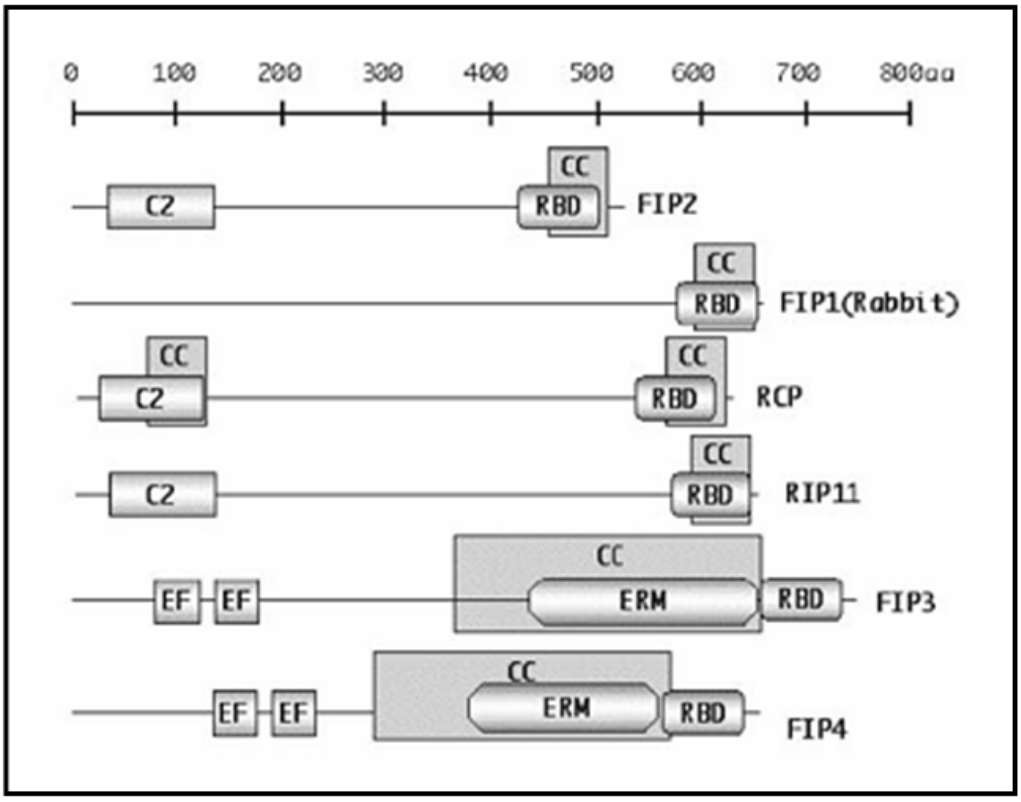

Figure 1.2: **Domain structure of different Rab11-FIPs**
RCP, Rip11 and FIP2 belong to class I Rab11-FIPs. They contain a C2 domain near their N-termini and the highly conserved 20 amino acid RBD (Rab Binding Domain) at their C-termini. The second class comprises FIP3 and FIP4, both containing EF hand motifs and an ERM domain. Class III contains just one member, FIP1, which does not have either a C2 domain nor EF hand domains.
Figure adapted from Wallace et al., 2002.

Basolateral transport of E-cadherin is Rab11-dependent Cells in epithels are connected by so called adherens junctions consisting of protein complexes. The major components are

cadherins, transmembrane proteins, which mediate cell-cell adhesion in a Ca^{2+}-dependent manner. The extracellular region of cadherins mediates the homotypic binding to a cadherin protein of an adjacent cell, whereas the cytoplasmic region binds to intracellular proteins, like ß-catenin.

E-cadherin, the epithelial cadherin, is trafficked and delivered to the basolateral cell surface. It is transported from the TGN to the plasma membrane by passing endosomal structures (Lock and Stow, 2005, Desclozeaux et al., 2008). By using GFP-tagged E-cadherin it has been shown that this transport is mediated by tubulovesicular carriers (Lock and Stow, 2005, Lock et al., 2005). Furthermore, Rab11-positive compartments are traversed by E-cadherin on its route to the plasma membrane. These studies demonstrated a Rab11-positive recycling endosome as an intermediate compartment for post-Golgi exocytosis of E-cadherin in HeLa cells. Overexpression of Rab11 results in an increased intracellular E-cadherin localization and a reduced cell surface delivery of E-cadherin supporting a functional role for Rab11 in E-cadherin trafficking (Lock and Stow, 2005).

2 *MATERIALS*

2.1 Expendable items

Item	Manufacturer	Order number
Autoclave tape (180°C)	distributed by A. Hartenstein Laborbedarf	STKH
Autoclave tape (120°C)	distributed by A. Hartenstein Laborbedarf	STKD
Blotting papers Grade 3 MM Chr	Whatman	3030.917
Cell culture flask T75 red cap	Sarstedt	83.1813.002
cell culture plates 6-Well	Greiner Bio-One	657160
Cell culture glass bottom dish	Willco wells	GWSt-5040
Conical reaction tubes (15 ml)	Greiner Bio-One	188271
Conical reaction tubes (50 ml)	Greiner Bio-One	227261
Cryovials (1 ml)	Thermo-Scientific, Nunc	366656
Embedding cassette	Carl-Roth	E478.1
Microscope cover glasses (15 mm diameter)	Marienfeld Laboratory Glassware	0111550
Microscope slides SuperFrost® Plus	Menzel, Thermo Scientific	J1800AMNZ
Neubauer counting chamber	Brand	

Nitrocellulose transfer membrane, PROTRAN® BA85, 0.45 µM pore size	Whatman	10401196
Parafilm® "M" Laboratory Film	Pechiney Plastic Packaging	PM-996
Pasteur pipettes	distributed by A. Hartenstein Laborbedarf	PP07
PCR-tubes (0.2 ml)	Axygen, distributed by Abimed	PCR-0208-CP-C
Petri dishes (94 x 16 mm)	distributed by A. Hartenstein Laborbedarf	PP90
Pipette tips (0.5-10 µl)	Axygen, distributed by Abimed	T-300
Pipette tips (100-1000 µl)	Axygen, distributed by Abimed	T-1000-B
Pipette tips (2-20 µl) and (20-200 µl)	Sarstedt	70.760.002
PIP Strips^{TM} membranes -set of 10-	Invitrogen	P23751
Reaction tubes (1.5 ml)	distributed by A. Hartenstein Laborbedarf	RK1G
Reaction tubes (2.0 ml)	distributed by A. Hartenstein Laborbedarf	RK2G
Scalpel	Megro	147222
Slide-A-Lyzer* Dialysis Cassettes, 10K MWCO, 0,5 ml	Thermo-Scientific	66383
Syringe (1 ml) with needle 0.45 x 10 mm	Becton-Dickinson	300015
Syringe (10 ml)	Braun	4606108V

Syringe (50 ml)	Dispomed	22050
Syringe filter (0.2 µm)	Sartorius Stedim Biotech	17597
X-ray film	FujiFilm	47410 08379

2.2 Chemicals

Item	Manufacturer	Order Number
Agar select	Sigma-Aldrich	A5054
Acrylaminde (30%)/ Bisacrylamide (0,8%) (37.5:1)	Carl-Roth	3029.1
Agarose, UltraPure™	Invitrogen, Molecular Probes	15510-027
Ammonium persulfate (APS)	Sigma-Aldrich	A3678
Ampicillin; Sodium crystalline	Sigma-Aldrich	A9518
BCP, phase separation reagent	MRC Molecular Research Center, Inc.	BP151
ß-Mercaptoethanol	Carl-Roth	4227.3
Boric acid	Sigma-Aldrich	B0252
Bovine serum albumin, Cohn V fraction	Sigma-Aldrich	A4503
Bromophenol blue	Carl-Roth	A512.1
Calcium chloride	Carl-Roth	A119.1
Chloramphenicol	Sigma-Aldrich	C0378
Complete, Mini, EDTA-free; Proteaseinhibitor	Roche	11836170001
Coomassie Blue G	Carl-Roth	9598.1
Diethyl Pyrocarbonate (DEPC)	Sigma-Aldrich	D5758
Dimethyl Sulfoxide (DMSO)	Sigma-Aldrich	D2650

ECL reagent	GE/Healthcare	RPN2109
EDTA	Sigma-Aldrich	E5134
Ethanol >99.8%, p.a.	Carl-Roth	9065.2
Ethanol denatured (+1% Mek)	Carl-Roth	K928.1
Ethidiumbromide	Carl-Roth	HP46.1
Fetal bovine serum Fetalclone III	Thermo Scientific; Hyclone	SH30109.03
Glutathione	Sigma-Aldrich	G4251
Glutathione agarose beads	GE/Healthcare	17-0756-01
Glycerine	Carl-Roth	3783.1
Glycerine solution (for microscopy)	Leica	11513872
Glycine	Sigma-Aldrich	G7126
Hydrochloric acid	Carl-Roth	6331.1
Imidazole	Sigma-Aldrich	I0125
IPTG	Sigma-Aldrich	I9003
Isopropanol	AppliChem	A0900
Kanamycin	Sigma-Aldrich	K-1377
LB	Sigma-Aldrich	L3022
Lipofectamine	Invitrogen, Molecular Probes	18324012
Magnesium chloride hexahydrate	Carl-Roth	2189.2
Methanol 99.9%	Carl-Roth	4627.2
Milk powder, blotting grade	Carl-Roth	T145.2
Mowiol	Calbiochem	475904
Ni-NTA Agarose	Qiagen	30210
Nitric acid	Carl-Roth	4989.1

Nonidet P-40	Biochemica; distributed by A. Hartenstein Laborbedarf	A1694,0500
Paraformaldehyde (PFA)	Carl-Roth	0335.1
PBS buffer (10X Dulbecco's) – powder	AppliChem	A0965
Phalloidin Rhodamine	Invitrogen, Molecular Probes	R415
Ponceau S	Sigma-Aldrich	P3504
Protein-G-Agarose beads	Roche	11 243 233 001
Rubidium chloride	Carl-Roth	4471.1
Sodium chloride	Sigma-Aldrich	S3014
Sodium citrate tribasic dihydrate	Sigma-Aldrich	S4641
Sodium dodecyl sulfate (SDS)	Sigma-Aldrich	L4390
Sodium hydroxide pellets	Merck	106462
Sodium phosphate	Sigma-Aldrich	S9638
TEMED	Sigma-Aldrich	T9281
Triton X 100	Carl-Roth	3051.3
Trizol® Reagent	Invitrogen, Molecular Probes	15596026
Tween 20	AppliChem	A1389

2.3 Kits

Kit	Manufacturer	Order number
NucleoTrap DNA Gel extraction Kit	Macherey-Nagel	740609.50
DNA Plasmid Maxi Kit	Qiagen	12163
DNA Plasmid Mini Kit	Qiagen	12123
QuantiTect Reverse Transcription	Qiagen	205311

One-Step RT-PCR	Qiagen	210212

2.4 Bacterial strains

Strain	Manufacturer	Annotation	Order number
NEB10ß	NEB	Genotype: araD139 Δ(ara,leu)7697 fhuA lacX74 galK16 galE15 mcrA f80d(lacZΔM15) recA1 relA1 endA1 nupG rpsL rph spoT1Δ(mrr hsdRMS mcrBC)	C3019H
E. coli Rosetta	Novagen / Merck	Increased protein expression rate by providing tRNAs rarely used in E. coli Genotype: F- ompT hsdSB(rB- mB-) gal dcm pRARE (CamR)	70953

2.5 Cultured cell lines

Cell line	ATTC number	Annotation
HeLa	CCL-2	an immortal cell line derived from cervical cancer cells taken from Henrietta Lacks
HEK 293	CRL-1573	human embryonic kidney 293 cells
MDCK	CCL-34	Madin-Darby canine kidney epithelial cell line
MDCK Myc-hs-Spir-2 stable cell line		pBABE-puro vector provides retrovirus sequences for the delivery of exogenous genes in mammalian cells

2.6 Expression vectors

Vector	Manufacturer	annotation
pGEX-4T-3	GE/Healthcare	Bacterial expression vector Genes cloned into the MCS will be expressed as fusions to the C-terminus of GST
pProEX HTb	Invitrogen, Molecular Probes	Bacterial expression vector Genes cloned into the MCS will be expressed as fusion proteins with an N-terminally 6xHis tag
pEGFP-C1	Clontech	Mammalian expression vector Genes cloned into the MCS will be expressed as fusions to the C-terminus of eGFP
pEGFP-N3	Clontech	Mammalian expression vector Genes cloned into the MCS will be expressed as fusions to the N-terminus of eGFP
mStrawberry	kindly provided by A. Akhmanova	Mammalian expression vector EGFP-C2 backbone (Clontech) eGFP substituted against mStrawberry Genes cloned into the MCS will be expressed as fusions to the N-terminus of the mStrawberry protein
pcDNA3	Invitrogen, Molecular Probes	Mammalian expression vector

2.7 Enzymes

Item	Manufacturer	Order number
BioTerm *Taq*-Polymerase	Genecraft	GC-002-0500
10x BioTherm buffer 15 mM $MgCl_2$	Genecraft	GC-002-006
Pfu-Polymerase	Promega	M774B
Pfx-Polymerase/Accuprime	Invitrogen, Molecular Probes	12344024
Phusion-High-Fidelity DNA Polymerase	NEB	F530S
Restrictionenzymes	NEB	
T4 DNA ligase (supplied with 10X Reaction Buffer)	NEB	M0202

2.8 Molecular Weight Standards

Item	Manufacturer	Order number
DNA ladder 1 kb	peqLab	25-2031
DNA ladder 100 bp	peqLab	25-2010
Precision Plus Protein dual color standard	Bio-Rad	1610374

2.9 Cell culture media and supplements

Item	Manufacturer	Order number
DMEM	Invitrogen, Molecular Probes	41965039
HEPES buffer 1 mM	Invitrogen, Molecular Probes	15630056
L-Glutamine 200 mM	Invitrogen, Molecular Probes	25030024
Poly-L-Lysine; 0,01% solution	Sigma-Aldrich	P 4707
Trypsin 0,05% EDTA	Invitrogen, Molecular Probes	25300054
PBS	Invitrogen, Molecular Probes	14190094

2.10 Antibodies

2.10.1 Primary antibodies

Antigen	Name	Species	Order number	Manufacturer
Anti-myc	Myc 9E10	mouse monoclonal	sc-40	Santa Cruz
E-cadherin	DECMA-1	rat monoclonal	sc-59778	Santa Cruz
Anti-His	penta-His-Antibody	mouse monoclonal	34660	Qiagen
Anti-alpha-Tubulin	alpha-Tubulin Antibody	mouse monoclonal	A-11126	Invitrogen, Molecular Probes
Anti-ERK1	ERK1 (C-16)	rabbit polyclonal	sc-93	Santa Cruz
Anti-EGFP	Living-colors EGFP A.v. Peptide Antibody	rabbit polyclonal	632376	Clontech
Anti-dsRed	Living-colors dsRed A.v. Peptide Antibody	rabbit polyclonal	632496	Clontech
Anti-GST	anti-GST	goat monoclonal	27-4577-01	GE Healthcare

2.10.2 Secondary antibodies

Antigen	Name	Species	Order number	Manufacturer
Anti-mouse	Flourescin (FITC)-conjugated AffiniPureDonkey anti-mouse IgG	donkey polyclonal	715-095-151	Jackson Immuno Research Laboratories

Anti-mouse	Rhodamine (TRITC)-conjugated AffiniPureDonkey anti-mouse IgG	donkey polyclonal	715-025-151	Jackson Immuno Research Laboratories
Anti-rat	Rhodamine (TRITC)-conjugated AffiniPureDonkey anti-rat IgG	donkey polyclonal	712-025-153	Jackson Immuno Research Laboratories
Anti-mouse	Cy5-conjugated AffiniPureDonkey anti-mouse IgG	donkey polyclonal	715-175-151	Jackson Immuno Research Laboratories
Anti-mouse	anti-mouse IgG horseradish-peroxidase linked	sheep polyclonal	NA 9310	Amersham Pharmacia biotech
Anti-rabbit	anti-rabbit IgG horseradish-peroxidase linked	sheep polyclonal	NA 9340	Amersham Pharmacia biotech
Anti-rat	anti-rat IgG horseradish-peroxidase linked	sheep polyclonal	NA 932	Amersham Pharmacia biotech
Anti-goat	bovine anti-goat IgG horseradish-peroxidase linked		sc-2350	Santa Cruz

2.11 Buffers and solutions

Acrylamid Gel electrophoresis (Protein SDS-PAGE)

Separating Gel

	6,5 %	7,5 %	10 %	12 %
H_2O dest	20,2 ml	17,1 ml	14,5 ml	12,3 ml
3M Tris-HCl pH 9,0	3,8 ml	3,8 ml	3,8 ml	3,8 ml
Acrylamid Roti 30	6,8 ml	7,9 ml	10,5 ml	12,7 ml
20 % SDS	0,15 ml	0,15 ml	0,15 ml	0,15 ml
TEMED	0,03 ml	0,03 ml	0,03 ml	0,03 ml
10 % APS	0,15 ml	0,15 ml	0,15 ml	0,15 ml

Stacking Gel

H_2O dest	7,7 ml
1M Tris-HCl pH 6,8	1,25 ml
Acrylamid Roti 30	1,66 ml
20 % SDS	0,05 ml
TEMED	0,015 ml
10 % APS	0,1 ml

Co-immunoprecipitation buffer with EDTA

- 25 mM Tris-HCl pH 7,4
- 150 mM NaCl
- 10 % (v/v) Glycerin
- 0,1 % NP-40

Co-immunoprecipitation buffer without EDTA (G proteins, myosin Vb)

- 25 mM Tris-HCl pH 7,4
- 150 mM NaCl
- 2,5 mM $MgCl_2$
- 1 mM DTT
- 10 % (v/v) Glycerin
- 0,1 % NP-40

1x DNA sample buffer

- 9 mM Tris-HCl pH 7,4
- 0,45 mM EDTA
- 46 % (v/v) Glycerin
- 0,2 % (w/v) SDS
- 0,05 % (w/v) Bromophenolblue

10x Electrophoresis buffer (Protein SDS-PAGE)

- 250 mM Tris
- 190 mM Glycin
- 0,1 % (w/v) SDS
- H_2O dest.
- pH 8,6

Elution buffer (Purification of 6xHis-tagged proteins)

- 50 mM NaH_2PO_4
- 300 mM NaCl
- 250 mM Imidazol
- pH 8,0

Elution buffer without phosphat (Purification of 6xHis-tagged proteins; protein-lipid overlay assay)

- 50 mM Tris-HCl
- 500 mM NaCl
- 250 mM Imidazol
- pH 8,0

Lysis buffer

- 50 mM NaH_2PO_4
- 300 mM NaCl
- 10 mM Imidazol
- pH 8,0

Elution buffer (Purification of GST-tagged proteins)

- 50 mM Tris
- 200 mM NaCl
- 25 mM Glutathione
- pH 8,8

5 % Milk solution (blocking reagent)

- 5 % (w/v) milk powder in PBST

Mowiol solution

- 15 % (w/v) Mowiol
- 30 % (v/v) Glycerin
- 2,25 % (w/v) N-propyl gallate in 1x PBS

1x PBS

- 9,55 g 10x Dulbecco's PBS powder in 1 l H_2O dest

PBST

- 0,05 % (v/v) Tween 20 in 1x PBS

Pull down buffer

- 25 mM Tris-HCl pH 7,4
- 300 mM NaCl
- 1 mM EDTA
- 0,1 % (v/v) NP-40
- 10 % (v/v) Glycerin

Rubidium chloride buffer

RFI

- 100 mM RbCl
- 30 mM KAc

- 10 mM $CaCl_2$
- 15 % (v/v) Glycerin
- pH 5,8

RFII

- 10 mM MOPS
- 10 mM RbCl
- 75 mM $CaCl_2$
- 15 % (v/v) Glycerin
- pH 6,8

1x SDS sample buffer (Protein sample buffer)

- 60mM Tris-HCl pH 6,8
- 10 % (v/v) Glycerin
- 3 % (w/v) SDS
- 5 % (v/v) β-Mercaptoethanol
- 0,005 % (w/v) Bromophenolblue

5x SDS sample buffer (Protein sample buffer)

- 300 mM Tris-HCl pH 6,8
- 50 % (v/v) Glycerin
- 15 % (w/v) SDS
- 25 % (v/v) β-Mercaptoethanol
- 0,025 % (w/v) Bromophenolblue

Stripping buffer

- 62,5 mM Tris
- 2 % (w/v) SDS
- pH 6,7

10x TBE buffer (DNA electrophoresis)

- 890 mM Tris
- 89 mM Boric acid
- 20 mM EDTA

TBST (Purification of GST-tagged proteins; protein-lipid overlay assay)

- 10 mM Tris-HCl pH 7,4
- 150 mM NaCl
- 0,1 % (v/v) Tween 20

Washing buffer (Purification of 6xHis-tagged proteins)

- 50 mM NaH_2PO_4
- 300 mM NaCl
- 20 mM Imidazol
- pH 8,0

Western blotting buffer (WB)

- 190 mM Glycine
- 125 mM Tris base
- 20 % methanol (v/v)

3 *METHODS*

3.1 Molecular Biological Methods

3.1.1 Cloning strategy

3.1.1.1 Amplification of a gene of interest

Reverse transcription PCR (RT-PCR)

The RT-PCR method is used to translate RNA to its DNA complement (complementary DNA, or cDNA) by using the enzyme reverse transcriptase. The cDNA is then amplified using a traditional PCR with a DNA polymerase. Three different types of primers could be used for the RT-step: random primers, oligo (dT) primers or gene specific primers.

There are two ways to perform a RT-PCR, first the RT-step could be performed in the same reaction tube like the following PCR-step (one-step RT-PCR). On the other hand, the PCR-step could be performed in another reaction tube (two-step RT-PCR).

DNA amplification (PCR)

To generate a DNA insert for cloning into a specific vector, the gene of interest must be amplified by using PCR. It is recommended to use a DNA polymerase, which possesses a proofreading ability, like *Pfu* or *Pfx* polymerases. The used primer pair must include restriction sites, which are required for the later digestion of the DNA insert and the cloning vector. The resulting DNA fragment contains specific restriction sites on both ends.

3.1.1.2 DNA recovery from agarose gels

Following the DNA amplification step, the PCR reaction was loaded on a 0,8 % agarose gel and electrophoretic separated. DNA fragments of interest were excised and recovered from the

gel by using the NucleoTrap Gel Extract Kit (Macherey & Nagel) following the manufacturers instructions.

3.1.1.3 DNA digestion

The cloning vector and the DNA fragment, which contain specific restriction sites, were incubated with restriction endonucleases (NEB) following the manufacturers instructions. Correct digestion was verified by agarose gel electrophoresis. The DNA fragment and the cloning vector were then recovered from the gel by using the NucleoTrap Gel Extract Kit (Macherey & Nagel).

3.1.1.4 Ligation

After generation and purification of DNA insert and cloning vector, both were eluted together in 1x T4 ligase buffer and T4 DNA ligase (NEB). The optimal molar ratio between insert and vector should be 3:1 to maximize the ligation rate. The optimal temperature for the T4 ligase is 16 °C. The ligation reaction was performed over night and the total reaction was used for transformation in competent cells.

3.1.1.5 Transformation

Transformation is the process of uptake of exogenous plasmid DNA into a bacterium. Bacteria that are capable of being transformed are called competent. Competent cells are prepared by treatment with rubidium chloride (RbCl). Cells are treated with a hypotonic solution containing RbCl. It increases the ability of a prokaryotic cell to incorporate plasmid DNA allowing them to be genetically transformed. The addition of rubidium chloride to a cell suspension promotes the binding of plasmid DNA to the cell surface, which can then pass into the cell.

The ligation reaction (see 3.1.1.4) was added to 100 µl competent *E. coli* (NEB10ß) cells, previously thawed on ice, gently mixed and incubated on ice for further 40 minutes. Afterwards, cells were heat shocked for 90 seconds at 42 °C and chilled on ice for 3 minutes. 500 µl LB was added and the cells were incubated under shaking for 1 hour at 37 °C. Subsequently, cells were harvested by centrifugation at 4000 rpm for 3 minutes at room temperature. The supernatant was discarded and the pellet was resolved in 150 µl H_2O. 50 and 100 µl were

plated out on LB agar plates containing the appropriate antibiotic. Plates were incubated overnight at 37 °C.

3.1.1.6 DNA purification

For subsequent plasmid purification, transformed *E. coli* clones were picked from the LB agar plate and inoculated over night in LB supplemented with the appropriate antibiotic at 37 °C with shaking. Finally, cells were pelleted and plasmid DNA was isolated employing the Plasmid Mini Kit or the Plasmid Maxi Kit (Qiagen). To verify the correct insertion of the DNA into the specific vector an average of 10 clones were picked and inoculated to perform a plasmid mini DNA preparation of each clone. The purified DNA was digested with the particular restriction enzymes, which are used for the cloning. The digested DNA was loaded on a 0,8 % agarose gel to verify the correct insert. The positive clone could than be used to perform a maxi DNA preparation.

3.1.1.7 Sequencing

DNA plasmids were sequenced by Eurofins MWG/Operon (Ebersberg)

3.1.2 Constructs designed for this study

pEGFP-N3-hs-Arf1 The hs-Arf1 (NCBI ID: NM_001024227.1) cDNA was generated by using mRNA from human cerebellum (kindly provided by the Institute of Pathology, University Hospital Regensburg). The Qiagen OneStep RT-PCR Kit was used. The PCR-fragment (546 bp) was digested with KpnI/BamHI and cloned into pEGFP-N3 linearized with KpnI/BamHI. The sequence was confirmed by DNA sequence analysis at MWG. Due to the fact, that Arf proteins are modified at their N-terminus it is recommended to use a C-terminally located tag. Therefore the pEGFP-N3 vector was used.

pEGFP-C1-hs-Rab11-FIP2 The Rab11-FIP2 cDNA (NCBI ID: NM_014904) was generated by employing human cerebellum mRNA. The Qiagen OneStep RT-PCR Kit was used. The RT-PCR-fragment (1539 bp) was digested with EcoRI/BamHI and cloned into pEGFP-C1 linearized with EcoRI/BamHI. Using the pEGFP-C1 vector the Rab11-FIP2 protein will be N-terminally tagged.

mStrawberry-hs-MyoVb-cc-tail The hs-MyoVb-cc-tail sequence (NCBI ID: NM_001080467) was subcloned from the pFAST -BacHT-A M5BHMM vector (kindly provided by Mitsuo Ikebe) into the mStrawberry vector. The used mStrawberry vector has a pEGFP-C2 backbone, in which the eGFP sequence is substituted against the strawberry sequence (the mStrawberry-Rab6a vector was kindly provided by Anna Akhmanova). The PCR-fragment (3820 bp) digested with HindIII/XbaI cloned into mStrawberry-Rab6a linearized with HindIII/XbaI. Using the pEGFP-C2 vector the MyoVb-cc-tail protein will be N-terminally tagged.

pcDNA3-Myc-hs-Spir-2-ΔKW The hs-Spir-2-ΔKW sequence (NCBI ID: AJ422077.1) was subcloned from the pcDNA3 -Myc-hs-Spir-2 vector into the pcDNA3 vector (Invitrogen). To add a Myc-epitope tag on the hs-Spir-2-ΔKW sequence the 5' primer contains the Myc epitope sequence. The PCR-fragment (1060 bp) was digested with BamHI/EcoRV cloned into pcDNA3 linearized with BamHI/EcoRV. Using the pcDNA3 vector the Spir-2 protein will be N-terminally tagged.

pGEX-4T-3-hs-Spir-2-ΔKW The hs-Spir-2-ΔKW sequence was subcloned from the pProEX HTb-hs-Spir-2-ΔKW vector. The hs-Spir-2-ΔKW insert was digested from pProEX HTb-hs-Spir-2-ΔKW by using BamHI/XhoI and cloned into pGEX-4T-3 linearized with BamHI/ XhoI. The GST-tag will be at the N-terminus of the Spir-2 protein.

pProEX HTb-mm-Spir-1-ΔKW The Spir-1-ΔKW cDNA (NCBI ID: NM_176832) was generated by employing mouse brain mRNA. The Qiagen OneStep RT-PCR Kit was used. The RT-PCR-fragment (1068 bp) digested with NcoI/XhoI cloned into pProEX HTb linearized with NcoI/XhoI. Using the pProEX HTb vector the Spir-1 protein will be N-terminally tagged. Supplemental table II summarizes the individual constructs, provides a description of the fragment boundaries and their purpose.

3.2 Protein Biochemical Methods

3.2.1 Electrophoretic protein separation

Polyacrylamide gel electrophoresis (PAGE) is used to separate proteins according to their electrophoretic mobility. Due to the fact that proteins are amphoteric compounds, their net

charge is determined by the pH of the solution. Throughout the course of this work protein samples were separated under denaturing conditions by using the anionic detergent sodium dodecyl sulfate (SDS). SDS disrupts the secondary and tertiary structure and confers a negative charge to the polypeptides in proportion to their length.

Protein samples were loaded on a discontinuous system, in which the tank and gel buffers are different from each other. A non-restrictive large-pore gel, called a stacking gel, overlays a smaller pore resolving gel. Prior to loading, protein samples were boiled in 1x- or 5x SDS sample buffer for 6 minutes at 95 °C. Protein sizes were analyzed using the prestained Protein Ladder (Bio-Rad) as a molecular mass marker. Electrophoresis was performed at 45 mA at room temperature until the bromophenol blue dye reached the bottom of the gel.

To stain protein bands directly after the separation via SDS-PAGE, Coomassie staining solution was used. The acrylamide gel was boiled in Coomassie staining solution for 1-2 minutes. After that, the gel was boiled 3-4 times in H_2O dest. and washed with H_2O dest. by gently agitation.

3.2.2 Western Blot and immunodetection

Separated proteins were transferred to a nitrocellulose membrane by electroblotting using a Sigma blotting tank. The transfer was performed for 1,5 hours at 150 mA at room temperature in Western blotting buffer. To verify the protein transfer the nitrocellulose was stained with Ponceau S solution (Sigma-Aldrich). The nitrocellulose was incubated in Ponceau S solution for 2 minutes at room temperature and washed with H_2O 3-5 times with shaking. To destain the nitrocellulose, PBST was used.

For immunodetection the nitrocellulose membrane was blocked in 5 % milk solution over night at 4 °C. After blocking the nitrocellulose was incubated in milk solution containing the particular primary antibody for 1-2 hours. Adjacent to the incubation with the primary antibody, the nitrocellulose was washed three times with PBST at room temperature with shaking for ten minutes. Subsequently, the nitrocellulose was incubated in a milk solution/PBST solution (1:3 ratio) containing the secondary horseradish peroxidase (HRP)-linked antibody for 30-45 minutes at room temperature with shaking. After the second antibody incubation step the nitrocellulose was washed three times for ten minutes at room temperature. Finally, the HRP-coupled secondary antibody was detected with an ECL reagent kit (enhanced chemo-

luminescence, Amersham). The light signal was detected by autoradiography using a x-ray film.

3.2.3 Western Blot stripping

Membrane stripping is the removal of antibodies (including primary and secondary) from a western blot membrane, to allow the further incubation of the membrane with other primary and secondary antibodies.

The membrane was incubated with prewarmed 50 ml Stripping buffer (ß-mercaptoethanol was freshly added) at 60 °C for 15 minutes. That incubation step was repeated 3 times. After the third incubation, the membrane was washed with PBST four times for 10 minutes at room temperature.

3.2.4 Protein expression in prokaryotes

For the expression of recombinant proteins, the *E. coli* strain Rosetta (Novagen) was used. The Rosetta strain contains a pRARE plasmid (chloramphenicol resistence) coding for tRNAs of the rarely used codons Arginine, Isoleucine, Glycine, Leucine and Proline, resulting in an increased protein expression rate. Protein expression is under the control of the lacZ promotor and is induced by the lactose analog isopropyl-β-D-thio-galactoside (IPTG). IPTG binds to the repressor and inactivates it, but is not a substrate for β-galactosidase. As it is not metabolized by *E. coli*, its concentration remains constant. Therefore the expression rate of the recombinant protein is also constant.

3.2.5 Ni-NTA based purification of 6xHis-tagged recombinant proteins

6xHis-tagged proteins could efficiently be purified by using nickel-nitrilotriacetic acid (Ni-NTA) metal-affinity chromatography matrices. The histidine residues of the recombinant protein of interest bind specific to the Ni-NTA matrix allowing the purification of proteins from bacterial lysates and the accumulation of these proteins in a large scale. For the expression of 6xHis-tagged proteins the pProEX HTb vector system was used. The 6xHis-tag is added to the N-terminus of the specific protein.

Procedure for 500 ml of a bacterial culture:

- Culture growth:

  50 ml of LB medium containing 10 % ampicillin (1:1000) and chloramphenicol (34 mg/ml) (1:1000) were inoculated over night at 37 ºC with continuous shaking. At the next day 500 ml of LB medium containg 10 % ampicillin (1:1000) and chloramphenicol (34 mg/ml) (1:1000) were inoculated 1:10 with the noninduced overnight culture. The culture grew at 37 ºC with shaking until an OD_{600} of 0,5 was reached. The temperature was lowered to 21 - 25 ºC and after on OD_{600} of 0,6 was reached the expression was induced by adding IPTG to a final concentration of 0,1 mM. The culture was incubated overnight at 21 - 25 ºC. One 500 µl sample was taken immediately before the induction (noninduced control t0), whereas another 500 µl sample was taken 2 hours after the induction and at the second day (induced control tI). The cells were harvested by centrifugation (Beckman Coulter; Avanti J26XP -> JA14 rotor) at 13000 rpm, 30 minutes, 4 ºC and pellets were frozen at -20 ºC.

- Protein extraction:

  The cell pellet was thawed on ice and resuspended in lysis buffer at 2-5 ml per gram wet weight. The cell lysate was sonificated 16x 10 seconds 80-100 % and centrifuged (Beckman Coulter; Avanti J26XP -> JA25.50 rotor) at 15000 rpm at 4 ºC for 30 minutes. The cleared lysate was saved and a sample of 40 µl was taken (soluble protein fraction). The pellet was resuspended in 5-10 ml lysis buffer and 20 µl were taken for the insoluble protein control (pellet). Proteins were purified by using a batch purification method under non-denaturing conditions. Ni-NTA beads (Qiagen) were washed two times with washing buffer and added to the cleared lysate. The cleared lysate and the Ni-NTA agarose beads were then rotated for 1-2 hours at 4 ºC on a rotator. Two additional controls were taken to control the binding of the 6xHis-tagged protein to the Ni-NTA matrix. After 1 hour and after 2 hours 40 µl of the cleared lysate was taken (flowthrough) After the binding of the 6xHis-tagged protein on the Ni-NTA matrix, the cleared lysate was washed three times with washing buffer (1 minute, 2000 rpm, 4 ºC). For reducing the unspecific binding of other His-containing proteins on the Ni-NTA agarose beads one washing step with 50 mM imidazole was performed. The 6xHis-tagged protein was then eluted in 1 ml elution buffer. One control sample was taken before elution from the Ni-NTA agarose beads to further test the protein binding to the matrix (tb). A second

control sample was taken after elution to check that the protein was completely eluted from the matrix (tb after elution). As a final control a sample of 30 µl was taken from the eluted fraction. All samples were boiled in 1x- or 5x SDS sample buffer at 95 ºC for 6 minutes and analyzed by SDS-PAGE.

3.2.6 Glutathione based purification of GST-tagged recombinant proteins

Glutathione-S-transferase (GST) binds to glutathione with high affinity and specificity. GST-tagged proteins can then be purified by using immobilized glutathione (glutathione sepharose). The purification was performed under non-denaturing conditions, because GST loses its ability to bind glutathione under denaturing conditions. For the bacterial expression of the protein of interest, the pGEX-4T-3 vector was used.

Procedure for a 500 ml bacterial culture:

- Culture growth:

  50 ml of LB Medium containing 10 % ampicillin (1:1000) and chloramphenicol (34 mg/ml) (1:1000) were inoculated over night at 37 ºC with continuous shaking. At the next day 500 ml of LB medium supplemented with 10 % ampicillin (1:1000) and chloramphenicol (34 mg/ml) (1:1000) were inoculated with the noninduced overnight culture (1:10). The culture grew at 37 ºC with shaking (160 rpm) until an OD_{600} of 0,5 was reached. The temperature was lowered to 21 ºC and after an OD_{600} of 0,6 was reached the expression was induced by adding IPTG to a final concentration of 0,1 mM. The culture was incubated overnight at 21 ºC. One 500 µl sample was taken immediatly before the induction (noninduced control t0), whereas another 500 µl sample was taken after the induction at the second day (induced control tI). The cells were harvested by centrifugation (Beckman Coulter; Avanti J26XP -> JA14 rotor) at 13000 rpm, 30 minutes, 4 ºC and pellets were frozen at -20 ºC.

- Protein extraction:

  The cell pellet was thawed on ice and resuspended in TBST at 2-5 ml per gram wet weight. The cell lysate was sonificated 16x 10 seconds 80-100 % and centrifuged (Beckman Coulter; Avanti J26XP -> JA25.50 rotor) at 15000 rpm at 4 ºC for 30 minutes. The cleared lysate was saved and a sample of 40 µl was taken (soluble protein fraction).

The pellet was resuspended in 5-10 ml TBST and 20 µl were taken for the insoluble protein control (pellet). Proteins were purified by using a batch purification method under non-denaturing conditions. Glutathion sepharose 4b beadsolution was washed three times with TBST and added to the supernatant. The supernatant and the glutathion sepharose beads were then rotated for 2 hours at 4 ^{o}C on a rotator. After the binding of the GST-tagged protein on the glutathion sepharose matrix the supernatant was washed three times with TBST (1 minute, 2000 rpm, 4 ^{o}C). All samples were boiled in 1x- or 5x SDS sample buffer at 95 ^{o}C for 6 minutes and analyzed by SDS-PAGE.

- Elution of the GST protein and the GST-tagged protein (for protein-lipid overlay assays)

  The GST protein respectively the GST-tagged protein bound to the GST-sepharose were incubated two times in 200 µl GST elution buffer at 4 ^{o}C on a rotator. The protein eluat was dialyzed over night in 1,5 l TBST at 4 ^{o}C by using Slide-A-Lyzer Dialysis cassettes (10000 MWCO) (ThermoScientific).

3.2.7 Protein-lipid overlay assay

By using a protein-lipid overlay assay potential protein-phospholipid interactions can be identified. Different phospholipid species are spotted on a membrane. That so-called PIP strip can than be incubated with purified GST- or 6xHis-tagged proteins. Phospholipid bound proteins can be detected with an antibody against the GST or the 6xHis tag and a secondary HRP-conjugated antibody. Finally, the HRP-linked antibody was detected by using an ECL reagent kit (enhanced chemiluminescence Amersham). The light signal was detected by autoradiography using a x-ray film.

Protein-lipid overlay assays were performed by using PIP strips from Invitrogen.

3.2.7.1 Experimental procedure

1. Block the membrane. The membrane was incubated for one hour at room temperature in TBST + 3% BSA with gently agitation.

2. Incubate the membrane. The membrane was incubated for 4 hours at room temperature with the protein of interest in TBST/3 % BSA.

3. Wash the membrane. The membrane was washed with TBST/3 % BSA three times using gently agitation at room temperature for 10 minutes each time.

4. Detect the protein. The membrane was blocked in TBST/5 % milk powder over night at 4 ºC. GST and GST-tagged proteins were detected by using an anti-GST antibody and a secondary HRP-conjugated anti goat antibody. 6xHis-tagged proteins were detected by using a penta-His antibody and a secondary HRP-conjugated anti mouse antibody.

3.3 Protein-Protein Interaction studies

3.3.1 Co-immunoprecipitation

Immunoprecipitation (IP) is used to isolate and concentrate a specific protein from a solution by using an antibody that specifically binds to that protein. The antibody is coupled to a solid substrate during the process of binding to the target protein. Immunoprecipitation of intact protein complexes is known as co-immunoprecipitation (Co-IP). Co-IP works by using an antibody that targets a known protein that is believed to be a member of a larger complex of proteins. By targeting this known member with an antibody it may become possible to pull the entire protein complex out of solution and thereby identify unknown members of the complex. Co-immunoprecipitations can be performed to determine if protein-protein interactions are occurring *in vivo*. Consequently, any cellular protein that interacts with the target protein will also be pulled out.

Throughout the course of this work N-terminally Myc-epitope tagged proteins were used. The Myc-epitope tagged protein acts as the "bait" to capture a putative binding partner (i.e., the "prey"). The putative binding partner was an eGFP- or mStrawberry-tagged fusion protein. To immunoprecipitate the “bait” from the cell lysate, an anti-Myc 9E10 antibody was used. The Myc-epitope tagged “bait” protein bound to the anti-Myc 9E10 antibody was then immobilized by binding to Protein-G-Agarose. Protein G binds the Fc-parts of most mammalian IgGs with high affinity.

Procedure

HEK 293 cells were seeded in four, with 10 % Poly-L-lysine solution coated, wells of a 6-well-plate. Cells were cotransfected with the Myc-epitope tagged protein and the eGFP- or mStrawberry-tagged protein. Cells were lysed after 48 hours in co-immunoprecipitation buffer (1 ml per 3 wells) with or without EDTA at 4 ^{o}C under rotation for 40 minutes. One well was lysed in 100 µl 1x SDS sample buffer and used as a control sample (total). The co-immunoprecipitation buffer was supplemented with Protease Inhibitors (complete, Mini, EDTA-free Protease Inhibitor Cocktail tablets; Roche). One tablet was used per 10 ml co-immunoprecipitation buffer. After centrifugation of the cell lysate (10 minutes, 4 ^{o}C, 14000 rpm) samples were taken from the supernatant and the pellet fraction. The Myc-epitope tagged protein was pulled with an anti-Myc 9E10 antibody (4 µg/ml). The anti-Myc 9E10 antibody was added and the cleared cell lysates were incubated at 4 ^{o}C for 1 hour. 50 µl Proteine-G-Agarose, earlier washed 3x with co-immunoprecipitation buffer, was added to the cell lysates and incubated at 4 ^{o}C for 2 hours under rotation. After 3 washing steps with co-immunoprecipitation buffer Proteine-G-Agarose beads were boiled in 30 µl 1x SDS sample buffer. Additionally, two controls were performed. First, HEK 293 cells were transfected with the Myc-epitope tagged protein and an empty pEGFP- or mStrawberry vector, to ensure that the binding doesn't depend on the eGFP- or mStrawberry-tag. Second, HEK 293 cells were only transfected with the eGFP- or mStrawberry-tagged protein, to show that the protein doesn't stick to the Protein-G-Agarose beads. All samples were boiled in 1x- or 5x SDS-sample buffer for 6 minutes at 95 ^{o}C and analyzed by SDS-PAGE.

3.3.2 Pull down assay with purified 6xHis-tagged and GST-tagged recombinant proteins

A pull down assay is a technique used to analyze protein-protein interaction. Throughout the course of this work a GST-pull down assay was performed. The "bait" protein was fused to a GST-tag, whereas the "prey", the putative binding partner, was fused to a 6xHis-tag. Both proteins were expressed in *E. coli* / Rosettas and purified. The GST-tagged protein bound to GST-beads were therefore incubated with the eluted 6xHis-tagged protein. As a control, GST bound to GST-beads were also incubated with the 6xHis-tagged protein to exclude that binding depends on the GST tag.

Procedure

The purified and eluted 6xHis-tagged protein was dialyzed over night in 1,5 l of pull down buffer at 4 ^{o}C by using a Slide-A-Lyzer Dialysis cassette (10000 MWCO) (ThermoScientific). To avoid unspecific binding to the GST-beads the eluted fraction of the 6xHis-tagged protein was preincubated with 100 µl GST-beads per 1 ml eluat for 30 minutes at 4 ^{o}C on a rotator. After that preincubation step the GST-beads/eluat was centrifuged at 4 ^{o}C for 5 minutes (14000 rpm). The supernatant was then used for the incubation with the GST-tagged protein bound to GST-beads or the GST protein as a control. Proteins were incubated for 1 hour on a rotator at 4 ^{o}C. After the binding step GST-beads were washed 5 times with pull down buffer (5 minute rotation at 4 ^{o}C; 5 minute centrifugation at 4 ^{o}C at 500 g). GST-beads were boiled in 30 µl 1x SDS sample buffer for 6 minutes at 95 ^{o}C. All samples were analyzed by SDS-PAGE.

3.4 Cell Biological Methods

3.4.1 Cell culture

HeLa, HEK 293 and MDCK cells were cultured in Dulbecco's modified Eagle's medium (DMEM, Invitrogen) supplemented with 10 % fetal calf serum (FCS; HyClone), 2 mM L-glutamate (Glu), and 100 units/ml penicillin and 100 µg/ml streptomycin at 37 ^{o}C and 10% CO_2.

3.4.2 Coating of 6-well plates with Poly-L-lysine

Poly-L-lysine coated 6-well plates provide higher adhesion, resulting in the reduced loss of cells during processing. Wells were incubated in 10 % Poly-L-lysine solution in H_2O dest. for 5 minutes at room temperature. Afterwards, the 10 % Poly-L-lysine solution was removed and wells were leave to dry. Finally, the 6-well plates were washed 3 times with PBS.

3.4.3 Establishing a stable cell line

Throughout the course of this work a stable constitutively expressing MDCK-Myc-Spir-2 cell line has been used. To deliver the exogenous Myc-epitope tagged Spir-2 into MDCK cells,

the pBABE-puro vector was used. This vector provides retrovirus sequences for the stable insertion and expression of exogenous genes. This cell line was already available and was used for further analysis.

3.4.4 Transfection

Cells were transfected with Lipofectamine according to the manufacturer's recommendations. Cells were seeded approximately 20 hours before transfection in DMEM full medium (10 % FCS, Pen/Strep, L-Glu). At the day of transfection the cells reached a confluency of 80-90 %. 6 µl of Lipofectamine were incubated with 1,4 - 2,0 µg of DNA in DMEM without FCS, Pen/Strep, L-Glu for 20 minutes and added to the cells. After 5-6 hours the medium was changed to DMEM containing FCS, Pen/Strep and L-Glu. Cells were allowed to express proteins for 20 - 48 hours.

3.4.5 Immunocytochemistry

HeLa cells were seeded on glass coverslips (15 mm diameter) in 6-well plates. The cells were transfected with the indicated plasmid vectors by a liposome transfection method (Lipofectamine, Invitrogen) at the next day. 24-36 hours after transfection the cells were fixed with 3,7 % paraformaldehyde in PBS (20 minutes, 4 ^{o}C) and permeabilized with 0,2 % Triton X-100 in PBS (3 1/2 minutes, room temperature). For immunodetection, the fixed cells were incubated for 1 hour in the presence of the indicated primary antibody, followed by three washing steps with PBS. After the incubation with the indicated secondary antibody for 1 hour, cells were washed 3 times with PBS and were mounted in a Mowiol solution.

The cells were analyzed with a Leica AF600LX imaging system equipped with a Leica HCX PL APO63X/1.30 glycerol objective and a Leica DFC350FX camera. For colocalization studies, images were deconvoluted (blind) with the deconvolution software from Leica (Leica Application Suite Advanced Flourescense) and further processed with ImageJ or Adobe Photoshop to optimize the contrast and brightness.

3.4.5.1 Detection of endogenous F-actin using Phalloidin

The phallotoxin phalloidin from death cap (*Amanita phalloides*) binds to F-actin and prevents its depolymerization leading to a decreased dissociation of actin monomers from F-actin.

Furthermore it inhibits ATP hydrolysis activity (Cooper, 1987, Barden et al., 1987). The specific binding to F-actin can be used to stain endogenous F-actin in immunocytochemical experiments. In this study endogenous F-actin in HeLa cells was detected with rhodamine-conjugated phalloidin (Molecular Probes) at a 1:20 dilution. Fixed cells were incubated for 1 hour in the presence of the indicated primary antibody and rhodamine-phalloidin, followed by three washing steps with PBS. After the incubation with the indicated secondary antibody for 1 hour, cells were washed 3 times with PBS and were mounted in mowiol solution.

3.4.6 Live cell imaging

HeLa cells were seeded on Willco glass bottom dishes. The cells were transfected at the next day and assayed 24-36 hours after transfection. The cells were analyzed with a Leica AF600LX imaging system (see 3.4.5 Immunocytochemistry).

3.4.6.1 Comparison of vesicle length and motility

Comparison of vesicle length

To measure and compare the length of different Spir-2 versions, HeLa cells were transiently transfected with eGFP-Spir-2, eGFP-Spir-2-ΔKW and eGFP-Spir-2-ΔKIND (Fig. 4.3) and used for live cell imaging experiments. 5 cells were imaged, and a total of 100 vesicles were measured of each Spir-2 protein version. Length of the vesicles was determined with the software from Leica (Leica Application Suite Advanced Flourescense).

To analyze the impact of Spir-2 and Spir-2-ΔKW on Rab11a-associated vesicles, HeLa cells were transfected with mStrawberry-Rab11a, mStrawberry-Rab11a + eGFP-Spir-2 and mStrawberry-Rab11a + eGFP-Spir-2-ΔKW. 3 cells were measured and a total of 100 vesicles were measured of each transfection.

Analogous to the effect of Spir-2 on Rab11a vesicles, Spir-2 has also an effect on myosin Vb- associated vesicles. To analyze the alteration of MyoVb-cc-tail-positive structures, HeLa cells were transfected with mStrawberry-MyoVb-cc-tail, mStrawberry-MyoVb-cc-tail + eGFP-Spir-2 and mStrawberry-MyoVb-cc-tail + eGFP-Spir-2-ΔKW. 4-5 cells were compared and a total of 100 vesicles were measured of each transfection.

Comparison of vesicle motility

To analyze the vesicle motility of eGFP-Spir-2, eGFP-Spir-2-ΔKW and eGFP-Spir-2-ΔKIND associated vesicles, time-lapse movies were made, by taking a picture every 2 seconds for one minute (31 pictures in total). To calculate the motility rate, 5 cells of each transfection were segmented in squares of 2,5 μm^2 size and the retention time of 20 vesicles per cell was measured.

3.4.6.2 Treatment of living HeLa cells with nocodazole

Nocodazole disrupts microtubules by promoting their depolymerization. To analyze the effect of microtubule depolymerization by nocodazole, transfected living HeLa cells were filmed for 1 minute before treatment with nocodazole. Cells were treated with 20 mM nocodazole in DMEM full medium with 20 mM 4-(2-hydroxyethyl)-1-piperazineethanesulfonic acid (HEPES). Another time-lapse movie was made after 30 minutes from the same cells. All movies were made by taking a picture every 2 seconds for one minute.

4 *RESULTS*

4.1 Aim of the work

Spir proteins are targeted towards intracellular membranes by a C-terminal modified FYVE zinc finger motif. Although a role for Spir-1 in vesicle transport processes of the exocytic pathway (Kerkhoff et al., 2001) and the transport beyond early endosomes (Morel et al., 2009) has been described, the function and regulation of the actin organizers at vesicular membranes is unknown. In the course of this work the role of the actin nucleation factor Spir-2 in intracellular vesicle transport processes was analyzed. The objective was to examine the recruitment of Spir-2 to specific membranes, to identify factors, which are important for Spir-2 targeting and to study the effect of Spir-2 deletion mutants on specific intracellular membrane compartments. The C-terminal part of Spir-2, consisting of the Spir-box and the modified FYVE zinc finger was analyzed with particular interest, assuming that this part of the protein is crucial for the membrane targeting and therefore for the function of Spir proteins in vesicle transport processes. Furthermore, the influence of the actin and the microtubule cytoskeleton on Spir-2 mediated vesicle transport processes should be elucidated.

4.2 Cellular localization of Spir-2

4.2.1 Spir-2 is located at tubular vesicular structures

To analyze the cellular localization of Spir-2 in HeLa cells, N-terminally eGFP-, and Myc-epitope tagged proteins were used. EGFP-Spir-2 and two truncated versions of Spir-2, Spir-2-ΔKW, in which the KIND domain and the 4 WH2 domains are deleted, and Spir-2-ΔKIND, were used for live cell imaging and immunofluorescence experiments (Fig. 4.1). To exclude, that the N-terminal tag alters the localization of Spir-2, eGFP-Spir-2-ΔKW and Myc-Spir-

2-ΔKW constructs were coexpressed in HeLa cells. Cells were fixed and the Myc-epitope tagged Spir-2-ΔKW protein was detected by using the anti-Myc 9E10 mouse monoclonal antibody (1,3 µg/ml, Santa Cruz) and a rhodamine isothiocyanate (TRITC)-conjugated donkey anti-mouse IgG secondary antibody (5 µg/ml) (Jackson ImmunoResearch Laboratories). An identical localization pattern was observed, supporting the fact that both tags don't modify the subcellular localization (Fig. 4.2).

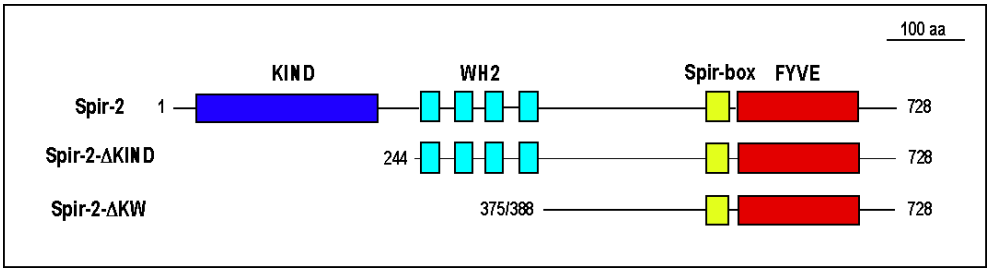

Figure 4.1: **Domain structure of the Spir-2 protein and two deletion constructs**

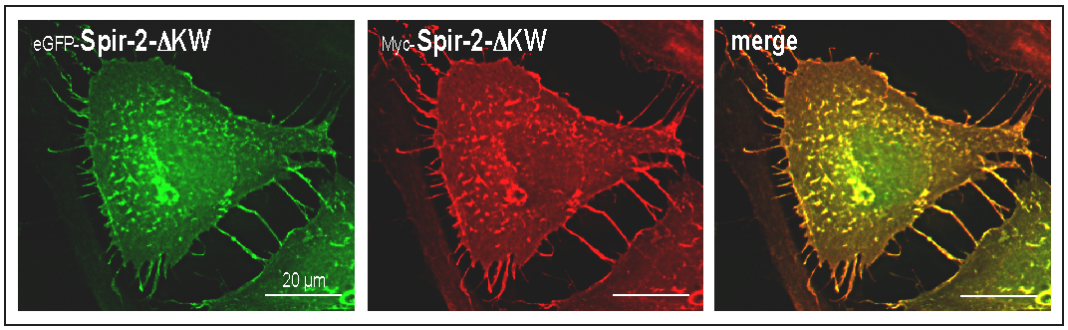

Figure 4.2: **Localization of Spir-2-ΔKW proteins**
HeLa cells were cotransfected with Myc-Spir-2-ΔKW and eGFP-Spir-2-ΔKW. The cellular localization of the Myc-Spir-2-ΔKW protein was determined by immunostain experiments (red fluorescence). The localization of eGFP-Spir-2-ΔKW was detected by GFP fluorescence (green fluorescence). Images were deconvoluted (blind) with the deconvolution software from Leica. They show an identical localization pattern, indicating that both tags don't change the subcellular localization.

To analyze the length and motility of Spir-2, Spir-2-ΔKW and Spir-2-ΔKIND-associated vesicles, live cell imaging experiments were performed. The different Spir-2 protein versions are all located to elongated tubular structures (Fig. 4.3). The comparison of the vesicle length, revealed that Spir-2 and Spir-2-ΔKIND-associated vesicles are very similar regarding their length. By comparison, Spir-2-ΔKW-associated vesicles show a more elongated morphology (Fig. 4.3 C). Although, the average elongation differs only slightly, the maximum length is increased up to 9 µm.

Furthermore, the motility of those three Spir-2 versions was compared in live cell imaging experiments. HeLa cells were transiently transfected with Spir-2, Spir-2-ΔKIND and Spir-2-ΔKW and one minute time-lapse movies were made, by taking a picture every 2 seconds. 100 vesicles of 5 cells per Spir-2 version were analyzed, regarding their vesicle retention time. Spir-2-ΔKIND-associated vesicles displayed a static behavior. In most cases, the vesicles exhibit the maximal retention time of 60 seconds. In contrast, Spir-2-ΔKW and Spir-2-associated vesicles are motile (Fig. 4.3 B,D). Spir-2-ΔKW exhibits the highest rate of motility.

Spir-2-ΔKW contains the Spir-box and the modified FYVE zinc finger motif, which is crucial for the membrane targeting of Spir proteins. Therefore, most experiments were performed with Spir-2-ΔKW to analyze the function of the C-terminus of Spir-2 in vesicle transport processes under the assumption that the C-terminal part without the 4 WH2-domains and the KIND domain is sufficient for the correct membrane targeting.

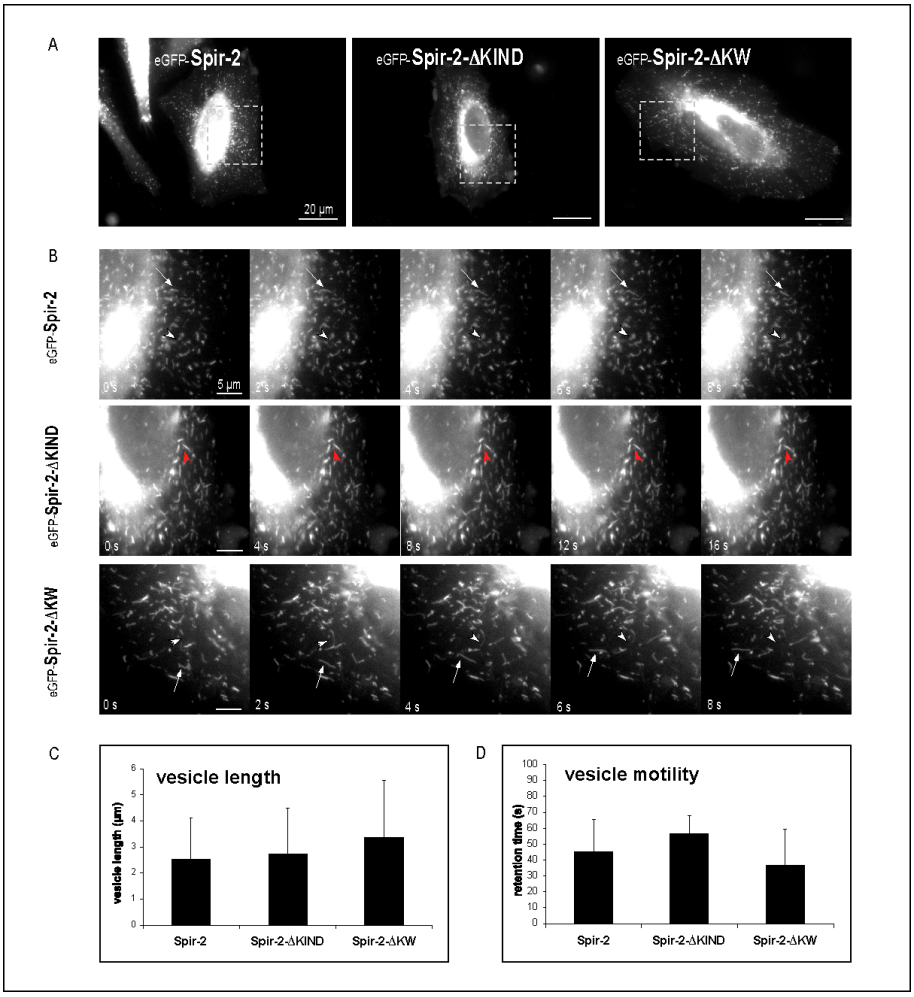

Figure 4.3: **Spir-2 proteins are found on tubular vesicular structures** Comparison of Spir-2 and two Spir-2 deletion mutants **A** Live cell imaging of HeLa cells transfected with expression vectors directing the expression of eGFP-Spir-2, eGFP-Spir-2-ΔKIND and eGFP-Spir-2-ΔKW. **B** Time-lapse movies of living HeLa cells were made by taking a picture every 2 seconds. Note that for eGFP-Spir-2 and eGFP-Spir-2-ΔKW the time interval between the shown pictures is 2 seconds, whereas for eGFP-Spir-2-ΔKIND the time interval is 4 seconds. **C** Comparison of the length of eGFP-Spir-2, eGFP-Spir-2-ΔKIND and eGFP-Spir-2-ΔKW-associated vesicles. 5 cells were imaged and a total of 100 vesicles was measured for each Spir-2 version. **D** Comparison of the motility of eGFP-Spir-2, eGFP-Spir-2-ΔKIND and eGFP-Spir-2-ΔKW-associated vesicles. 5 cells were imaged and a total of 100 vesicles was measured for each Spir-2 version. Cells were segmented in squares of 2,5 µm^2 and the retention time of 20 vesicles per cell was measured.

4.2.2 Spir-2 shows partial colocalization to Rab11a but not to Rab6a

To determine the exact subcellular localization of Spir-2, HeLa cells were cotransfected with mStrawberry-tagged Rab11a together with eGFP-tagged Spir-2 and Spir-2-ΔKW. Several tubular structures could be detected which contain both proteins (Fig. 4.4 A). Rab proteins are used as markers for specific membrane compartments and it is well known, that they function as regulators of vesicle transport processes. The fact that Spir-2 and Rab11a are present at the same motile structures support the role for Spir-2 in regulation of vesicle trafficking processes. To characterize the identity of Spir-2-positive tubular vesicles in more detail the small G protein Rab6a was used to show if Spir-2 is localized at Rab6a-positive compartments. Rab6a is localized at *medial*- and *trans*-Golgi membranes and mediates intra-Golgi transport processes, like retrograde Golgi to endoplasmic reticulum traffic (Nery et al., 2006), but also post Golgi transport of secretory vesicles to the plasma membrane (Grigoriev et al., 2007). By performing live cell imaging experiments with eGFP-Spir-2-ΔKW/mStrawberry-Rab6a transfected Hela cells it was shown that Spir-2 doesn't show colocalization to Rab6a-positive membrane structures (Fig. 4.5). This suggests, that Spir-2 regulates vesicle traffic along the Rab11 but not along the Rab6-pathway.

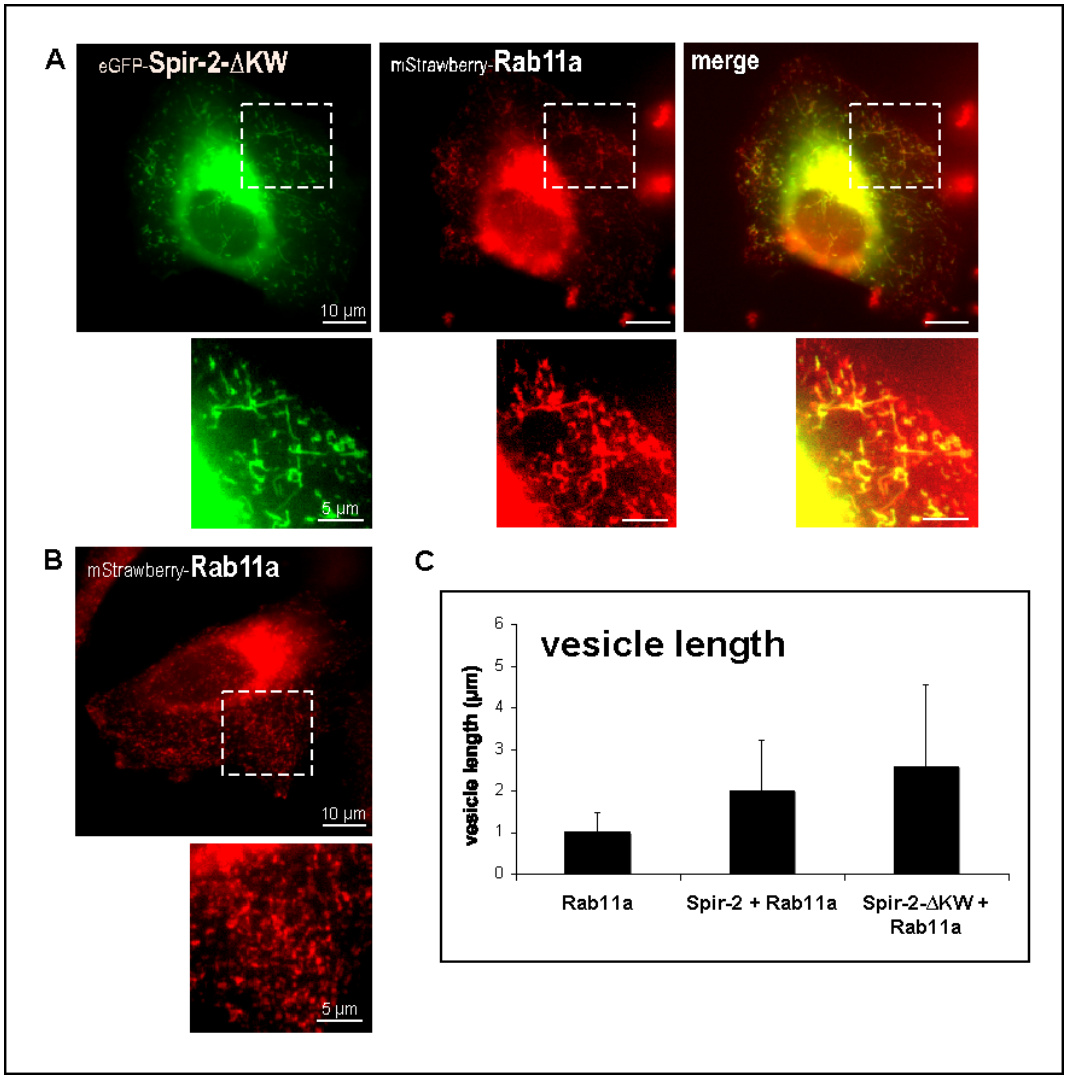

Figure 4.4: **Partial colocalization of Spir-2 and Rab11a**
Spir-2-ΔKW alters the morphology of Rab11a-positive vesicles **A** HeLa cells were cotransfected with eGFP-Spir-2-ΔKW and mStrawberry-Rab11a. The localization of both proteins were analyzed in living HeLa cells, where they show colocalization on elongated tubular vesicles. **B** HeLa cells were transfected with strawberry-Rab11a. Rab11a is located at dotlike vesicles in contrast to the elongated tubular structures in eGFP-Spir-2-ΔKW and mStrawberry-Rab11a transfected HeLa cells. **C** Comparison of the length of eGFP-Spir-2-ΔKW/mStrawberry-Rab11a-associated vesicles in **A**, with eGFP-Spir-2/mStrawberry-Rab11a-associated vesicles and mStrawberry-Rab11a-positive vesicles in **B**. 3 cells were imaged in all experiments and a total of 100 vesicles are measured for each transfection.

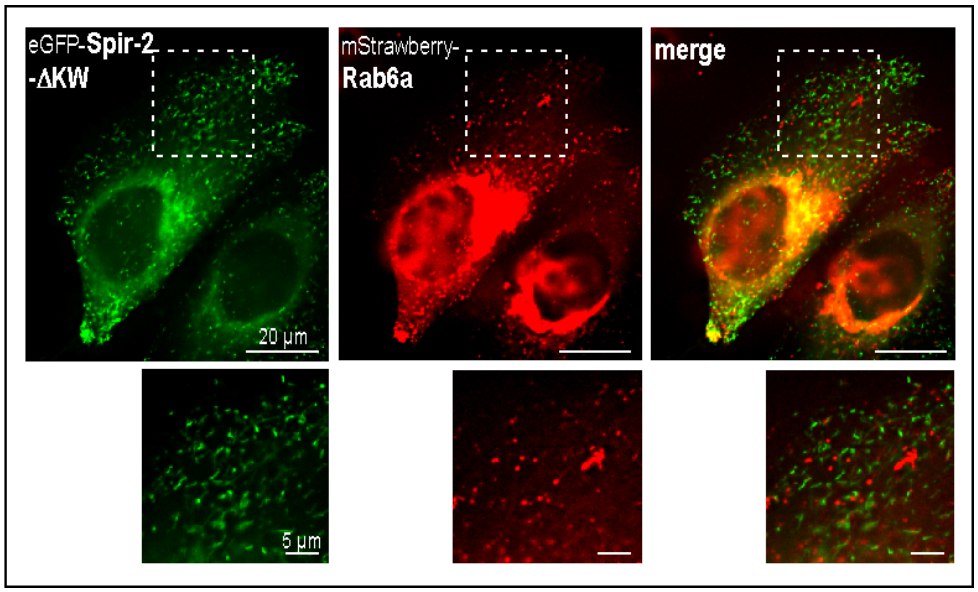

Figure 4.5: **Spir-2 shows no colocalization to Rab6a-positive compartments** HeLa cells were cotransfected with eGFP-Spir-2-ΔKW and mStrawberry-Rab6a. Living HeLa cells were imaged and the localization of both proteins was compared. Rab6a shows a different localization pattern as Spir-2-ΔKW. Rab6a-positive vesicles show no elongation, like Rab11a-associated vesicles, suggesting that Spir-2-ΔKW has no effect on Rab6a-positive compartments.

Rab11a is implicated in transport processes along the recycling pathway, but it is also localized to the TGN, involved in post Golgi secretory traffic. Furthermore, a role for Rab11a in retrograde traffic between recycling endosome and the TGN has also been shown, where it plays a role in exit of membranes from recycling endosomes (Wilcke et al., 2000). Although, Spir-2 colocalizes partially with Rab11a on intracellular membranes an interaction between Spir-2-ΔKW and Rab11a, Rab25 or Rab11-FIP2 couldn't be shown (Fig. 4.6; Fig. 4.7). Therefore, other proteins, like the GTP-binding proteins of the Arf family were analyzed with respect to their function in Spir-2 membrane recruitment.

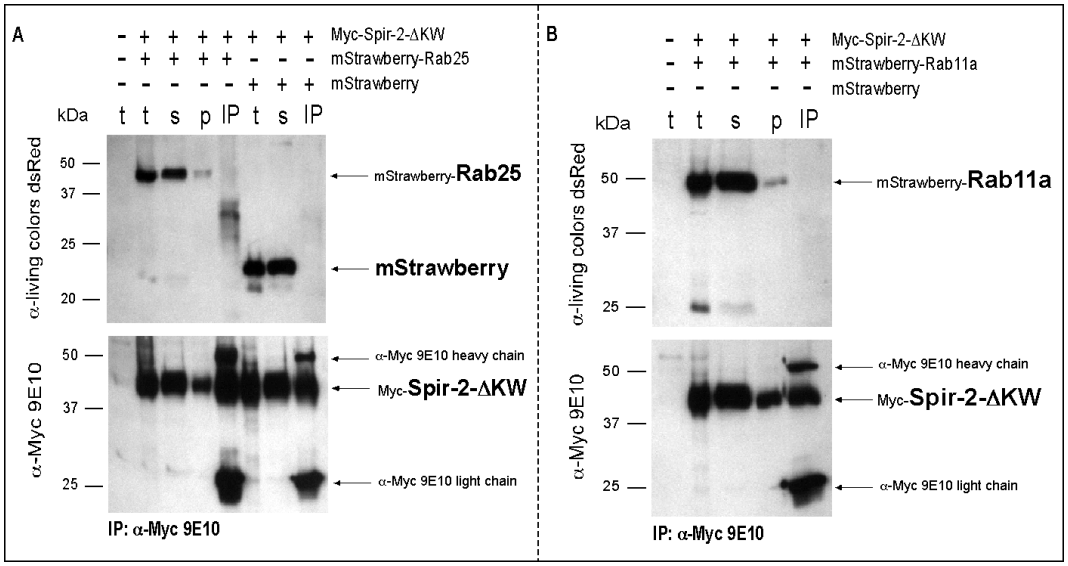

Figure 4.6: **Neither Rab11a nor Rab25 interact with Spir-2-ΔKW**
Co-IP of Myc-Spir-2-ΔKW and mStrawberry-Rab25/mStrawberry-Rab11a. Myc-Spir-2-ΔKW was pulled from a HEK 293 cell lysate using the anti-Myc 9E10 antibody (4 µg/ml). mStrawberry-Rab25 or mStrawberry-Rab11a couldn't be immunoprecipitated. The mStrawberry protein was used as a negative control. SDS-PAGE: 10% Polyacrylamide gel; Immunodetection: α-living colors dsRed (1:1000); α-rabbit-HRP (1:5000); α-Myc 9E10 (1:200); α-mouse-HRP (1:4000); Abbreviations: **kDa** kilo Dalton; **IP** immunoprecipitation; **t** total; **s** supernatant (soluble protein fraction; supernatant fraction after centrifugation at 14000 rpm); **p** pellet (insoluble protein fraction; pellet fraction after centrifugation at 14000 rpm)
This figure is representative of two separate experiments.

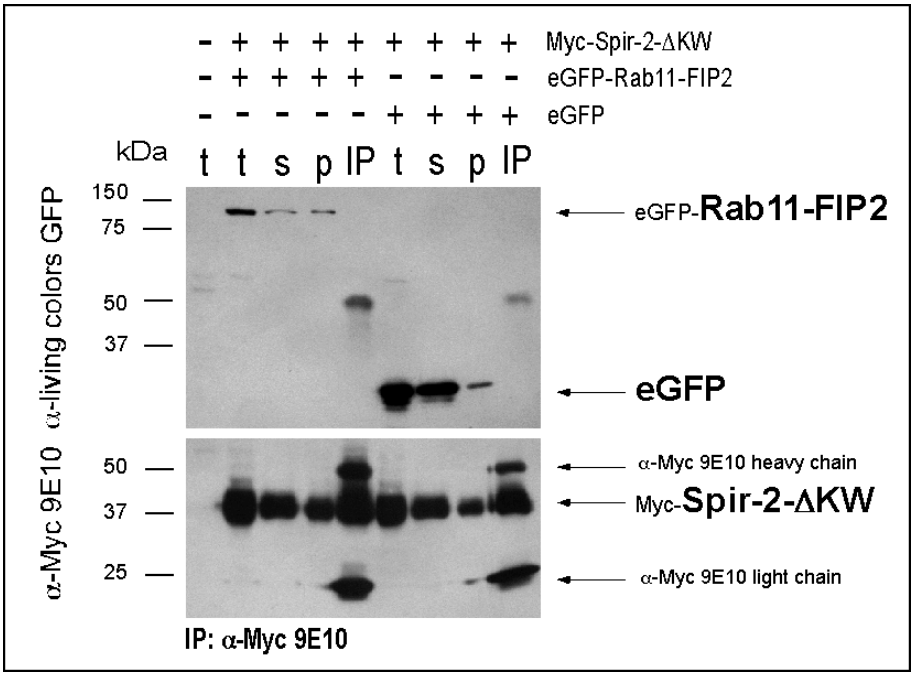

Figure 4.7: **Rab11-FIP2 doesn't interact with Spir-2-ΔKW**
Co-IP of Myc-Spir-2-ΔKW and eGFP-Rab11-FIP2. Myc-Spir-2-ΔKW was pulled from a HEK 293 cell lysate using the anti-Myc 9E10 antibody (4 µg/ml). eGFP-Rab11-FIP2 was not immunoprecipitated. The eGFP protein was used as a negative control. eGFP-Rab11-FIP2 was not immunoprecipitated from HEK 293 lysates when Myc-Spir-2-ΔKW was absent. SDS-PAGE: 7,5% Polyacrylamide gel; Immunodetection: α-living colors GFP (1:100); α-rabbit-HRP (1:5000); α-Myc 9E10 (1:200); α-mouse-HRP (1:4000); Abbreviations: **kDa** kilo Dalton; **IP** immunoprecipitation; **t** total; **s** supernatant (soluble protein fraction, supernatant fraction after centrifugation at 14000 rpm); **p** pellet (insoluble protein fraction; pellet fraction after centrifugation at 14000 rpm)
This figure is representative of two separate experiments.

4.2.3 Spir-2 colocalizes to the small G protein Arf1

Arf1 regulates many transport processes at the Golgi apparatus. It controls intra-Golgi traffic and also TGN to plasma membrane transport via endosomal structures. Arf1 is implicated in vesicle formation by recruiting coat proteins, regulating the phospholipid environment and

modulating actin structures (Bonifacino and Lippincott-Schwartz, 2003, Godi et al., 1999, Myers and Casanova, 2008).

To elucidate if Spir-2-associated vesicles are somehow regulated by Arf1, HeLa cells were cotransfected with Myc-epitope tagged Spir-2-ΔKW and Arf1-eGFP, and the subcellular localization of both proteins was determined by immunofluorescence staining experiments. The Myc-epitope tagged Spir-2-ΔKW protein was detected with an anti-Myc9E10 antibody and a TRITC-conjugated anti-mouse IgG secondary antibody. Arf1 and Spir-2-ΔKW are colocalized on vesicular structures (Fig. 4.8). To further confirm the connection between Spir-2 and Arf1 a co-immunoprecipitation experiment was performed. It could be shown that Spir-2-ΔKW and Arf1 co-immunoprecipitates in a complex (Fig. 4.9), supporting an interaction between both proteins. Therefore, a Spir-2/Arf1 complex mediates transport of tubular vesicles.

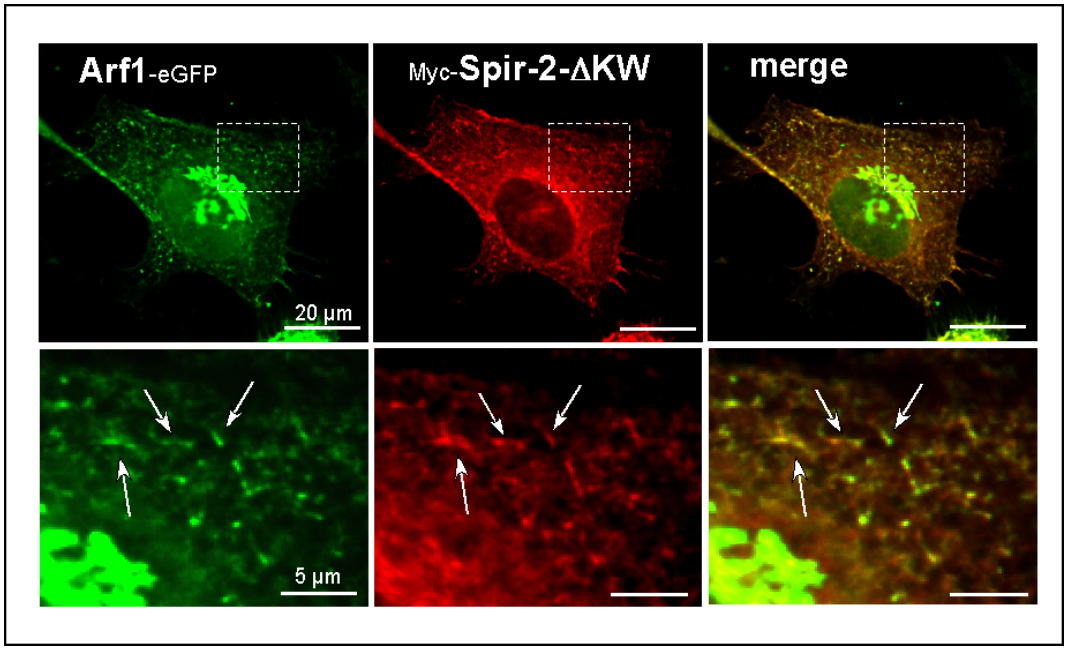

Figure 4.8: **Spir-2 is localized at Arf1-positive compartments**
HeLa cells were cotransfected with Myc-Spir-2-ΔKW and Arf1-eGFP. Images were deconvoluted (blind) with the deconvolution software from Leica. Arf1 and Spir-2-ΔKW colocalize on tubular vesicles

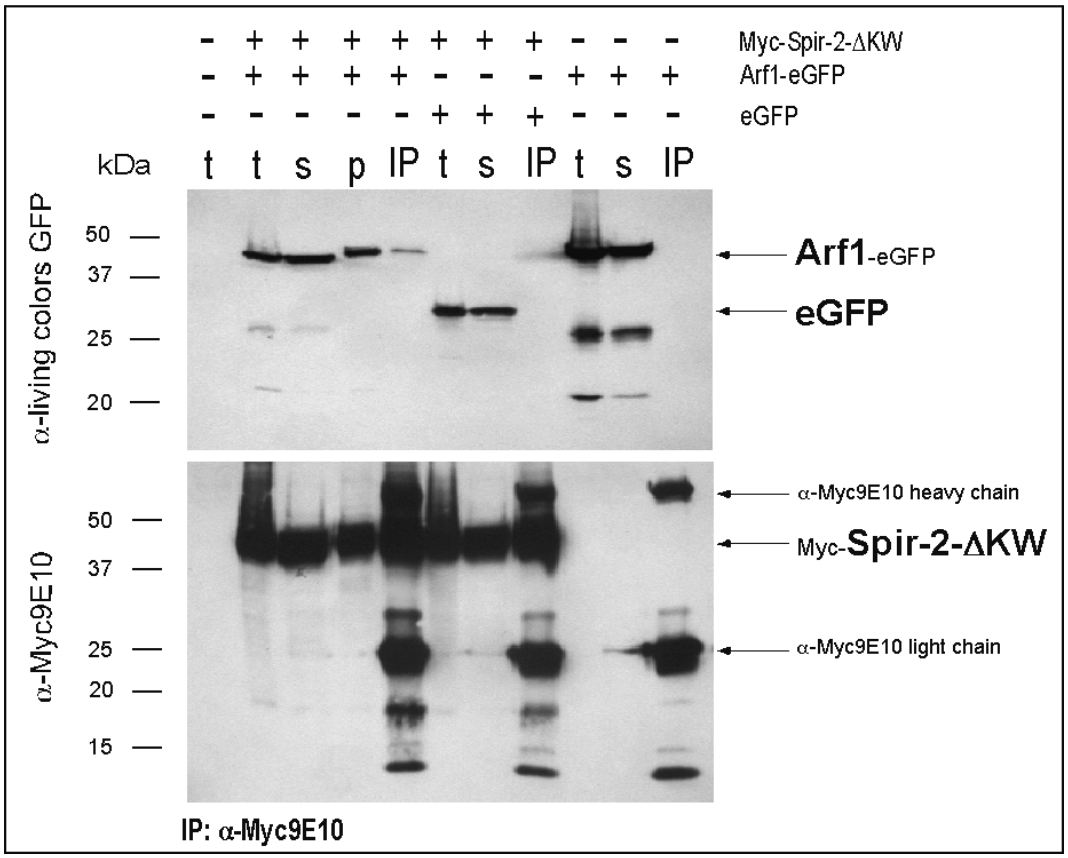

Figure 4.9: **Arf1 is in a complex with Spir-2-ΔKW**

Co-IP of Myc-Spir-2-ΔKW and Arf1-eGFP. Myc-Spir-2-ΔKW was pulled from a HEK 293 cell lysate using the anti-Myc 9E10 antibody (4 µg/ml). Arf1-eGFP but not eGFP was immunoprecipitated with Spir-2-ΔKW. Arf1-eGFP was not immunoprecipitated from HEK 293 lysates when Myc-Spir-2-ΔKW was absent.

SDS-PAGE: 10% Polyacrylamide gel; Immunodetection: α-living colors GFP (1:100); α-rabbit-HRP (1:5000); α-Myc9E10 (1:200); α-mouse-HRP (1:4000); Abbreviations: **kDa** kilo Dalton; **IP** immunoprecipitation; **t** total; **s** supernatant (soluble protein fraction; supernatant fraction after centrifugation at 14000 rpm); **p** pellet (insoluble protein fraction; pellet fraction after centrifugation at 14000 rpm)

This figure is representative of three separate experiments.

4.2.4 Spir-2-ΔKW vesicles are localized to microtubules

A major question to be answered was, in which way the cytoskeleton regulates Spir-2 mediated membrane transport. First, the role of the microtubule cytoskeleton in Spir-2-mediated vesicle traffic was examined. HeLa cells were therefore coexpressed with eGFP-Spir-2-ΔKW, fixed and endogenous α-tubulin was detected with an anti-α-tubulin mouse monoclonal antibody (1 µg/ml) to stain the microtubule cytoskeleton. Spir-2-ΔKW partially colocalized with endogenous α-tubulin, suggesting that the transport of Spir-2-associated vesicles could depend on microtubule filaments (Fig. 4.10).

To test this dependency between Spir-2-driven vesicle transport and the microtubule cytoskeleton, eGFP-Spir-2-ΔKW transfected HeLa cells were treated with the microtubule depolymerizing drug nocodazole. 1 minute movies from cells were taken before and after treatment with nocodazole to analyze the alteration of vesicle motility and morphology. Depolymerization of microtubule filaments by nocodazole (20 mM) completely disrupts Spir-2-ΔKW-positive structures with respect to their length and also their motility (30 minutes after treatment). Almost all Spir-2-ΔKW vesicles showed a decreased elongation (Fig. 4.11). Furthermore, also the motility of Spir-2-ΔKW was severely limited. This suggests, that the elongation of Spir-2 vesicles depends on an intact microtubule cytoskeleton, supposing a model in which Spir-2-mediated vesicle transport requires microtubules.

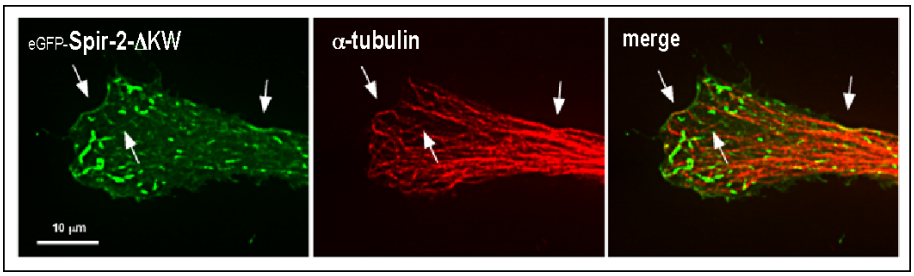

Figure 4.10: **Spir-2 vesicles are localized to microtubules**
HeLa cells were transiently transfected with pEGFP-C1-Spir-2-ΔKW. The subcellular localization of endogenous α-tubulin was determined by immunostain experiments (red fluorescence) and the localization of eGFP-Spir-2-ΔKW was detected by GFP fluorescence (green fluorescence). Localization of Spir-2-ΔKW on microtubules is indicated (white arrows).

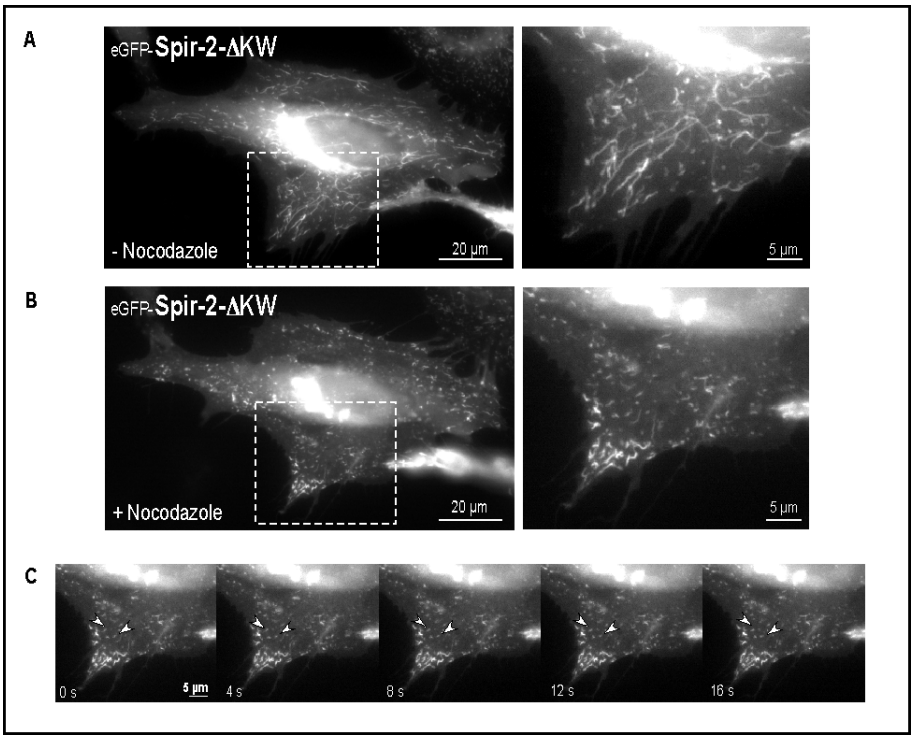

Figure 4.11: **Spir-2 vesicle elongation depends on microtubules**
Live cell imaging of HeLa cells transiently transfected with pEGFP-C1-Spir-2-ΔKW **A** Before treatment with the microtubule depolymerizing drug nocodazole, long and motile tubular structures are present. **B** After treatment with nocodazole (30 minutes) tubular structures are collapsed and exhibit decreased motility **C**. Decreased motility of Spir-2 vesicles is indicated by white arrows **C**.

4.2.5 Tubular Spir-2-ΔKW vesicles are coated with F-actin

Considering the fact that Spir is an actin nucleation factor and therefore regulates the actin cytoskeleton directly it was important to analyze the influence of the actin cytoskeleton of Spir-2- mediated vesicle transport. To show the association of endogenous F-actin and Spir-2 in HeLa cells, cells were transfected with Myc-Spir-2-ΔKW. After fixation and permeabilization, endogenous F-actin was detected with rhodamine-phalloidin, whereas transfected

exogenous Myc-Spir-2-ΔKW was detected with an anti-Myc 9E10 antibody and a fluorescin-isothiocyanate (FITC)-conjugated donkey anti-mouse secondary antibody. Spir-2-ΔKW was found to be localized on F-actin-positive vesicles, suggesting that in addition to the microtubule cytoskeleton also actin filaments are required for Spir-2-dependent vesicle transport (Fig. 4.12).

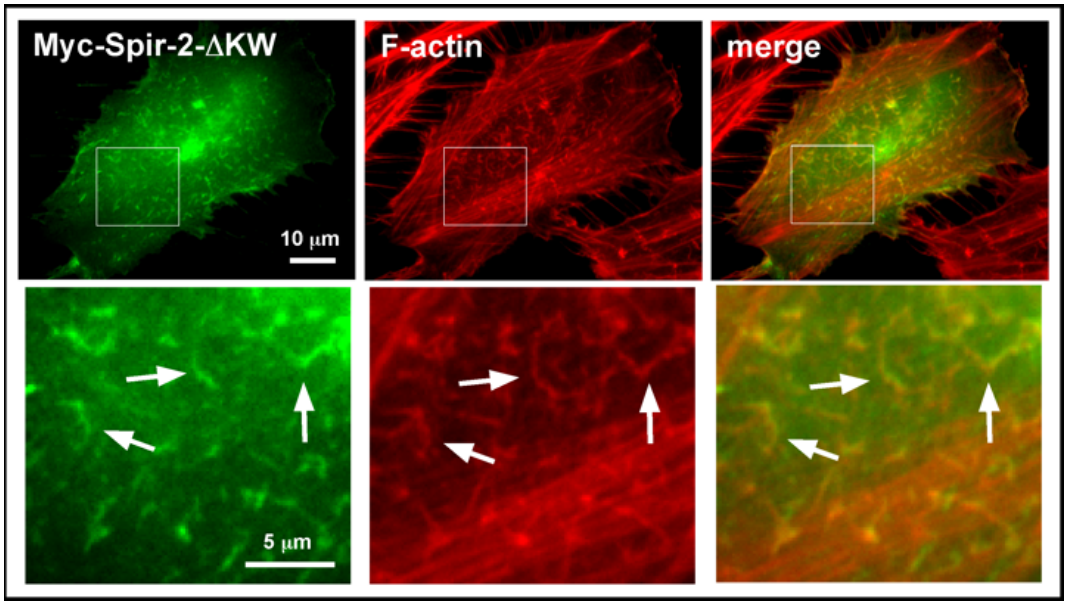

Figure 4.12: **Spir-2-ΔKW vesicles are F-actin coated**
HeLa cells were transfected with Myc-Spir-2-ΔKW, fixed and F-actin was detected with Rhodamine-Phalloidin (red fluorescence), whereas the Myc-Spir-2-ΔKW protein was detected with an anti-Myc 9E10 antibody and a secondary FITC-conjugated antibody (green fluorescence). Images were deconvoluted (blind) with the deconvolution software from Leica. Spir-2-ΔKW is localized to F-actin-positive tubular vesicles (white arrows).

4.2.6 Spir-2-ΔKW colocalizes and is in complex with the tail domain of myosin Vb

An interesting observation was that Spir-2-ΔKW, which lacks the KIND domain and the four WH2 domains and therefore the ability to nucleate actin filaments, also shows colocalization

to actin (Fig. 4.12). This suggests that the actin nucleation function of Spir is not crucial for the association of Spir-2-positive vesicles with the actin cytoskeleton.

It has been shown, that myosin Vb and Rab11a are involved in several transport processes (Volpicelli et al., 2002, Fan et al., 2004, Hales et al., 2002, Swiatecka-Urban et al., 2007). Localization of myosin Vb and Rab11 in HeLa and MDCK cells shows a very similar cellular distribution of both proteins (Lapierre et al., 2001). Throughout the course of this work a C-terminal fragment of the actin motor protein myosin Vb was used, which contain the cargo binding globular tail domain and the adjacent coiled coil domains (Fig. 4.13 A). Coexpression of mStrawberry-tagged MyoVb-cc-tail and eGFP-Rab11a in HeLa cells shows a very similar localization pattern of both proteins (Fig. 4.13 B).

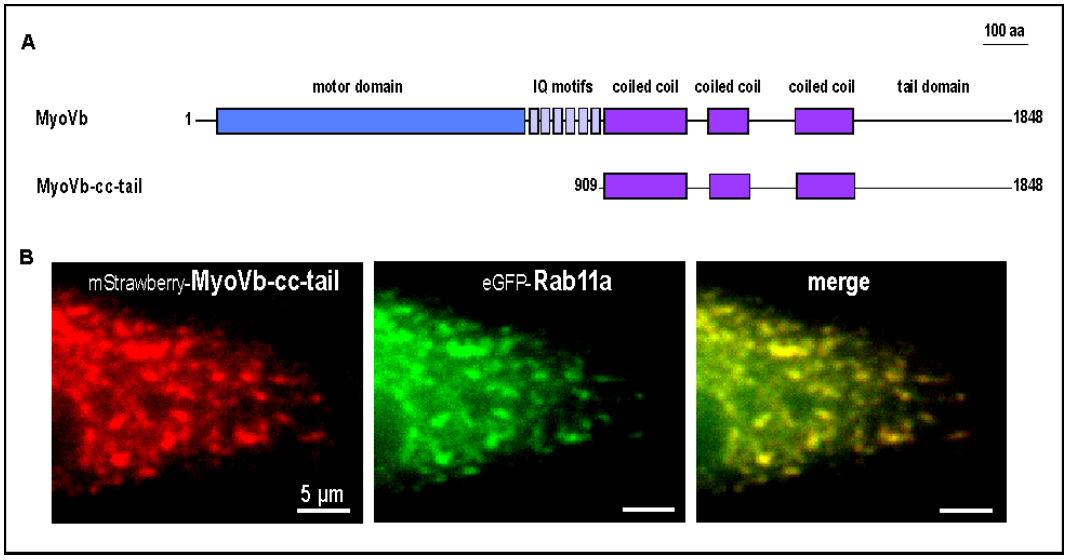

Figure 4.13: **Colocalization of the tail domain of myosin Vb and Rab11a in HeLa cells**

A Domain structure of the actin-dependent motor protein myosin Vb. Tail domain fragments of myosin Vb (MyoVb-cc-tail) are used as dominant negative mutants specifically for myosin Vb-dependent vesicle transport.

B Live cell imaging of HeLa cells transfected with expression vectors directing the expression of eGFP-Rab11a and mStrawberry-MyoVb-cc-tail. They show an identical localization pattern.

To elucidate the potential relation between Spir-2 and myosin Vb, HeLa cells were cotransfected with eGFP-Spir-2-ΔKW and mStrawberry-MyoVb-cc-tail. The tail domain of myosin Vb is often used as a dominant negative mutant for myosin Vb-dependent vesicle transport processes. This mutant has the ability to bind myosin Vb-specific cargo but does not actively transport it. Spir-2-ΔKW and MyoVb-cc-tail both localized to the same elongated tubular structures (Fig. 4.14).

To confirm the connection of Spir-2 and myosin Vb, interaction studies were performed. Myc-Spir-2-ΔKW and mStrawberry-MyoVb-cc-tail were cotransfected in HEK 293 cells. That study showed that MyoVb-cc-tail was immunoprecipitated with Spir-2-ΔKW, supporting an interaction between Spir-2 and myosin Vb (Fig. 4.15).

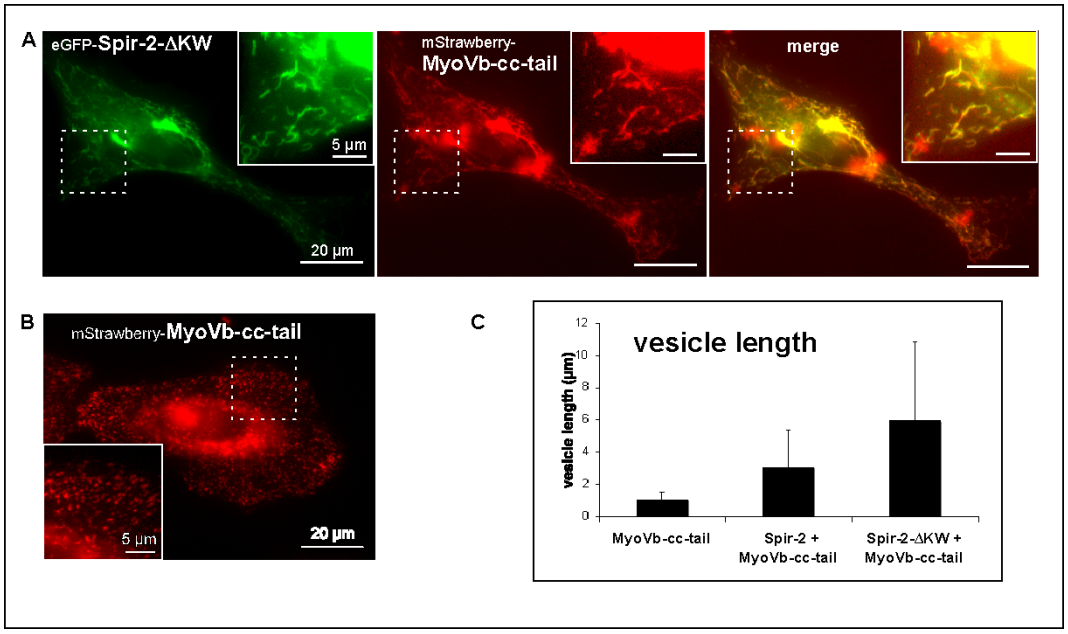

Figure 4.14: **Spir-2 shows colocalization to the tail domain of myosin Vb** Spir-2-ΔKW alters the morphology of MyoVb-cc-tail-positive vesicles **A** HeLa cells were co-transfected with eGFP-Spir-2-ΔKW and mStrawberry-MyoVb-cc-tail. The localization of both proteins were analyzed in living HeLa cells, were they show colocalization at tubular elongated vesicles. **B** HeLa cells were transfected with mStrawberry-MyoVb-cc-tail. MyoVb-cc-tail is located at dotlike vesicles in contrast to the elongated tubular structures in eGFP-Spir-2-ΔKW and mStrawberry-MyoVb-cc-tail transfected HeLa cells. **C** Comparison of the length of vesicles. 3 cells were imaged and a total of 100 vesicles are measured for each transfection.

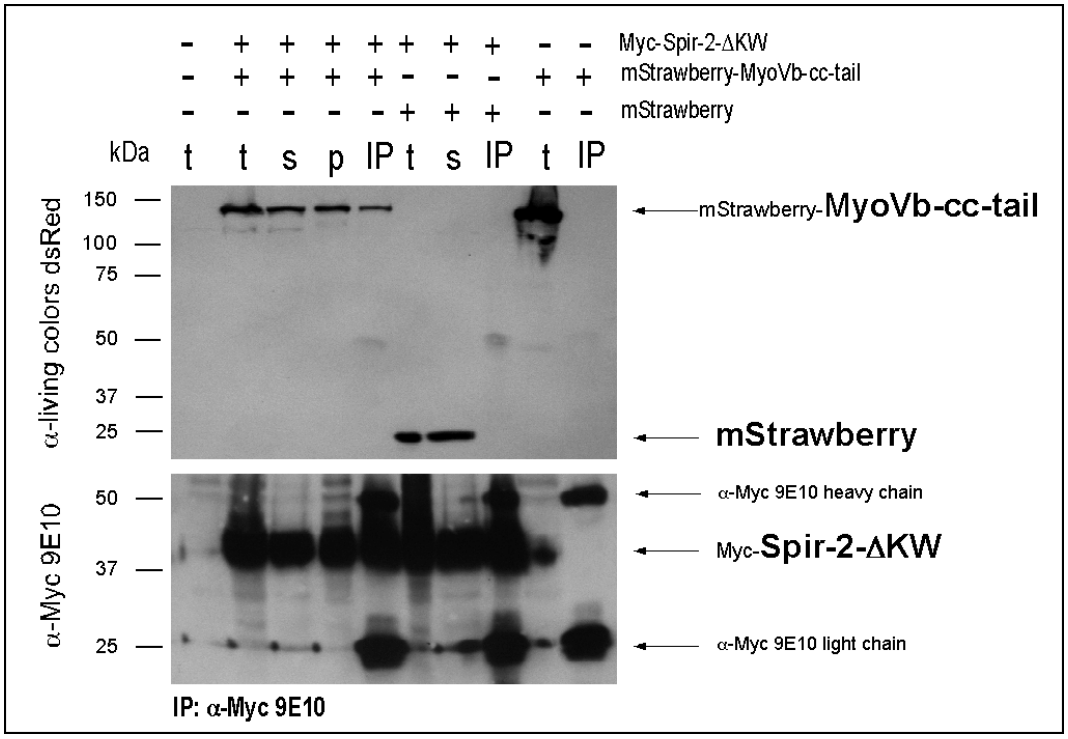

Figure 4.15: **MyoVb-cc-tail is in a complex with Spir-2-ΔKW**
Co-IP of Myc-Spir-2-ΔKW and mStrawberry-MyoVb-cc-tail. Myc-Spir-2-ΔKW was pulled from a HEK 293 cell lysate using an anti-Myc 9E10 antibody (4 µg/ml). mStrawberry-MyoVb-cc-tail but not mStrawberry was immunoprecipitated with Myc-Spir-2-ΔKW. SDS-PAGE: 7,5 % Polyacrylamide gel; Immunodetection: α-living colors dsRed (1:1000); α-rabbit-HRP (1:5000); α-Myc 9E10 (1:200); α-mouse-HRP (1:4000); Abbreviations: **kDa** kilo Dalton; **IP** immunoprecipitation; **t** total; **s** supernatant (soluble protein fraction; supernatant fraction after centrifugation at 14000 rpm); **p** pellet (insoluble protein fraction; pellet fraction after centrifugation at 14000 rpm)
This figure is representative of three separate experiments.

4.3 Function of Spir-2 in vesicle trafficking

4.3.1 Spir-2 and Spir-2-ΔKW alter the morphology of Rab11a-associated vesicles

Spir-2 shows specific localization to Rab11a-positive vesicles. To analyze if Spir-2 has an effect on Rab11a vesicle morphology, HeLa cells were transfected with N-terminally mStrawberry-tagged Rab11a alone and together with eGFP-Spir-2 or eGFP-Spir-2-ΔKW. To measure the vesicle length, 100 vesicles of 3 cells per transfection, were analyzed. Expression of Rab11a results in Rab11a-associated vesicles with an average length of 1 µm (Fig. 4.4 B,C). In comparison, coexpression of Rab11a and Spir-2 or Spir-2-ΔKW leads to elongated Rab11a/Spir-2 or Rab11a/Spir-2-ΔKW-positive vesicles, with an average length of 2-3 µm (Fig. 4.4). Rab11a/Spir-2 and Rab11a/Spir-2-ΔKW-associated vesicles displayed a similar length to Spir-2 or Spir-2-ΔKW vesicles (Fig. 4.4 A,C), suggesting that Spir-2 induced vesicle elongation affects the morphology of Rab11a compartments. Rab11a/Spir-2-ΔKW-associated vesicles showed a slightly increased elongation rate compared with Rab11a/Spir-2-positive vesicles, very similar to the differences of Spir-2 and Spir-2-ΔKW-associated vesicles (Fig. 4.3 C). This supports the assumption, that the alterations of the Rab11a compartment are specifically induced by Spir-2 function.

4.3.2 Spir-2 and Spir-2-ΔKW alter the morphology of myosin Vb vesicles

The C-terminal tail domain of myosin Vb mediates cargo binding but lacks the motor domain. MyoVb-cc-tail constructs could therefore be used as dominant negative mutants, which inhibit myosin Vb-dependent transport specifically. Myosin Vb and Spir-2 show colocalization in HeLa cells (Fig. 4.14 A) and interact with each other via their C-termini (Fig. 4.15). To measure the vesicle length, 100 vesicles of 4-5 cells per transfection were analyzed. As well as Rab11a vesicles were altered by Spir-2, MyoVb-cc-tail-positive structures were also modified by Spir-2 and Spir-2-ΔKW (Fig. 4.14). Besides, MyoVb-cc-tail/Spir-2-ΔKW-associated vesicles exhibited an increased elongation rate up to 11 µm, suggesting that inhibition of Spir-2 dependent actin nucleation leads to the elongation of those vesicles. Furthermore, coexpression of MyoVb-cc-tail and Spir-2-ΔKW results in highly elongated tubular vesicles whose motility is inhibited (Fig. 4.16).

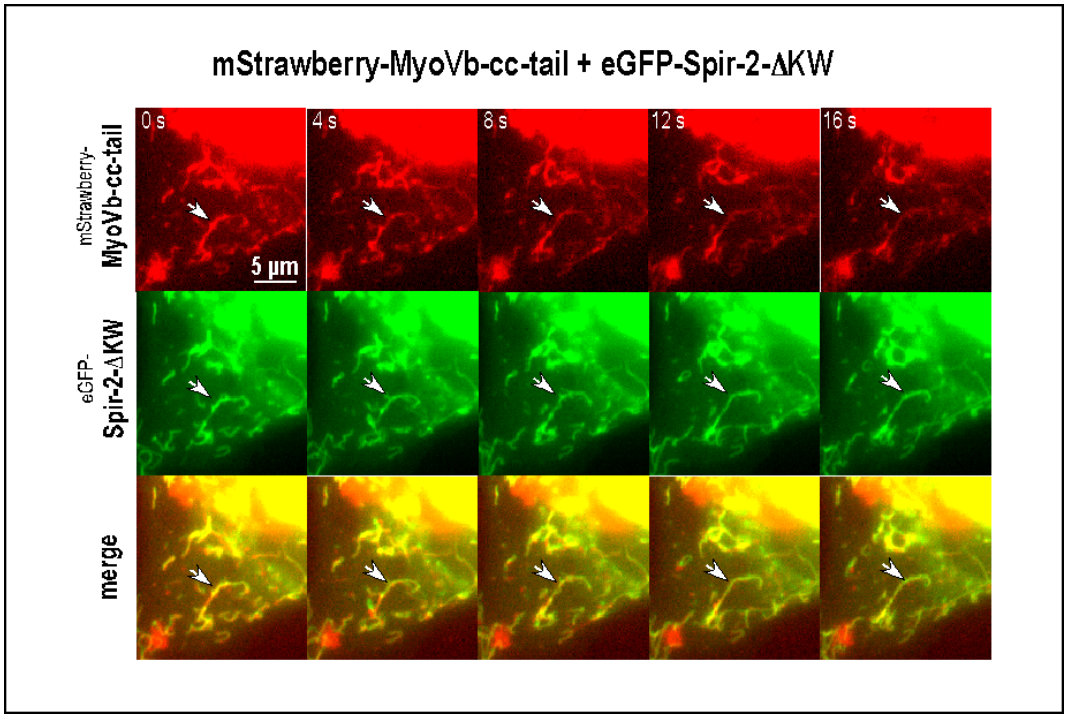

Figure 4.16: **MyoVb-cc-tail/Spir-2-ΔKW-positive vesicles exhibit decreased motility**

Live cell imaging of HeLa cells cotransfected with expression vectors directing the expression of mStrawberry-MyoVb-cc-tail and eGFP-Spir-2-ΔKW. Time-lapse movies were made by taking a picture every two seconds. Note that the time interval between the shown pictures is 4 seconds. MyoVb-cc-tail/Spir-2-ΔKW-positive vesicles are highly elongated (Fig. 4.14) and exhibit decreased motility (white arrow).

4.4 Spir-2 and Spir-1 C-termini form homo- and heteromers and mediate binding to phospholipids

4.4.1 Purification of GST-Spir-2-ΔKW, 6xHis-Spir-2-ΔKW, 6xHis-Spir-1-ΔKW and 6xHis-SOS1-PH

To analyze the subcellular function of the Spir-box and the modified Spir FYVE domain Spir-2-ΔKW and Spir-1-ΔKW proteins were expressed by using bacterial expression vectors and finally purified. These purified proteins could then be used for protein-lipid overlay assays and pull down experiments. The Ras GEF SOS1 (Son of sevenless) (NCBI ID: NM_005633) activates Ras at the plasma membrane. The recruitment of SOS1 to the plasma membrane via its pleckstrin homology (PH) domain requires phosphatidic acid generated by PLD2 (Zhao et al., 2007). The PH domain of SOS1 is a phosphatidic acid binding domain. An N-terminally 6xHis-tagged PH domain was used as a positive control for the protein-lipid overlay assay.

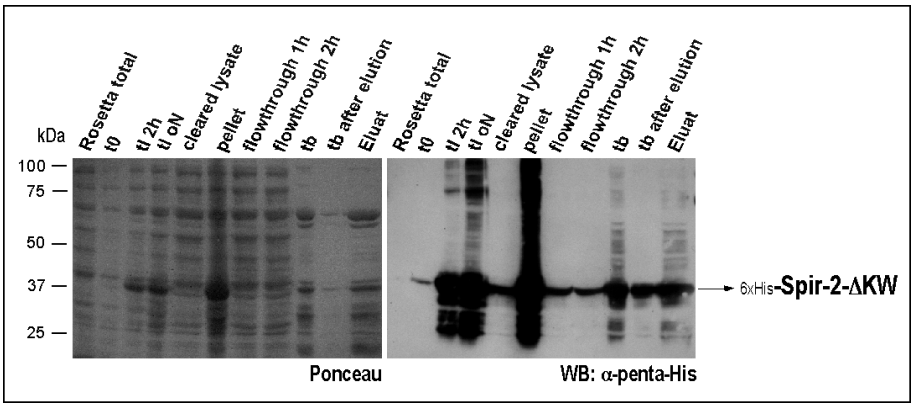

Figure 4.17: **Purification of 6xHis-Spir-2-ΔKW**
Spir-2-ΔKW was N-terminally tagged with 6xHis residues. 6xHis tagged proteins could be efficiently purified by using nickel-nitrilotriacetic acid (Ni-NTA) agarose. and purified by using a Ni-NTA batch purification method under non-denaturing conditions (Qiagen).
Expression conditions: 0,1 mM IPTG, over night, 25 ºC; SDS-PAGE: 7,5 % Polyacrylamide gel; Immunodetection: α-penta-His (1:1000); α-mouse-HRP (1:4000); Abbreviations: **kDa** kilo Dalton; **t0** non induced control; **tI** induced control; **tb** protein fraction bound to beads

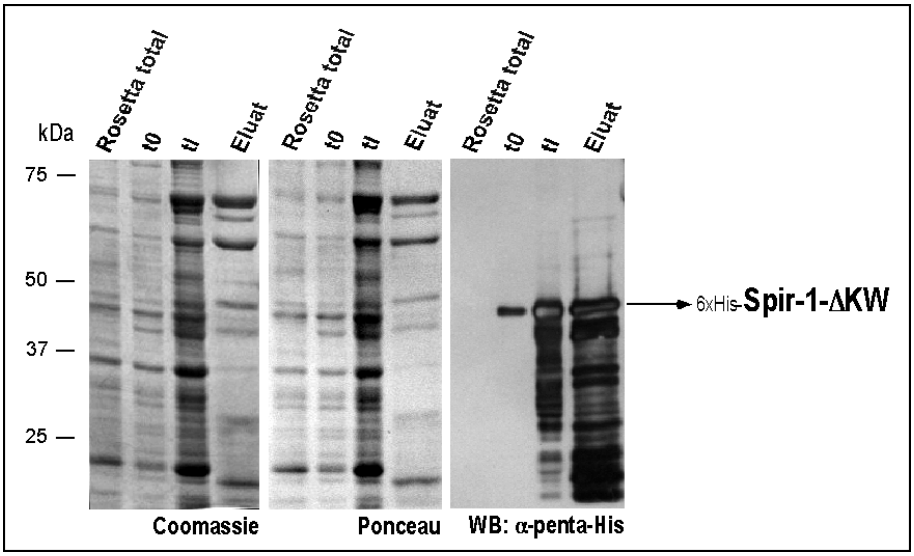

Figure 4.18: **Purification of 6xHis-Spir-1-ΔKW**

Spir-1-ΔKW was also N-terminally tagged with 6 His residues, comparable to the Spir-2-ΔKW protein and was purified by using Ni-NTA agarose beads from Qiagen under non-denaturing conditions.

Expression conditions: 0,1 mM IPTG, over night, 25 ^{o}C; SDS-PAGE: 7,5 % Polyacrylamide gel; Immunodetection: α-penta-His (1:1000); α-mouse-HRP (1:4000), Abbreviations: **kDa** kilo Dalton; **t0** non induced control; **tI** induced control

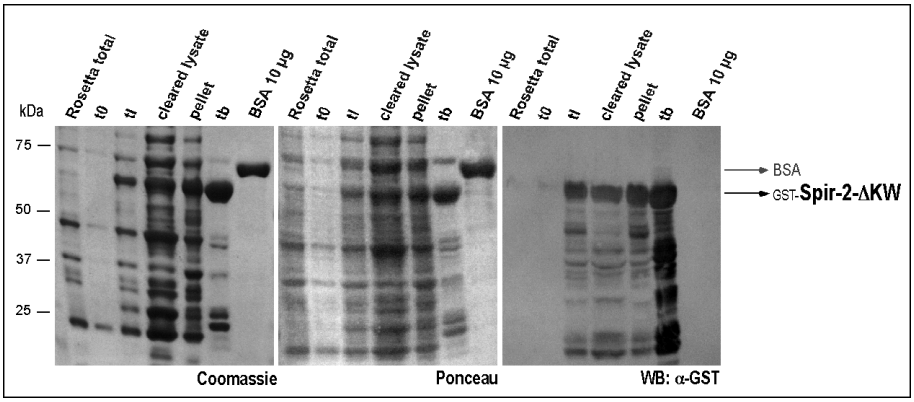

Figure 4.19: **Purification of GST-Spir-2-ΔKW (for pull down assays)**
Additionally to the 6xHis-tagged Spir-2-ΔKW protein also a N-terminally GST-tagged Spir-2-ΔKW protein was purified. The GST-tag leads to a much better solubility of the Spir-2 protein, which results in an increased yield of purified protein.
Expression conditions: 0,1 mM IPTG, over night, 21 ^{o}C; SDS-PAGE: 7,5 % Polyacrylamide gel; Immunodetection: α-GST (1:5000); α-goat-HRP (1:7000), Abbreviations: **kDa** kilo Dalton; **t0** non induced control; **tI** induced control, **tb** protein fraction bound to beads

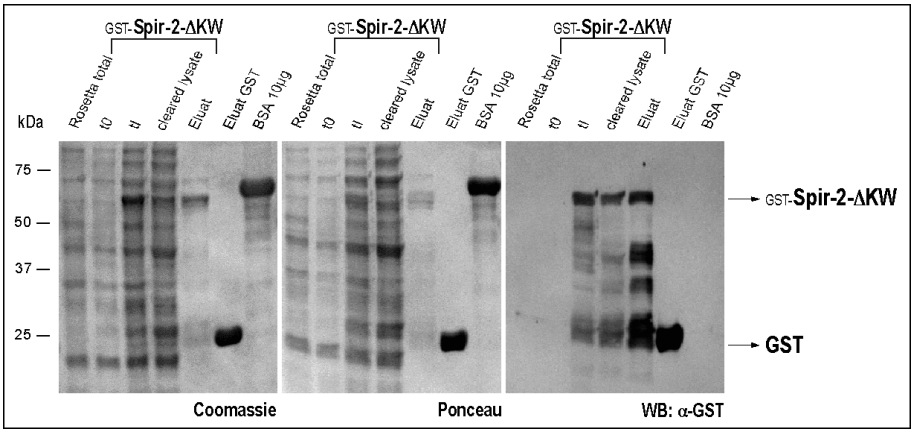

Figure 4.20: **Purification of GST-Spir-2-ΔKW and GST-control (for protein-lipid overlay assays)**
To analyze the phospholipid binding properties, the GST-tagged Spir-2-ΔKW protein was eluted from the GST-beads. Expression conditions: 0,1 mM IPTG, over night, 21 ^{o}C; SDS-PAGE: 10 % Polyacrylamide gel; Immunodetection: α-GST (1:5000); α-goat-HRP (1:7000); Abbreviations: **kDa** kilo Dalton; **t0** non induced control; **tI** induced control

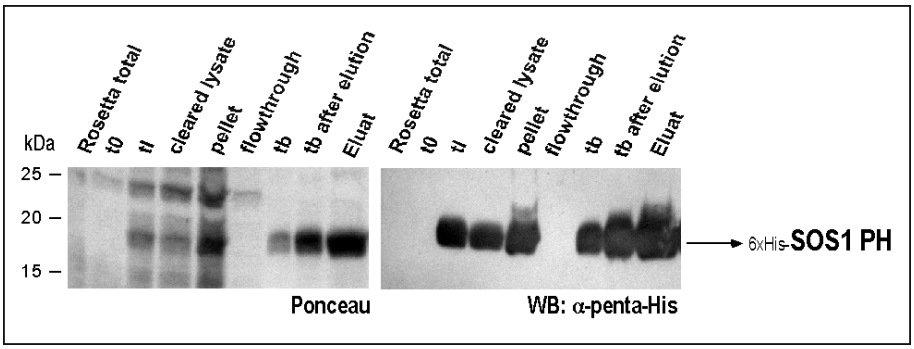

Figure 4.21: **Purification of 6xHis-SOS1-PH**
The PH domain of SOS1 is a phosphatidic acid binding domain. An N-terminally 6xHis-tagged PH domain was used as a positive control for the protein-lipid overlay assay.
Expression conditions: 0,1 mM IPTG, over night, 25 ^{o}C; SDS-PAGE: 11 % Polyacrylamide gel; Immunodetection: α-penta-His (1:1000); α-mouse-HRP (1:4000), Abbreviations: **kDa** kilo Dalton; **t0** non induced control; **tI** induced control, **tb** protein fraction bound to Ni-NTA beads

4.4.2 Interaction of the C-terminal part of Spir-2 and Spir-1

To further elucidate the mechanism in which Spir-membrane-targeting could be regulated, interaction studies of C-terminal parts of Spir-1 and Spir-2 were performed. A well studied FYVE domain containing protein is EEA1 (early endosome antigen 1). The localization of EEA1 to early endosomal membranes depends on its C-terminus, which contains a Rab5 interaction site and a FYVE domain. The FYVE domain selectively binds phosphatidylinositol 3-phosphat (PtdIns(3)P). Another important feature of EEA1 is its ability to dimerize (Dumas et al., 2001). The formation of EEA1 dimers is crucial for binding to early endosomal membranes. Adjacent to the FYVE domain is a coiled coil domain, which is needed for the dimerization. Considering that Spir proteins also consist of a FYVE domain it was obvious to test the ability of Spir proteins to dimerize and to analyze the function of Spir dimerization regarding membrane targeting and recruitment.

First, a co-immunoprecipitation assay was performed. HEK 293 cells were transfected with eGFP-Spir-2-ΔKW and Myc-Spir-2-ΔKW. The co-immunoprecipitation experiment revealed that eGFP-Spir-2-ΔKW co-immunoprecipitate with Myc-Spir-2-ΔKW (Fig. 4.22).

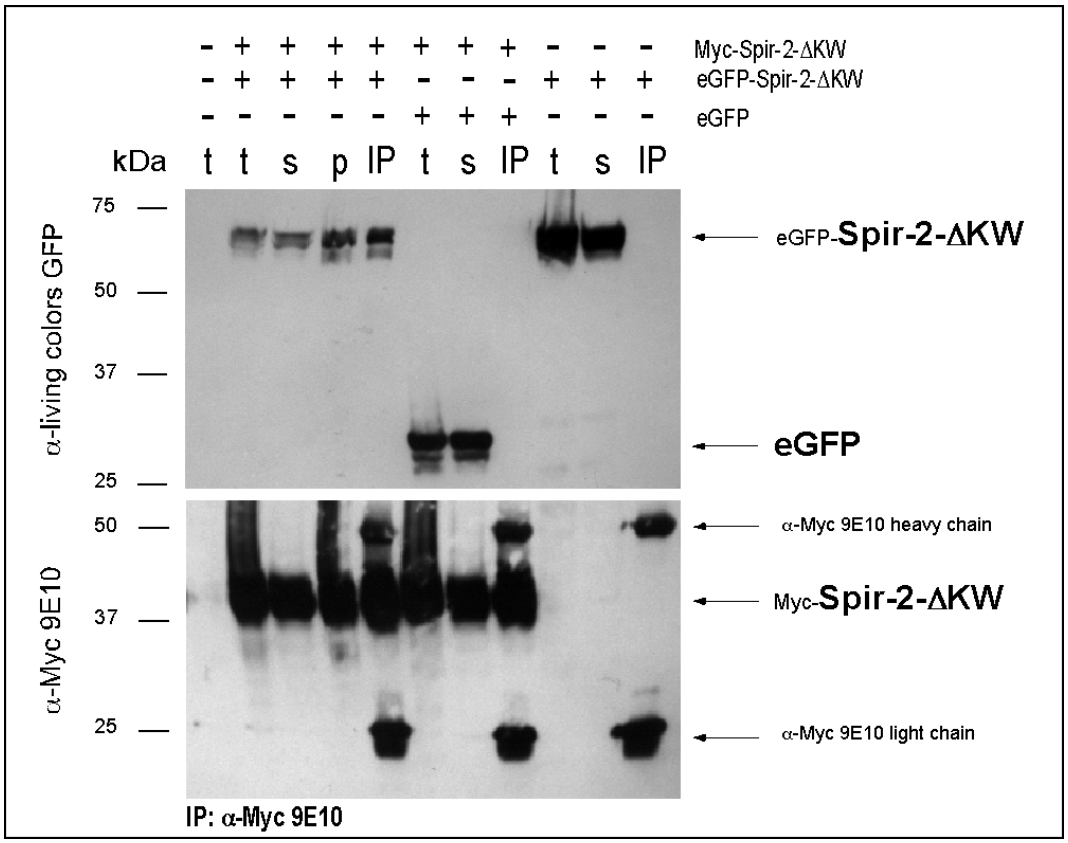

Figure 4.22: **Spir-2 proteins interact via their C-termini**
Co-IP of Myc-Spir-2-ΔKW and eGFP-Spir-2-ΔKW. Myc-Spir-2-ΔKW was pulled from a HEK 293 cell lysate using the anti-Myc 9E10 antibody (4 µg/ml). eGFP-Spir-2-ΔKW but not eGFP was immunoprecipitated. eGFP-Spir-2-ΔKW was not immunoprecipitated from HEK 293 lysates when Myc-Spir-2-ΔKW was absent.
SDS-PAGE: 7,5% Polyacrylamide gel; Immunodetection: α-living colors GFP (1:100); α-rabbit-HRP (1:5000); α-Myc 9E10 (1:200); α-mouse-HRP (1:4000); Abbreviations: **kDa** kilo Dalton; **IP** immunoprecipitation; **t** total; **s** supernatant (soluble protein fraction; supernatant fraction after centrifugation at 14000 rpm); **p** pellet (insoluble protein fraction; pellet fraction after centrifugation at 14000 rpm)
This figure is representative of three separate experiments.

To further confirm, that the Spir-2 C-termini interact directly, GST- and 6xHis-tagged Spir-2-ΔKW proteins were purified and used for pull-down experiments. GST-Spir-2-ΔKW bound to GST-beads was therefore incubated with eluted 6xHis-Spir-2-ΔKW protein. As a control, GST bound to GST-beads were also incubated with 6xHis-Spir-2-ΔKW to exclude that the binding depends on the GST-tag. 6xHis-Spir-2-ΔKW was pulled with GST-Spir-2-ΔKW but not with GST alone (Fig. 4.23). Additionally, 6xHis-tagged Spir-1-ΔKW was also purified and incubated with GST-Spir-ΔKW/beads, respectively GST/beads, to examine a possible heteromerization ability of Spir proteins. The pull-down assay showed that also 6xHis-Spir-1-ΔKW could be pulled with GST-Spir-2-ΔKW but not with GST (Fig. 4.24), suggesting a Spir-2/Spir-1 heteromer.

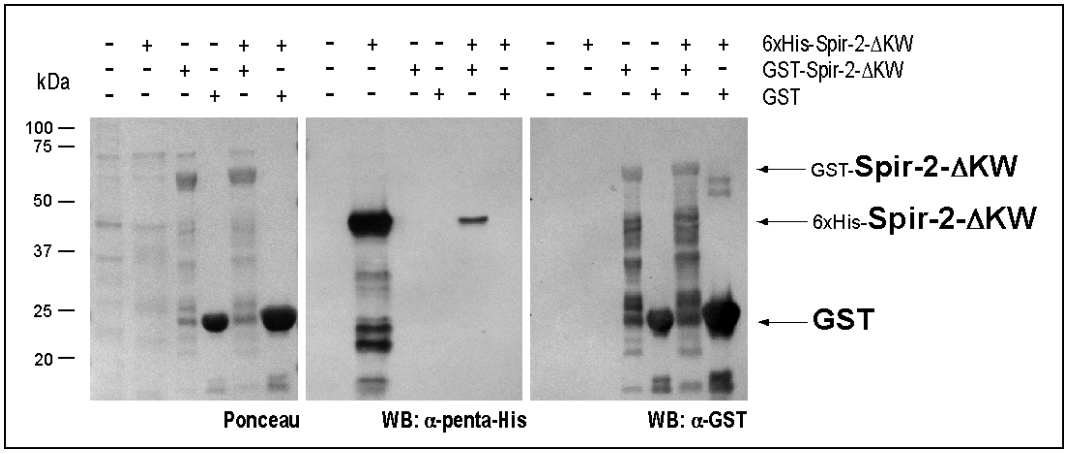

Figure 4.23: **Spir-2 proteins interact directly via their C-termini**
Pull down of GST-Spir-2-ΔKW and 6xHis-Spir-2-ΔKW. The 6xHis-Spir-2-ΔKW was pulled with GST-Spir-2-ΔKW but not with GST, indicating the direct interaction of Spir-2 proteins. This figure is representative of two separate experiments.

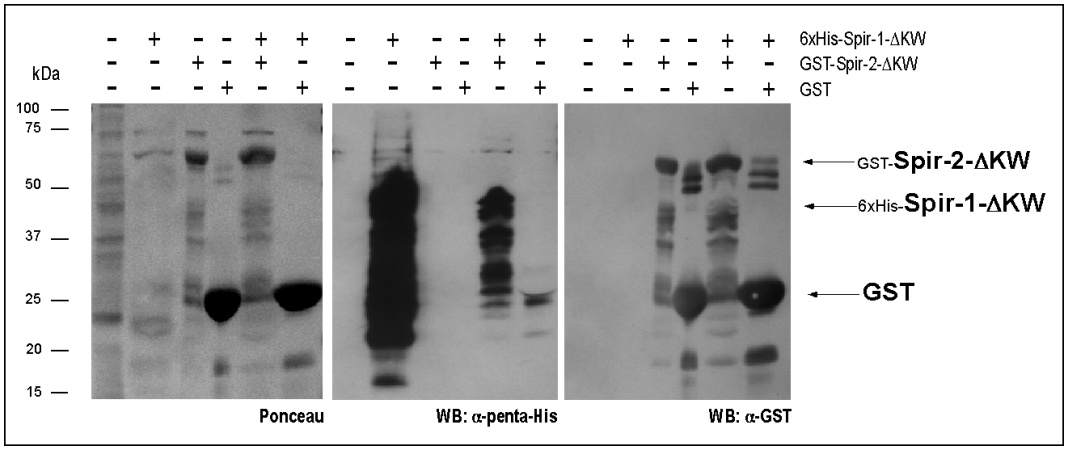

Figure 4.24: **Spir-2 and Spir-1 interact directly via their C-termini**
Pull down of GST-Spir-2-ΔKW and 6xHis-Spir-1-ΔKW. The 6xHis-Spir-1-ΔKW protein was pulled with GST-Spir-2-ΔKW but not with GST, indicating the direct interaction between Spir-2 and Spir-1.
This figure is representative of two separate experiments.

4.4.3 Phospholipid interaction of Spir-1 and Spir-2

FYVE domains are known phospholipid interaction modules, which mediate membrane targeting of several proteins. To test the interaction of the Spir FYVE domain, GST-Spir-2-ΔKW, 6xHis-Spir-2-ΔKW and 6xHis-Spir-1-ΔKW were purified and used for protein-lipid overlay assays. The PH domain of the Ras GEF SOS1, which is known to bind phosphatidic acid (Zhao et al., 2007), was used as a positive control. Purified GST protein was used as a negative control. The GST protein exhibits no binding to any phospholipid, which indicates, that the GST-tag has no influence on the phospholipid binding property. In contrast, GST-Spir-2-ΔKW, 6xHis-Spir-2-ΔKW and 6xHis-Spir-1-ΔKW exhibit a binding to phosphatidic acid, like 6xHis-SOS1-PH (Fig. 4.25). All proteins show a binding to PtdIns(3)P, PtdIns(4)P and PtdIns(5)P. Additionally, GST-Spir-2-ΔKW, 6xHis-Spir-2-ΔKW and 6xHis-SOS1-PH weakly bound to PtdIns(3,4)P_2, PtdIns(3,5)P_2, PtdIns(4,5)P_2 and PtdIns(3,4,5)P_3. The binding affinity of GST-Spir-2-ΔKW to PtdIns(3,5)P_2 was higher in contrast to 6xHis-Spir-2-ΔKW. Regarding the fact that the PH domain of SOS1 also shows a weak binding to the different

phosphatidylinositolphosphate species that binding can be considered as unspecific. The Spir FYVE domain could also bind to PtdIns(3)P, like other FYVE domains, regardless of the lacking basic cluster between cysteines 2 and 3. Spir FYVE domains have therefore the ability to bind different phospholipids. For this reason it is possible that Spir-recruitment to specific target membranes requires further factors, such as Arf proteins.

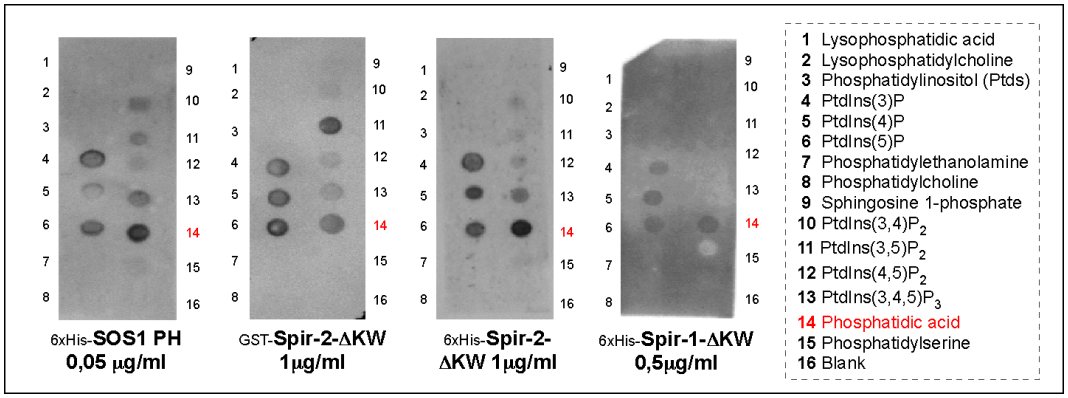

Figure 4.25: **Phospholipid binding ability of the Spir FYVE domain** Purified Spir-2-ΔKW, Spir-1-ΔKW and SOS1-PH proteins were used for protein-lipid overlay assays. The purified PH domain of SOS1 was used as a positive control. Spir-2-ΔKW and Spir-1-ΔKW bind to phosphatidic acid. Purified GST protein was used as a negative control. GST alone shows no binding to any phospholipid.

5 *DISCUSSION*

5.1 Spir-2 regulates actin/microtubule dependent transport of tubular vesicles

Spir-2 is targeted to membrane structures via its C-terminal FYVE domain. The analysis of living HeLa cells expressing eGFP-tagged Spir-2, Spir-2-ΔKIND and Spir-2-ΔKW showed Spir-2-associated tubular structures, which differ in their length and motility. Spir-2-ΔKW-associated vesicles exhibit the highest degree of elongation and furthermore, showed a slightly increased motility (Fig. 4.3 C,D) as compared to wildtype Spir-2. In contrast, Spir-ΔKIND, which encodes the four WH2 domains sufficient for *in vitro* actin nucleation, shows no difference regarding the vesicle length, to full length Spir-2, but Spir-2-ΔKIND-associated vesicles display a relative static behavior (Fig. 4.3 D). A possible explanation for the differences of vesicle motility between Spir-2 and Spir-2-ΔKIND, could be that Spir proteins are autoinhibited. For Spir-1, it has been shown, that a Spir-1-KIND CAAX construct recruits Spir-1-FYVE, which is cytoplasmic, to membrane structures (Fig. 5.1). This suggests, that Spir KIND domains have the ability to bind Spir FYVE domains, which could cause a folded Spir protein, with no actin nucleation activity. Regarding the fact, that Spir domains are highly conserved between different Spir proteins, the FYVE/KIND interaction is also possible for Spir-2. Spir-2-ΔKIND could therefore be a dominant active Spir protein. It is therefore possible that increased actin levels on Spir-2-ΔKIND vesicles disrupt their motility. Considering that Spir-2-ΔKW and Spir-2-ΔKIND both lack the ability to bind a formin actin nucleator exhibit contrary effects on vesicle motility, raises the question in which way the actin nucleation function of formin contributes to the Spir-2-mediated transport of tubular vesicles.

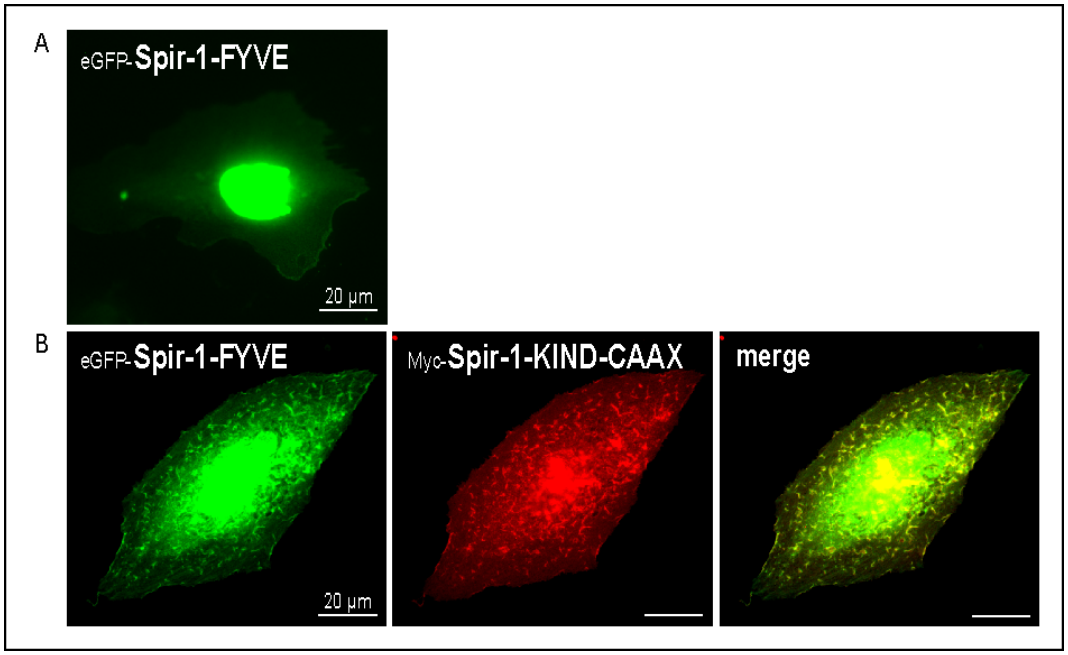

Figure 5.1: **Spir-1 KIND-FYVE interaction**
Spir-1-KIND-CAAX recruits Spir-1-FYVE to tubular membrane structures **A** HeLa cells were transfected with eGFP-Spir-1-FYVE. The FYVE domain exhibits a nuclear localization. **B** HeLa cells were cotransfected with eGFP-Spir-1-FYVE and Myc-Spir-1-KIND-CAAX. eGFP-Spir-1-FYVE is recruited to membranes, suggesting a KIND-FYVE interaction of Spir-1 proteins. Spir-1 proteins could therefore be autoinhibited.

By depolymerizing microtubule filaments with the drug nocodazole the data presented here show that the elongation of this tubular vesicles is disrupted. This suggests, that an intact microtubule cytoskeleton is necessary for the formation of those tubular vesicles. It was found that actin is still present on the WH2-domain deficient Spir-2-ΔKW protein. Furthermore, the actin dependent motor protein myosin Vb could be immunoprecipitated with Spir-2-ΔKW and a good colocalization of Spir-2-ΔKW and MyoVb-cc-tail in living HeLa cells could also be observed. The tail domain of myosin Vb is often used as a dominant negative mutant for myosin Vb-dependent vesicle transport processes. This mutant has the ability to bind myosin Vb-specific cargo but does not actively transport it. Expression of mStrawberry-tagged MyoVb-cc-tail protein in HeLa cells shows a punctate pattern, which shows colocalization to

Rab11a (Fig. 4.13). Coexpression of Spir-2-ΔKW together with MyoVb-cc-tail in living HeLa cells change the morphology of MyoVb-cc-tail-associated vesicles. Spir-2-ΔKW/MyoVb-cc-tail-positive vesicles are highly elongated also in comparison to Spir-2-ΔKW vesicles. Coexpression of the full length Spir-2 protein together with MyoVb-cc-tail results also in an elongation of MyoVb-cc-tail- associated vesicles but they have the same average length like the Spir-2-positive vesicles. An inhibition of the nucleation activity results in highly elongated tubular vesicles whose motility is inhibited (Fig. 4.14 and Fig. 4.16). The cooperativity of both dominant negative effects suggests that the actin nucleation function of Spir-2 and the actin-dependent motor activity of myosin Vb both have an effect on Spir-2-mediated vesicle trafficking.

These results argues for a model, in which Spir-2 vesicles move along microtubule filaments, branch and fuse with each other, and have the ability to switch to another microtubule filament. The actin cytoskeleton is supposed to be crucial for the crossing of those Spir-2 vesicles from one microtubule filament to another.

5.1.1 Spir-2 and Rab11a mediate vesicle transport along the same pathway

Exogenous eGFP-tagged Spir-2 and Spir-2-ΔKW proteins are localized to membraneous structures in HeLa cells. Coexpression of mStrawberry-tagged Rab11a revealed a colocalization of Spir-2 and the small G protein Rab11a on tubular structures. Rab11a is involved in transport processes along the secretory and the endocytic pathway (Ullrich et al., 1996, Chen et al., 1998) and shows a localization to recycling endosomes and also to the TGN. It has been shown, that a dominant negative Rab11 mutant (Rab11S25N) causes a block of exocytosis of VSV-G protein and results in an accumulation of that protein into the Golgi (Chen et al., 1998).

Furthermore, the expression of Rab11S25N results in a TfR-positiv extended tubular network, suggesting a role for Rab11 in vesicle budding from recycling endosomal structures (Wilcke et al., 2000). In contrast, the expression of dominant active Rab11Q70L leads to a dispersed, punctate pattern of TfR-positive vesicles throughout the cytoplasm (Wilcke et al., 2000). By using markers for different transport pathways, like Shiga toxin B (STxB), which uses the retrograde endosome to TGN route, TGN38, which cycles between the plasma membrane and the TGN via endosomes, and transferrin receptor (TfR), which is a marker for the recycling pathway, it has been shown that Rab11 plays a role in the exit of membranes from

the recycling endosome (Wilcke et al., 2000). The fact that after nocodazole treatment the tubular network was no longer visible, suggests that Rab11S25N induced tubules depend on an intact microtubule cytoskeleton.

For Spir-1-CT, a truncated version of the Spir-1 protein, which lacks the N-terminal KIND and the four WH2 domains, it has been shown that VSV-G transport is partially blocked in NIH3T3 cells coexpressing VSV-G and Spir-1-CT (Kerkhoff et al., 2001). This suggests, that Spir plays a role in the regulation of post-Golgi vesicle transport. A possible function for Spir-1 has also been shown in the endocytic pathway. Spir-1 and annexin A2 are required for the nucleation of actin patches on early endosomal structures (Morel et al., 2009).

Although, an interaction of Spir proteins with Rab11a, Rab25 or the Rab11-interacting protein FIP2 could not be detected here (Fig. 4.6 and Fig. 4.7), Spir-2 has an effect on the morphology of Rab11a vesicles. The observed elongation of Rab11a/Spir-2 vesicles indicates an active role for Spir-2 in Rab11a-regulated vesicle transport. Several studies show a cooperation of Rab11a and myosin Vb in recycling processes (Hales et al., 2002, Fan et al., 2004, Swiatecka-Urban et al., 2007, Volpicelli et al., 2002, Chu et al., 2009). A Rab11a/Rab11-FIP2/myosin Vb-complex regulates actin dependent transport of vesicles along the recycling pathway (Hales et al., 2002, Lapierre et al., 2001). Therefore, the recruitment of Spir-2 to Rab11a-positive membranes via binding to myosin Vb, could explain the Spir-2/Rab11a colocalization. This leads to the assumption, that the motor protein myosin Vb is required for Spir-2-driven transport along the Rab11 pathway.

5.1.2 Spir-2 influences the basolateral targeting of E-cadherin in MDCK cells

It has been shown, that the basolateral transport of newly synthesized E-cadherin depends on Rab11a. Overexpression of Rab11 disrupts the localization of E-cadherin, leading to an increased intracellular localization of exogenous E-cadherin in HeLa cells (Lock et al., 2005, Lock and Stow, 2005). E-cadherin-eGFP exits the TGN in elongated, highly motile transport carriers and travels to the plasma membrane by passing Rab11-positive recycling endosomal structures (Lock and Stow, 2005). Considering the observation that Spir-2 alters the morphology of Rab11a-positive structures, leading to highly elongated Spir-2/Rab11a-associated tubular vesicles, suggests that Spir-2 regulates vesicle traffic along that Rab11-pathway. MDCK-cells, which are stably transfected with Myc-Spir-2 show a loss of cell-cell contacts, a mechanism

which is called epithelial-mesenchymal transition (EMT) (Yang and Weinberg, 2008). Analysis of E-cadherin expression revealed that E-cadherin protein levels are highly decreased in this cell line (Fig. 5.2).

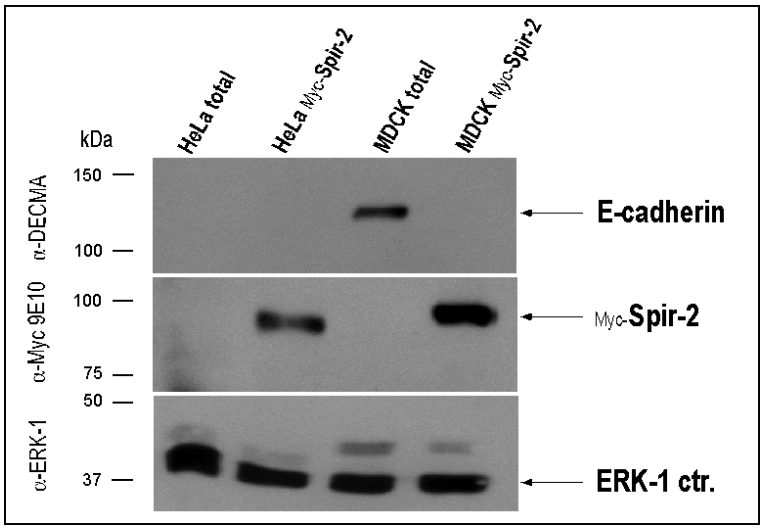

Figure 5.2: **Loss of endogenous E-cadherin in MDCK-Myc-Spir-2 cells**
E-cadherin expression in MDCK-Myc-Spir-2 cell. Endogenous E-cadherin was detected by using an anti-E-cadherin antibody. ERK1 is used as a standard to show that equal amounts of cell lysats are used. A HeLa cell lysat is used as a negative control, due to the fact that HeLa cells don't have endogenous E-cadherin.

The functional loss of E-cadherin is a common feature of EMT (Frixen et al., 1991, Perl et al., 1998, Schmalhofer et al., 2009). The E-cadherin loss is mediated by repression of E-cadherin transcription. Several zinc-finger transcription factors have been found to be capable of repressing E-cadherin transcription, these include Slug, a close relative of Snail (Hajra et al., 2002), and two members of the ZEB family of transcription factors, ZEB1 (dEF1) (Eger et al., 2005) and ZEB2 (SIP1) (Comijn et al., 2001). One additional attractive candidate for downregulation of E-cadherin expression is ß-catenin. The disappearance of E-cadherin from adherens junctions results in the release of its partner, ß-catenin, into the cytosol, which then has the potential to enter the nucleus where it can activate transcription factors, which

are involved in the repression of E-cadherin translation (Schmalhofer et al., 2009). Although, the contribution of the adherens junction-associated ß-catenin pool to transcription is still a matter of debate, several studies suggest that ß-catenin-mediated transcription can induce the expression of Slug (Conacci-Sorrell et al., 2003) and Twist1 (Onder et al., 2008), thereby contributing to the EMT program. A possible explanation for the loss of endogenous E-cadherin in MDCK-Myc-Spir-2 cells is therefore, that increased Spir-2 levels disrupt Rab11-dependent E-cadherin transport. Free ß-catenin could than induce repression of E-cadherin transcription. Moreover, in this study it has been shown, that transfection of eGFP-Rab11a or eGFP-Spir-2 in MDCK cells, leads to an increased intracellular distribution of endogenous E-cadherin (Fig. 5.3), supporting the idea that overexpression of Spir-2 and Rab11a disrupts E-cadherin transport to the plasma membrane.

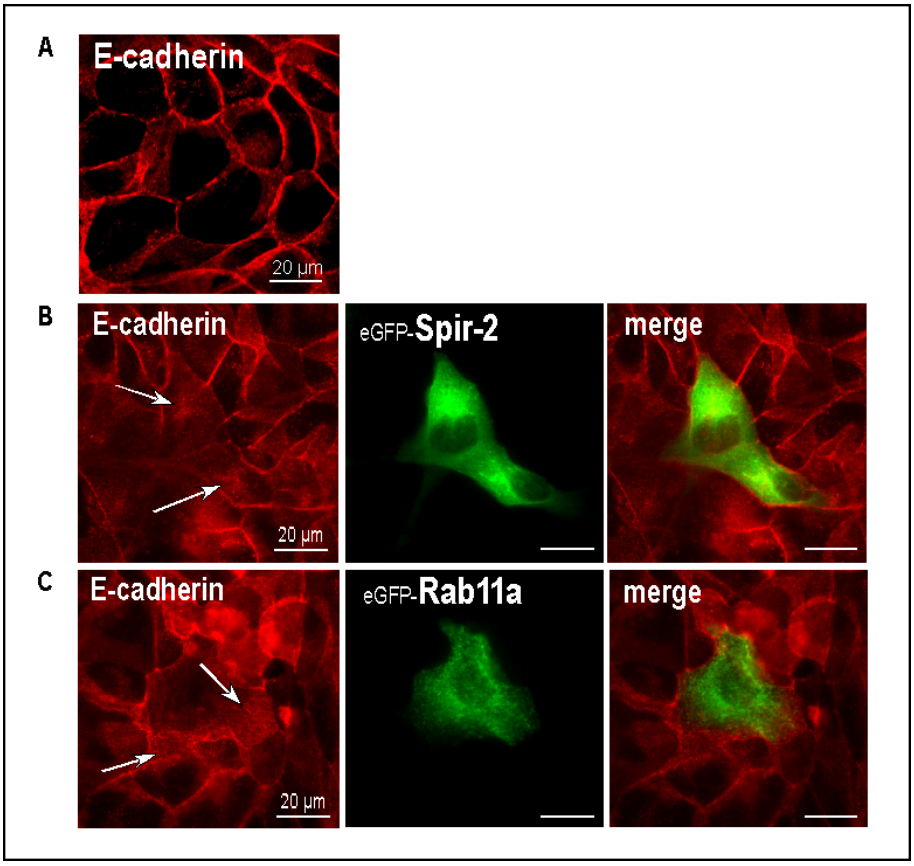

Figure 5.3: **Altered E-cadherin expression**
Endogenous E-cadherin in MDCK cells is localized at the plasma membrane **A**. The localization of E-cadherin was determined by immunostaining (red fluorescence).
Expression of eGFP-Spir-2 **B** and eGFP-Rab11a **C** alter the E-cadherin localization resulting in a more cytoplasmic distribution of the E-cadherin protein (white arrows).

5.1.3 An Arf1/Spir-2 complex is localized to tubular vesicles

The ADP-ribosylation factor (Arf) family of proteins belongs to the Ras superfamily of small G proteins. The first Arf protein was identified as an allosteric activator of cholera toxin ADP-ribosyltransferase activity (Kahn and Gilman, 1984). They have now been shown to regulate vesicular traffic and organelle structure by recruiting coat proteins (Bonifacino and Lippincott-

Schwartz, 2003, Nie et al., 2003), regulating phospholipid metabolism (Matteis et al., 2005, Godi et al., 1999, 2004, Liscovitch et al., 1994, Pertile et al., 1995, Jones et al., 2000a) and modulating the structure of actin (Myers and Casanova, 2008, Cao et al., 2005, Stamnes, 2002, Randazzo and Hirsch, 2004). All Arf proteins are myristoylated at the N-terminus, a lipid modification that is required for biological function of Arf proteins (Antonny et al., 1997, Goldberg, 1998, Franco et al., 1993, Liu et al., 2009). The mechanism by which the myristate functions in Arf membrane binding is not fully understood (Serafini et al., 1991, Franco et al., 1993). A current model suggests that myristoylation contributes to both the regulation of guanine nucleotide exchange and stable membrane association (Liu et al., 2009). There are six Arfs in mammals, which are structurally divided into three classes: class I, Arf1-Arf3, class II, Arf4 and Arf5, class III contains only Arf6 (Wallace et al., 2002, Donaldson and Honda, 2005). Like the Rab small G proteins the Arf proteins cycle between a GTP-bound and GDP-bound conformation. They require accessory proteins to facilitate nucleotide exchange. The hydrolysis of GTP is mediated by GTPase-activating proteins (GAPs), whereas the exchange of GDP for GTP is mediated by guanine-exchange factors (GEFs) (Donaldson and Klausner, 1994, Peyroche et al., 1996, Chardin et al., 1996).

Eukaryotic Arf GEFs can be divided into five families based on their domain organization: Golgi BFA-resistance factor 1/BFA-inhibited GEF (GBF/BIG), Arf nucleotide binding site opener (ARNO)/cytohesin, exchange factor for Arf6 (EFA6), Brefeldin resistant Arf GEF (BRAG) and F-box only protein 8 (FBX8) (Casanova, 2007). All Arf GEFs contain a so called Sec7 domain, which is highly conserved (Jackson and Casanova, 2000). The Sec7 domain is crucial for the activation of Arfs. Most important for the activation of Arf G proteins is one highly conserved glutamate residue at the tip of a hydrophilic loop between helix 6 and 7, referred to as a 'glutamic finger', which is localized in the nucleotide binding fold (Renault et al., 2003, Robert et al., 2004). Binding of a Sec7 domain to an Arf protein results in a rotation of the Arf protein core that drives the nucleotide binding fold into the glutamic finger, thereby displacing the bound GDP (Robert et al., 2004). The fungal toxin Brefeldin A (BFA) inhibits the nucleotide exchange by binding to the Arf-GDP-Sec7 domain complex and prevents the conformational changes necessary to bring the catalytic glutamate into contact with the GDP (Klausner et al., 1992). Mammals express three BFA sensitive Arf GEFs: GBF1, BIG1 and BIG2.

The Arf GAPs could be subdivided into 6 groups according to their domain structure: Arf GAP1/2/3; Git1/2; ASAP1/2/3; ACAP1/2/3; ARAP1/2/3 and AGAP1/2/3 (Randazzo and Hirsch, 2004). Arf GAPs bind to Arf proteins, which results in the hydrolysis of GTP. It has also been shown, that Arf GAPs bind to cargo and coat proteins, suggesting a function for them as subunits of coat proteins rather than simply Arf regulators (Nie et al., 2003, 2005). There is evidence that Arf GAPs are needed for sorting of cargo into vesicles and that Arf GAP activity is sensitive for membrane curvature (Bigay et al., 2003). Until now it is not completely understood how exactly GTP hydrolysis contributes to vesicle formation, cargo sorting and vesicle uncoating (Nie and Randazzo, 2006).

Arf1 is a multifunctional regulator of vesicular traffic, which controls intra-Golgi traffic in addition to TGN to plasma membrane and TGN to endosome/lysosome pathways (Peters et al., 1995, Gu and Gruenberg, 2000). It reversibly associates with Golgi membranes. Furthermore, it has been shown, that Arf1 is also recruited to endosomal membranes (Gu and Gruenberg, 2000), where it regulates transferrin recycling (Volpicelli-Daley et al., 2005). According to the 'myristoyl-GTP switch' model Arf1 is associated with membranes in its activated, GTP-bound conformation, whereas upon inactivation, Arf1 is released from membranes into the cytosol (Serafini et al., 1991). Guanine nucleotide exchange triggers a conformational change in the Arf1 protein which then exposes its N-terminal myristoyl anchor and amphipathic helix, inserting the myristate and the hydrophobic residues of the helix into the membrane (Antonny et al., 1997, Goldberg, 1998). It has been shown that myristoylated Arf1-GDP partially binds to phospholipid membranes (Franco et al., 1995) challenging the proposed 'myristoyl-GTP switch' model. The cycle of association and dissociaton is regulated by several GEFs and GAPs, which are specifically localized to different regions of the Golgi complex and endosomes (Donaldson and Klausner, 1994, Presley et al., 2002, Majoul et al., 2001). Arf1 is crucial for the morphology of the Golgi apparatus. First, it recruits coat proteins to Golgi membranes, such as the coat protein complex I (COPI) (Kartberg et al., 2010) and clathrin through the recruitment of heterotetrameric adaptorprotein (AP-1, AP-3, AP-4) complexes (Donaldson and Klausner, 1994, Faundez et al., 1998, Ooi et al., 1998), as well as monomeric Golgi-localized γ-ear-containing Arf-binding proteins (GGA) (Shiba et al., 2003). Second, Arf1 also regulates the actin cytoskeleton on the Golgi complex. Several actin-binding and actin-regulatory proteins localize to the Golgi (Stamnes, 2002) and some of them rapidly dis-

sociate from the Golgi upon treatment with BFA. Drebrin, mAbp1 and cortactin are recruited to the Golgi upon Arf1 activation (Fucini et al., 2002, Cao et al., 2005). Also the association of Cdc42 is sensitive to BFA (Erickson et al., 1996, Myers and Casanova, 2008).

Arf1 also plays an important role in the regulation of phosphoinositides at the Golgi compartment. It modulates the lipid composition of the Golgi, by stimulating the activity of phospholipidkinases and phospholipase D (Donaldson et al., 2005, Godi et al., 1999, 2004, Haynes et al., 2005). The phosphoinositide kinase PI4K, which phosphorylates PtdIns at the D-4 position generating PtdIns(4)P, is recruitet to Golgi membranes by Arf1 (Godi et al., 1999, Haynes et al., 2005). Furthermore, it has been shown, that Arf1 activates both PLD isoforms but especially PLD1, which is located at endosomes and the Golgi apparatus (Hammond et al., 1995, 1997).

It has been shown that Arf1 induces membrane tubulation of liposomes *in vitro* and Arf1 in its GTP-bound state is associated with curved membrane buds and tubules originating from the Golgi-apparatus (Krauss et al., 2008). The N-terminal amphipathic helix is crucial for this tubulation. This suggests, that Arf1-GTP has the ability to locally induce high curvature in membranes and in this way drives membrane deformation. The membrane tubulation function of Arf1 could be essential for Spir-2-associated tubular vesicles. The observation that Spir-2-ΔKW interacts with Arf1, as shown in co-immunoprecipitation assays, implies, that Arf1 could be required for the recruitment of Spir-2 to tubular vesicle membranes and that recruitment could be regulated by the GTP-GDP cycle of Arf1 by specific Arf GEFs and GAPs. Arf GEFs and GAPs show a specific localization pattern on membrane compartments, which determines the regulation of Arf1 (Donaldson et al., 2005). Thus could also regulate Spir-2 function indirectly.

5.1.4 Spir-2, Arf1 and Rab11a colocalize on the same tubular vesicles

Experimental data of this study have been shown that Spir-2-ΔKW alters the morphology of Rab11a/Spir-2-ΔKW-positive vesicles and it is furthermore colocalized to Arf1 on tubular structures. To check if Spir-2-ΔKW, Arf1 and Rab11a are present on the same tubular membranes a triple coexpression of Myc-Spir-2-ΔKW, eGFP-Arf1 and mStrawberry-Rab11a was performed. Transfected HeLa cells were fixed 24 hours after transfection and Myc-Spir-2-ΔKW was detected with an anti-Myc 9E10 antibody and a polyclonal Cy5-conjugated donkey

anti-mouse secondary antibody. All 3 proteins were found on the same tubular structures (Fig. 5.4), suggesting that the different regulators of vesicle transport processes, small G proteins of the Arf and Rab family together with an actin nucleation factor, Spir-2, mediate vesicle transport along the same pathway.

The Arf GEF BIG2 has been shown to be implicated in the structural integrity of the recycling endosome by activating class I Arfs (Arf1 and Arf3) (Shin et al., 2004, Shen et al., 2006). A catalytically inactive BIG2 mutant selectively induces membrane tubules on recycling endosomes (Shin et al., 2004), implicating a role for BIG2 in maintaining endosome structure. It has been shown, that deletion of BIG2, by siRNA treatment, leads to an increased content of TfR/Tf in Rab11-positive recycling endosomes, suggesting a role for BIG2 in the endocytic pathway (Shen et al., 2006). The Arf1 GAP AGAP2 is involved in retrograde transport of STxB from endosomes to the TGN. It has been shown that depletion of AGAP2 results in an accumulation of STxB in transferrin-positive recycling endosomes (Shiba et al., 2010). If BIG2, AGAP2 or other GEFs and GAPs are implicated in the regulation of Spir-2/Arf1-mediated vesicle transport requires further investigation.

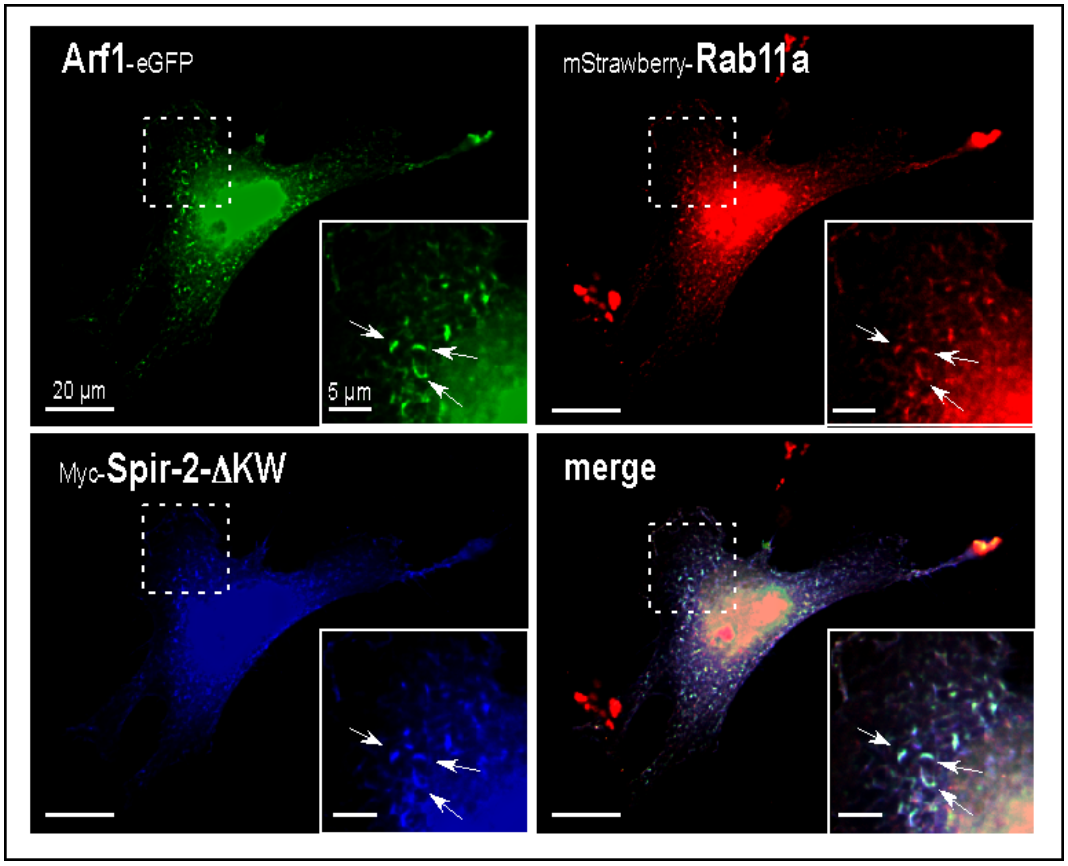

Figure 5.4: **Localization of Arf1, Spir-2-ΔKW and Rab11a on the same tubular vesicles**

HeLa cells were cotransfected with Arf1-eGFP, Myc-Spir-2-ΔKW and mStrawberry-Rab11a, fixed, and Myc-Spir-2-ΔKW was detected with an anti-Myc 9E10 antibody and a secondary Cy5-conjugated anti-mouse IgG antibody (blue fluorescence). The localization of Arf1-eGFP and mStrawberry-Rab11a was determined by GFP and mStrawberry fluorescence. Images were deconvoluted (blind) with the deconvolution software from Leica. 3 tubular vesicles, which are associated with Rab11a, Spir-2-ΔKW and Arf1 are indicated (white arrows).

5.1.5 The Spir-box and FYVE domain containing C-terminus of Spir-2 and Spir-1 is a phospholipid-binding module

FYVE domains are known phospholipid interaction modules, which mediate the binding to phosphatidylinositol 3-phosphat (PtdIns(3)P). In contrast to that, Spir consists of a modified FYVE domain, lacking the basic cluster between cysteines 2 and 3 and having a loop insertion between cysteines 6 and 7. Therefore, it was tempting to speculate that Spir facilitates binding to other phospholipid species than PtdIns(3)P. Experiments of this study show, that Spir-1-ΔKW and Spir-2-ΔKW bind to phosphatidic acid (PA).

The small phospholipid phosphatidic acid is generated by phospholipase D (PLD). PLD1 is found throughout the cell, primarily localizes to perinuclear endosomes and the Golgi apparatus (Brown et al., 1998, Freyberg et al., 2001, Hughes and Parker, 2001). PLD2 is mostly localized at the plasma membrane (Czarny et al., 1999). PA is a versatile second messenger, which plays a role in many cellular processes like membrane trafficking and actin cytoskeleton remodeling (Jenkins and Frohman, 2005). PLD is regulated by protein kinase C isoforms, small G proteins of the Rho and Arf family (Hammond et al., 1995, 1997, Henage et al., 2006, Hiroyama and Exton, 2005, Sung et al., 1999, Frohman et al., 2000) and, particularly, by the phosphoinositide phosphatidylinositol 4,5-bisphosphate (PtdIns(4,5)P_2) (Liscovitch et al., 1994, Pertile et al., 1995). PA stimulates PIP5K, recruits proteins to specific membranes by binding to phospholipid binding-domains, like the PH domain of SOS1 (Zhao et al., 2007), and facilitates membrane curvature. PA favors negatively curved membranes and could therefore play a role in vesicle formation (Roth, 2008).

PA is also localized to the Golgi apparatus. Inhibition of PA generation alters the structure of the Golgi apparatus and blocks TGN exit (Siddhanta et al., 2000). This supports a role for PA in promoting vesicle formation at the TGN. Considering that PA is generated by phospholipase D (PLD), which is activated by Arf proteins (Hammond et al., 1995, 1997, Henage et al., 2006, Hiroyama and Exton, 2005) Arf1 could recruit Spir-2 to membranes in two ways, first, by activation of PA synthesis and second, by binding to Spir-2. PA has a small polar head group and is more stable in a membrane with negative curvature. Therefore it is likely, that PA induces or facilitates negative curvature of membranes. Considering the tubular morphology of Spir-2-associated vesicles, it is possible that Spir-2 is recruited to specific membranes in an Arf1/PA-dependent manner. According to the "coincidence detection code"

model (Paolo and Camilli, 2006) higher affinities and thus more stable protein-membrane interaction could be achieved by parallel binding of two or more factors. Other studies have shown that Arf G proteins promote release of nascent secretory vesicles from the TGN and this depends on an enhancement of PLD activity (Chen and Shields, 1996, Chen et al., 1997).

5.1.6 Spir-2 proteins could perform homotypic and heterotypic interaction via their C-terminal parts

To further elucidate mechanisms in which Spir protein function could be regulated, homo- and hetero-interaction studies were performed. In this study it has been demonstrated that Spir-2 has the ability to directly interact with another Spir-2 protein via its C-terminal part but also with a C-terminally Spir-1 protein. Cotransfection of Spir-2 and Spir-1 proteins in HeLa cells revealed a similar but not identical localization pattern of both proteins. Several structures could be detected, which are Spir-2/Spir-1-positive but there are also several structures, which contain just one of the proteins (Fig. 5.5). The fact that Spir-1 and Spir-2 both show colocalization to Rab11a and display a similar phospholipid binding pattern, suggests that they are recruitet to the same membranes.

Hypothetically, Spir recruitment to membranes could require dimerization, like it has been shown for EEA1, in which the formation of an EEA1 dimer is crucial for the binding to early endosomes (Dumas et al., 2001). Dimerization could also be required for the binding to PA, Arf1 or myosin Vb. Another possibility for the role of Spir dimerization could be, that Spir autoinhibition by binding of the KIND domain to the FYVE domain could be removed. Theoretically, KIND domains and FYVE domains could compete with each other in terms of binding to another FYVE domain. If and in which way dimerization regulates Spir actin nucleation needs further investigation.

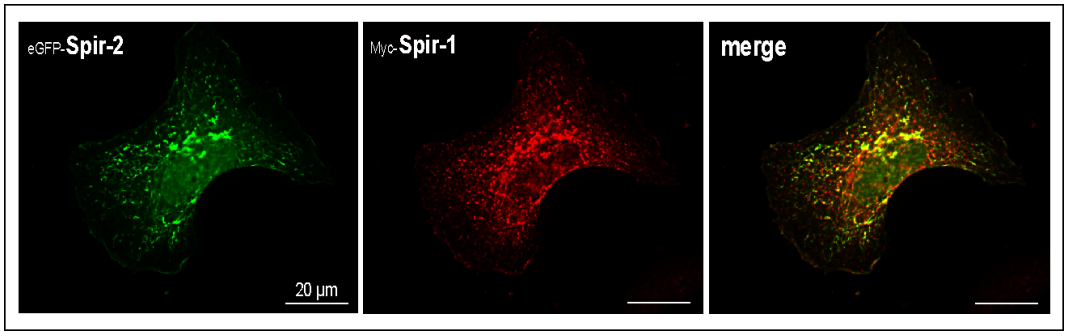

Figure 5.5: **Localization of Spir-2 and Spir-1 in HeLa cells**
HeLa cells were cotransfected with expression vectors directing the expression of eGFP-Spir-2 and Myc-Spir-1. Cells were fixed and protein localization was determined by immunostain experiments. Spir-2 and Spir-1 proteins exhibit a similar cellular localization. Several Spir-2/Spir-1-associated vesicles are present, suggesting a Spir-2/Spir-1 heteromer.

5.1.7 Spir-2 mediated vesicle transport: secretory or endocytic pathway?

Spir-2 regulates vesicle transport in a myosin Vb-dependent manner. The actin-dependent motor protein myosin Vb is implicated in the regulation of recycling traffic together with Rab11a/Rab11-FIP2. Spir-2 also interacts with the small G protein Arf1, which plays a role in the formation of nascent secretory vesicles at intra-Golgi structures and at the TGN (Chen and Shields, 1996, Chen et al., 1997). This raises the question on which pathway Spir-2 acts. Arf1 also regulates the phospholipid environment by activating PLD, thereby generating PA and increasing PIP_2 levels (Hammond et al., 1995, 1997, Jones et al., 2000b). PA is located on membranes with negative curvature and facilitates vesicle formation at the TGN like Arf1 (Siddhanta and Shields, 1998, Siddhanta et al., 2000, Roth, 2008). There are several interconnections between the endocytic and the secretory pathway. The TGN, as an important sorting station for secreted proteins also receives retrograde membrane traffic (Gleeson et al., 2004, Bonifacino and Rojas, 2006). The proposed 'tubular endosomal network' (Bonifacino and Rojas, 2006), challenges the idea in which the endosomal system has a stable appearance. That new model proposes an endosomal network consisting of several specific domains with various connections to specific target membrane compartments, for example the TGN.

There are two independent retrograde pathways from early endosomes to the TGN. On the one hand traffic from early endosomes to the Golgi via late endosomes, using cation-independent mannose 6-phosphate receptor (CI-MPR) as a marker (Lombardi et al., 1993, Ganley et al., 2004, Pfeffer, 2009), otherwise there is also a direct route from early endosomes to the Golgi. Shiga toxin B-fragment (STxB) and TGN38 use this pathway (Mallard et al., 1998, Ghosh et al., 1998, Pfeffer, 2009). Clathrin/AP-1 coats may be involved in retrograde as well as anterograde transport between TGN and endosomes. Previous studies have indicated a role for clathrin, the clathrin adaptor AP-1 and the retromer complex in retrograde sorting from early/recycling endosomes to the TGN. (Popoff et al., 2007, Natsume et al., 2006). Depletion of clathrin results in the accumulation of STxB in recycling endosomes. Traffic through the early/recyling endosome to TGN pathway could pass Rab11-positive recycling endosomal structures. Overexpression of Rab11 mutants affects the transport of STxB to the TGN (Wilcke et al., 2000). Rab11a/b and its binding protein FIP1/RCP are required for the retrograde delivery of TGN38 and Shiga toxin from early/recycling endosomes to the TGN, but not for the retrieval of cation-independent mannose 6-phosphate receptor from late endosomes (Jing et al., 2010). Arf1 and its GAP AGAP2 have also been shown to be involved in retrograde transport processes from endosomes to the TGN (Shiba et al., 2010). AGAP2 depletion results in an accumulation of STxB in transferrin-positive recycling endosomes (Shiba et al., 2010).

It has been shown that Rab11 is also involved in the exit of membranes from the recycling endosome (Wilcke et al., 2000), and that an intact microtubule cytoskeleton is necessary for that vesicle transport. Spir-2 and Rab11a are located at the same vesicles and Spir-2 alters the morphology of Rab11a-associated vesicles. Moreover, elongation of Spir-2 vesicles is also microtubule-dependent, suggesting that Spir-2 together with Rab11a and/or Arf1 maybe regulate retrograde transport from endosomal structures back to the TGN, or could be crucial for the maintainance of the 'tubular endosomal network' by regulating vesicle fusion and/or fission of that membraneous structure. Arf1 could be the crucial factor for Spir-2 recruitment to PA-enriched membranes. Spir-2 could furthermore be involved in basolateral transport of E-cadherin. E-cadherin is transported from the TGN to the plasma membrane by passing recycling endosomal structures (Lock and Stow, 2005, Lock et al., 2005), respectively Rab11-positive compartments of the 'tubular endosomal network'. Moreover, it remains an open

question, if Spir-2 regulates TGN to endosome traffic, exit of vesicles from endosomes, such as retrograde traffic from endosomal structures to the TGN, or anterograde traffic from endosomes to the plasma membrane.

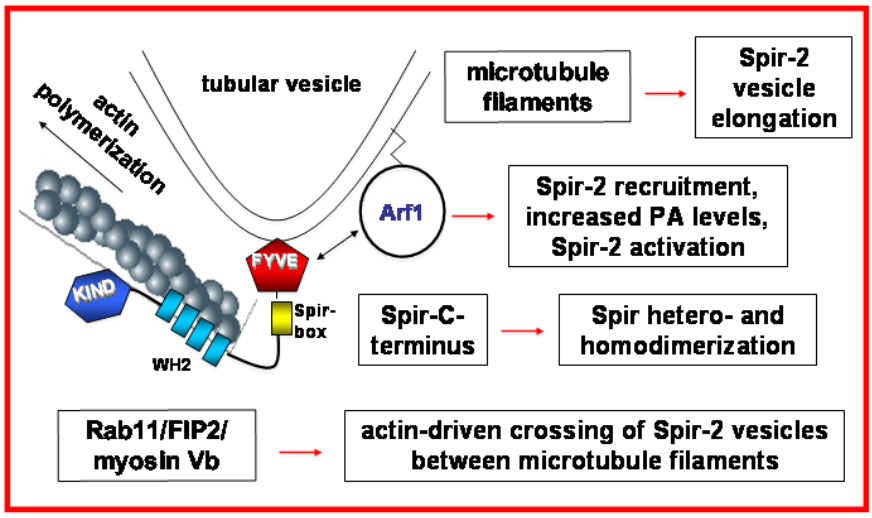

Figure 5.6: **Model of Spir-2 recruitment to intracellular membranes**
The C-terminal part of Spir-2, consisting of the Spir-box and the modified FYVE zinc finger is crucial for the membrane targeting and therefore for the function of Spir proteins in vesicle transport processes. Arf1 regulates PA synthesis at membranes by activating PLD and has the ability to locally induce high curvature in membranes and in this way drives membrane deformation. The membrane tubulation function of Arf1 could be essential for Spir-2-associated tubular vesicles. Arf1 could be required for the recruitment of Spir-2 to tubular vesicle membranes and that recruitment could be regulated by the GTP-GDP cycle of Arf1 by specific Arf GEFs and GAPs. The actin and the microtubule cytoskeleton has an important impact on Spir-2-mediated vesicle transport processes. An intact microtubule cytoskeleton is necessary for the elongation of Spir-2-associated tubular vesicles. It was found that actin is still present on the WH2-domain deficient Spir-2-ΔKW vesicles and Spir-2-ΔKW is in a complex with the actin-dependent motor protein myosin Vb. Spir-2 vesicles move along microtubule filaments, branch and fuse with each other, and have the ability to switch to another microtubule filament. The actin cytoskeleton is supposed to be crucial for the crossing of those Spir-2 vesicles from one microtubule filament to another.

Appendix I Supplemental table I: Primersequences

All primers were acquired from MWG BIOTECH of standard HPSF quality, diluted in H_2O to 10 pm/µl and stored at -20°C.

Primer name	Sequence 5'-3'	annotation
NcoI mSpir-1-CT long 5'	5' CATG CCATGG GA CCA GAA GAA ATT AGA CGG AGC 3'	cloning of pProEX HTb-mm-Spir-1-ΔKW
m-Spir-1-CT XhoI 3'	5' CCG CTCGAG TCA GAT CTC GTT GAT AGT CCG 3'	
BamHI Myc hSpir2 375 st 5'	5' GC GGATCC GCC GCC GCC ATG GAG CAG AAG CTG ATC TCC GAG GAG GAC CTG ATC CTC AAC GCC TGC TCC 3'	cloning of pcDNA3-Myc-hs-Spir-2-ΔKW
hSpir2 375 EcoRV 3'	5' GATATC TCA CTT GAA GTC AAG AGT CCT GGT 3'	
EcoRI hFIP2 5'	5' CG GAATTC T ATG ATG CTG TCC GAG CAA GCC 3'	cloning of pEGFP-C1-hs-FIP2
hFIP2 BamHI 3'	5'CG GGATCC TTA ACT GTT AGAGAA TTT GCC AGC TTT TCC 3'	

HindIII hMyoVb 5'	5' CCC AAGCTT C GAG GCC CGC TCA GCA GAG 3'	cloning of mStrawberry-hs-MyoVb tail
hMyoVb XbaI 3'	5' GC TCTAGA GAC TTC ATT GAG GAA TTC CAG ATT 3'	
KpnI hArf1 st5'	5' GG GGTACC GCC GCC GCC ATG GGG AAC ATC TTC GCC AAC CTC 3'	cloning of pEGFP-N3-hs-Arf1
hArf1end BamHI3'	5' CG GGATCC CTT CTG GTT CCG GAG CTG ATT 3'	

Appendix II Supplemental table II: Construct overview

Construct	Description	Fragment boundaries (Restriction sites)	Purification	Purpose
pcDNA3-Myc-hs-Spir-2-ΔKW	Myc-Spir-2-ΔKW	aa 388-728 BamHI/EcoRI		cell imaging, co-immuno-precipitation
pEGFP-N3-hs-Arf1	Arf1-eGFP	KpnI/BamHI		cell imaging, co-immuno-precipitation
pEGFP-C1-hs-Spir-2	eGFP-Spir-2	BamHI/XbaI		cell imaging
pEGFP-C1-hs-Spir-2-ΔKW	eGFP-Spir-2-ΔKW	aa 375-728 EcoRI/XbaI		cell imaging
pEGFP-C1-hs-Spir-2-ΔKIND	eGFP-Spir-2-ΔKIND	aa 244-728 EcoRI/KpnI		cell imaging
pEGFP-C1-hs-Rab11-FIP2	eGFP-Rab11-FIP2	EcoRI/BamHI		co-immuno-precipitation
mStrawberry-hs-MyoVb-cc-tail	mStrawberry-MyoVb-cc-tail	aa 909-1849 HindIII/XbaI		cell imaging, co-immuno-precipitation
pEGFP-cl-Rab11a (kindly provided by Marino Zerial)	eGFP-Rab11a			cell imaging co-immuno-precipitation
mStrawberry-mm-Rab11a	mStrawberry-Rab11a	EcoRI/BamHI		cell imaging co-immuno-precipitation

mStrawberry-mm-Rab25	mStrawberry-Rab25	EcoRI/XbaI		co-immuno-precipitation
mStrawberry-mm-Rab6a (pEGFP-C2 vector backbone)	mStrawberry-Rab6a	EcoRI/BamHI		cell imaging
pEGFP-C1-Spir-1-FYVE	eGFP-Spir-1-FYVE	aa 586-715 XhoI/BamHI		cell imaging
pcDNA3-Myc-Spir-1-KIND-CAAX	Myc-Spir-1-KIND-CAAX	BamHI/EcoRI		cell imaging
pGEX-4T-3-hs-Spir-2-ΔKW	GST-Spir-2-ΔKW	aa 375-728 BamHI/XhoI	Glutathione Sepharose 4b resin (*Amersham*)	pull down, phospholipid overlay assay
pProEX HTb-mm-Spir-1-ΔKW	6xHis-Spir-1-ΔKW	aa 160-515 NcoI/XhoI	Ni-NTA matrix (*Qiagen*)	pull down, phospholipid overlay assay
pProEX HTb-hs-Spir-2-ΔKW	6xHis-Spir-2-ΔKW	aa 375-728 BamHI/XhoI	Ni-NTA matrix (*Qiagen*)	pull down, phospholipid overlay assay
pProEX HTb-hs-SOS1-PH	6xHis-SOS1-PH	aa 422-551 BamHI/XhoI	Ni-NTA matrix (*Qiagen*)	phospholipid overlay assay

Appendix III Lebenslauf

Persönliche Daten

Name	Sabine Weiß
Geburtsort	Suhl
Geburtsdatum	25.09.1981

Ausbildung

1992-2000	Carl-Fiedler-Gymnasium (Allgemeine Hochschulreife)
2000-2006	Studium der Biologie an der Julius-Maximilians-Universität Würzburg Akademischer Grad: Diplom Biologin; Abschlussnote: sehr gut Schwerpunkt: Genetik (Hauptfach), Neurobiologie und Bioinformatik (Nebenfächer) Thema der Diplomarbeit: „Untersuchungen zur Expression und Funktion der *Drosophila melanogaster* Aktinorganisatoren p150 Spir und Cappuccino" Prof. Dr. Thomas Raabe
2006-2007	Beginn der Dissertation, Universität Würzburg, Institut für medizinische Strahlenkunde und Zellforschung
2007-2011	Universität Regensburg, Institut für funktionelle Genomik Prof. Dr. Eugen Kerkhoff

List of Abbreviations

ACAP Arf GAP with coiled-coil domains, ANK repeats and PH domain

ADF actin-depolymerizing factor

AGAP Arf GAP with GLD domain, ANK repeats and PH domain

AMPA alpha-amino-3-hydroxy-5-methyl-4-isoxazolepropionic acid receptor

AP-1,-2,-3,-4 adaptorprotein 1, 2, 3 and 4

APS Ammonium persulfate

ARAP Arf GAP with Rho GAP domain, ANK repeats and PH domain

Arf ADP-ribosylation factor

ARNO Arf nucleotide binding site opener

Arp2/3 actin-related protein 2 and 3

ASAP Arf GAP with SH3 domain, ANK repeats and PH domain

BCP 1-bromo-3-chloropropane

BFA Brefeldin A

ADP adenosin diphosphate

ATP adenosin triphosphate

eGFP enhanced green fluorescent protein

FYVE Fab1p, YOTB, Vac1p, EEA1

GST glutathione S-transferase

KIND kinase noncatalytical C-lobe domain

bp base pairs

BRAG Brefeldin resistant Arf GEF

BSA Bovine serum albumin

CAAX 'C' is Cysteine, 'A' is an aliphatic amino acid, and 'X' is variable

Capu Cappuccino

Cdc42 Cell division cycle 42

cDNA complementary DNA

CI-MPR cation-independent mannose 6-phosphate receptor

Co-IP co-immunoprecipitation

Cobl Cordon-bleu

COPI/II coat protein complex I and II

Cy5 Cyanine 5

DAAM dishevelled-associated activator of morphogenesis

DAD diaphanous autoregulatory domain

DEPC Diethyl Pyrocarbonate

Dia diaphanous

DID diaphanous inhibitory domain

DMEM Dulbecco's modified Eagle's medium

DMSO Dimethyl Sulfoxide

DNA Deoxyribonucleic acid

E-cadherin epithelial cadherin

E. coli Escherichia coli

ECL enhanced chemiluminescent light detection

EDTA Ethylenediaminetetraacetic acid

EEA1 early endosome antigen 1

EFA6 exchange factor for Arf6

EMT epithelial-mesenchymal transition

ERK1 extracellular-signal-regulated kinase 1

ERM Ezrin Radixin Moesin

F-actin filamentous actin

FBX8 F-box only protein 8

Fc-region fragment crystallizable region

FCS fetal calf serum

FH1 formin homology 1

FH2 formin homology 2

FHOD formin homology domain-containing protein

FIP2 family of interacting proteins

FITC Fluorescin isothiocyanate

FRL formin-related gene in leukocytes

FSI formin-Spir-interaction site

G proteins guanine nucleotide-binding proteins

G-actin globular actin

GAP GTPase-activating protein

GDF GDI-displacement factor

GDI GDP-dissociation inhibitor

GDP Guanosine diphosphate

GEF guanine nucleotide exchange factor

GGA Golgi-localized gamma-ear-containing Arf-binding protein

GGTase geranylgeranyltransferase

Glu Glutamate

GST glutathione S-transferase

GTP Guanosine-5'-triphosphate

HEK 293 human embryonic kidney 293 cells

HeLa an immortal cell line derived from cervical cancer cells taken from Henrietta Lacks

HEPES 4-(2-hydroxyethyl)-1-piperazineethanesulfonic acid

His Histidine

HRP horseradish peroxidase

IgG Immunoglobulin G

INF1/2 inverted formin 1 and 2

IP Immunoprecipitation

IPTG Isopropyl beta-D-1-thiogalactopyranoside

JMY junction-mediating regulatory protein

kb kilo bases

kDa kilo Dalton

L-3 linker region 3

LB luria bertani

Lmod-2 Leiomodin-2

LTP long-term potentiation

mA milliampere

mAbp1 mammalian actin-binding protein 1

MCS multiple cloning site

MDCK Madin-Darby canine kidney epithelial cell line

ml milliliter

mM millimolar

MOPS 3-(N-Morpholino)propanesulfonic acid

MWCO molecular-weight cutoff

NEB New England Biolabs

Ni-NTA nickel-nitrilotriacetic acid

NPF nucleation promoting factor

OD Optical density

PA phosphatidic acid

PAGE Polyacrylamide gel electrophoresis

PBS phosphate buffered saline

PCR polymerase chain reaction

Pen Penicillin

PFA Paraformaldehyde

Pfu Pyrococcus furiosus

PLD phospholipase D

PtdIns(3)P Phosphatidyl 3-phosphat

PtdIns(3,4)P2 Phosphatidyl 3,4-bisphosphat

PtdIns(3,4,5)P3 Phosphatidyl 3,4,5-trisphosphat

PtdIns(3,5)P2 Phosphatidyl 3,5-bisphosphat

PtdIns(4)P Phosphatidyl 4-phosphat

PtdIns(4,5)P2 Phosphatidyl 4,5-bisphosphat

PtdIns(5)P Phosphatidyl 5-phosphat

Rab Ras-related in brain

RBD Rab Binding Domain

RCP Rab coupling protein

REP Rab escort protein

rpm rounds per minute

RT-PCR Reverse transcriptase PCR

SCAR suppressor of cAMP receptor

SDS Sodium dodecyl sulfate

SH3 SRC homology 3

SOS1 son of sevenless 1

Strep Streptomycin

STxB Shiga toxin B

Taq Thermus aquaticus

TARP translocated actin recruiting phosphoprotein

TBST Tris-Buffered Saline-Tween

TEMED Tetramethylethylenediamine

Tf Transferrin

TfR Transferrin receptor

TGN trans-Golgi network

TRITC Tetramethyl Rhodamine Isothiocyanate

tRNA transfer RNA

VSV-G Vesicular stomatitis virus glycoprotein

WASH WASP and SCAR homologue

WASP Wiskott-Aldrich syndrome protein

WAVE WASp family verprolin homologous protein

WB Western Blot

WH2 WASP-homology

WHAMM Wiskott Aldrich syndrome protein homologue associated with actin, golgi membranes and microtubules

WHIF1 WH2 domain-containing formin 1

ZEB1/2 Zinc finger E-box-binding homeobox 1 and 2

^{o}C degree Celsius

Bibliography

R Agarwal, I Jurisica, GB Mills, and KW Cheng. The emerging role of the RAB25 small GTPase in cancer. *Traffic*, 10(11):1561–8, 2009.

Rashmi Ahuja, Roser Pinyol, Nicole Reichenbach, Laura Custer, John Klingensmith, Michael M Kessels, and Britta Qualmann. Cordon-bleu is an actin nucleation factor and controls neuronal morphology. *Cell*, 131(2):337–50, 2007.

K Alexandrov, H Horiuchi, O Steele-Mortimer, MC Seabra, and M Zerial. Rab escort protein-1 is a multifunctional protein that accompanies newly prenylated rab proteins to their target membranes. *EMBO J*, 13(22):5262–73, 1994.

B Antonny, S Beraud-Dufour, P Chardin, and M Chabre. N-terminal hydrophobic residues of the G-protein ADP-ribosylation factor-1 insert into membrane phospholipids upon GDP to GTP exchange. *Biochemistry*, 36(15):4675–84, 1997.

Jessica Azoury, Karen W Lee, Virginie Georget, Pascale Rassinier, Benjamin Leader, and Marie-Helene Verlhac. Spindle positioning in mouse oocytes relies on a dynamic meshwork of actin filaments. *Curr Biol*, 18(19):1514–9, 2008.

J A Barden, M Miki, B D Hambly, and C G Dos Remedios. Localization of the phalloidin and nucleotide-binding sites on actin. *Eur J Biochem*, 162(3):583–8, 1987.

F Barr and DG Lambright. Rab GEFs and GAPs. *Curr Opin Cell Biol*, 22(4):461–70, 2010.

S G Bhartur, B C Calhoun, J Woodrum, J Kurkjian, S Iyer, F Lai, and J R Goldenring. Genomic structure of murine Rab11 family members. *Biochem Biophys Res Commun*, 269 (2):611–7, 2000.

Joelle Bigay, Pierre Gounon, Sylviane Robineau, and Bruno Antonny. Lipid packing sensed by ArfGAP1 couples COPI coat disassembly to membrane bilayer curvature. *Nature*, 426 (6966):563–6, 2003.

L Blanchoin and TD Pollard. Mechanism of interaction of Acanthamoeba actophorin (ADF/Cofilin) with actin filaments. *J Biol Chem*, 274(22):15538–46, 1999.

L Blanchoin and TD Pollard. Hydrolysis of ATP by polymerized actin depends on the bound divalent cation but not profilin. *Biochemistry*, 41(2):597–602, 2002.

L Blanchoin, TD Pollard, and RD Mullins. Interactions of ADF/cofilin, Arp2/3 complex, capping protein and profilin in remodeling of branched actin filament networks. *Curr Biol*, 10(20):1273–82, 2000.

JS Bonifacino and J Lippincott-Schwartz. Coat proteins: shaping membrane transport. *Nat Rev Mol Cell Biol*, 4(5):409–14, 2003.

Juan S Bonifacino and Raul Rojas. Retrograde transport from endosomes to the trans-Golgi network. *Nat Rev Mol Cell Biol*, 7(8):568–79, 2006.

JL Bos, H Rehmann, and A Wittinghofer. GEFs and GAPs: critical elements in the control of small G proteins. *Cell*, 129(5):865–77, 2007.

F D Brown, N Thompson, K M Saqib, J M Clark, D Powner, N T Thompson, R Solari, and M J Wakelam. Phospholipase D1 localises to secretory granules and lysosomes and is plasma-membrane translocated on cellular stimulation. *Curr Biol*, 8(14):835–8, 1998.

C G Burd and S D Emr. Phosphatidylinositol(3)-phosphate signaling mediated by specific binding to RING FYVE domains. *Mol Cell*, 2(1):157–62, 1998.

BC Calhoun, LA Lapierre, CS Chew, and JR Goldenring. Rab11a redistributes to apical secretory canaliculus during stimulation of gastric parietal cells. *Am J Physiol*, 275(1 Pt 1): C163–70, 1998.

Kenneth G Campellone, Neil J Webb, Elizabeth A Znameroski, and Matthew D Welch. WHAMM is an Arp2/3 complex activator that binds microtubules and functions in ER to Golgi transport. *Cell*, 134(1):148–61, 2008.

Hong Cao, Shaun Weller, James D Orth, Jing Chen, Bing Huang, Ji-Long Chen, Mark Stamnes, and Mark A McNiven. Actin and Arf1-dependent recruitment of a cortactin-dynamin complex to the Golgi regulates post-Golgi transport. *Nat Cell Biol*, 7(5):483–92, 2005.

MF Carlier, D Pantaloni, JA Evans, PK Lambooy, ED Korn, and MR Webb. The hydrolysis of ATP that accompanies actin polymerization is essentially irreversible. *FEBS Lett*, 235 (1-2):211–4, 1988.

MF Carlier, V Laurent, J Santolini, R Melki, D Didry, GX Xia, Y Hong, NH Chua, and D Pantaloni. Actin depolymerizing factor (ADF/cofilin) enhances the rate of filament turnover: implication in actin-based motility. *J Cell Biol*, 136(6):1307–22, 1997.

Elizabeth A Carroll, Dianne Gerrelli, Stephan Gasca, Elizabeth Berg, David R Beier, Andrew J Copp, and John Klingensmith. Cordon-bleu is a conserved gene involved in neural tube formation. *Dev Biol*, 262(1):16–31, 2003.

JE Casanova. Regulation of Arf activation: the Sec7 family of guanine nucleotide exchange factors. *Traffic*, 8(11):1476–85, 2007.

P J Casey and M C Seabra. Protein prenyltransferases. *J Biol Chem*, 271(10):5289–92, 1996.

PT Caswell, HJ Spence, M Parsons, DP White, K Clark, KW Cheng, GB Mills, MJ Humphries, AJ Messent, KI Anderson, MW McCaffrey, BW Ozanne, and JC Norman. Rab25 associates with alpha5beta1 integrin to promote invasive migration in 3D microenvironments. *Dev Cell*, 13(4):496–510, 2007.

PT Caswell, M Chan, AJ Lindsay, MW McCaffrey, D Boettiger, and JC Norman. Rab-coupling protein coordinates recycling of alpha5beta1 integrin and EGFR1 to promote cell migration in 3D microenvironments. *J Cell Biol*, 183(1):143–55, 2008.

P Chardin, S Paris, B Antonny, S Robineau, S Beraud-Dufour, C L Jackson, and M Chabre. A human exchange factor for ARF contains Sec7- and pleckstrin-homology domains. *Nature*, 384(6608):481–4, 1996.

P Chavrier, J P Gorvel, E Stelzer, K Simons, J Gruenberg, and M Zerial. Hypervariable C-terminal domain of rab proteins acts as a targeting signal. *Nature*, 353(6346):769–72, 1991.

W Chen, Y Feng, D Chen, and A Wandinger-Ness. Rab11 is required for trans-golgi network-to-plasma membrane transport and a preferential target for GDP dissociation inhibitor. *Mol Biol Cell*, 9(11):3241–57, 1998.

Y G Chen and D Shields. ADP-ribosylation factor-1 stimulates formation of nascent secretory vesicles from the trans-Golgi network of endocrine cells. *J Biol Chem*, 271(10):5297–300, 1996.

Y G Chen, A Siddhanta, C D Austin, S M Hammond, T C Sung, M A Frohman, A J Morris, and D Shields. Phospholipase D stimulates release of nascent secretory vesicles from the trans-Golgi network. *J Cell Biol*, 138(3):495–504, 1997.

KW Cheng, JP Lahad, WL Kuo, A Lapuk, K Yamada, N Auersperg, J Liu, K Smith-McCune, KH Lu, D Fishman, JW Gray, and GB Mills. The RAB25 small GTPase determines aggressiveness of ovarian and breast cancers. *Nat Med*, 10(11):1251–6, 2004.

David Chereau, Frederic Kerff, Philip Graceffa, Zenon Grabarek, Knut Langsetmo, and Roberto Dominguez. Actin-bound structures of Wiskott-Aldrich syndrome protein (WASP)-homology domain 2 and the implications for filament assembly. *Proc Natl Acad Sci U S A*, 102(46):16644–9, 2005.

David Chereau, Malgorzata Boczkowska, Aneta Skwarek-Maruszewska, Ikuko Fujiwara, David B Hayes, Grzegorz Rebowski, Pekka Lappalainen, Thomas D Pollard, and Roberto Dominguez. Leiomodin is an actin filament nucleator in muscle cells. *Science*, 320(5873): 239–43, 2008.

MA Chesarone and BL Goode. Actin nucleation and elongation factors: mechanisms and interplay. *Curr Opin Cell Biol*, 21(1):28–37, 2009.

Bei-Bei Chu, Liang Ge, Chang Xie, Yang Zhao, Hong-Hua Miao, Jing Wang, Bo-Liang Li, and Bao-Liang Song. Requirement of myosin Vb.Rab11a.Rab11-FIP2 complex in cholesterol-

regulated translocation of NPC1L1 to the cell surface. *J Biol Chem*, 284(33):22481–90, 2009.

Francesca D Ciccarelli, Peer Bork, and Eugen Kerkhoff. The KIND module: a putative signalling domain evolved from the C lobe of the protein kinase fold. *Trends Biochem Sci*, 28(7):349–52, 2003.

J Comijn, G Berx, P Vermassen, K Verschueren, L van Grunsven, E Bruyneel, M Mareel, D Huylebroeck, and F van Roy. The two-handed E box binding zinc finger protein SIP1 downregulates E-cadherin and induces invasion. *Mol Cell*, 7(6):1267–78, 2001.

Maralice Conacci-Sorrell, Inbal Simcha, Tamar Ben-Yedidia, Janna Blechman, Pierre Savagner, and Avri Ben-Ze'ev. Autoregulation of E-cadherin expression by cadherin-cadherin interactions: the roles of beta-catenin signaling, Slug, and MAPK. *J Cell Biol*, 163(4): 847–57, 2003.

J A Cooper. Effects of cytochalasin and phalloidin on actin. *J Cell Biol*, 105(4):1473–8, 1987.

M Czarny, Y Lavie, G Fiucci, and M Liscovitch. Localization of phospholipase D in detergent-insoluble, caveolin-rich membrane domains. Modulation by caveolin-1 expression and caveolin-182-101. *J Biol Chem*, 274(5):2717–24, 1999.

Katja Dahlgaard, Alexandre A S F Raposo, Teresa Niccoli, and Daniel St Johnston. Capu and Spire assemble a cytoplasmic actin mesh that maintains microtubule organization in the Drosophila oocyte. *Dev Cell*, 13(4):539–53, 2007.

D Deretic. Rab proteins and post-Golgi trafficking of rhodopsin in photoreceptor cells. *Electrophoresis*, 18(14):2537–41, 1997.

Marion Desclozeaux, Juliana Venturato, Fiona G Wylie, Jason G Kay, Shannon R Joseph, Huong T Le, and Jennifer L Stow. Active Rab11 and functional recycling endosome are required for E-cadherin trafficking and lumen formation during epithelial morphogenesis. *Am J Physiol Cell Physiol*, 295(2):C545–56, 2008.

M Dettenhofer, F Zhou, and P Leder. Formin 1-isoform IV deficient cells exhibit defects in cell spreading and focal adhesion formation. *PLoS One*, 3(6):e2497, 2008.

A B Dirac-Svejstrup, T Sumizawa, and S R Pfeffer. Identification of a GDI displacement factor that releases endosomal Rab GTPases from Rab-GDI. *EMBO J*, 16(3):465–72, 1997.

R Dominguez. Actin-binding proteins–a unifying hypothesis. *Trends Biochem Sci*, 29(11): 572–8, 2004.

R Dominguez. The beta-thymosin/WH2 fold: multifunctionality and structure. *Ann N Y Acad Sci*, 1112:86–94, 2007.

R Dominguez and KC Holmes. Actin Structure And Function. *Annu Rev Biophys*, 2010.

J G Donaldson and R D Klausner. ARF: a key regulatory switch in membrane traffic and organelle structure. *Curr Opin Cell Biol*, 6(4):527–32, 1994.

JG Donaldson and A Honda. Localization and function of Arf family GTPases. *Biochem Soc Trans*, 33(Pt 4):639–42, 2005.

Julie G Donaldson, Akira Honda, and Roberto Weigert. Multiple activities for Arf1 at the Golgi complex. *Biochim Biophys Acta*, 1744(3):364–73, 2005.

J J Dumas, E Merithew, E Sudharshan, D Rajamani, S Hayes, D Lawe, S Corvera, and D G Lambright. Multivalent endosome targeting by homodimeric EEA1. *Mol Cell*, 8(5):947–58, 2001.

S Eathiraj, X Pan, C Ritacco, and DG Lambright. Structural basis of family-wide Rab GTPase recognition by rabenosyn-5. *Nature*, 436(7049):415–9, 2005.

J Edwards. Are beta-thymosins WH2 domains? *FEBS Lett*, 573(1-3):231–2; author reply 233, 2004.

Andreas Eger, Kirsten Aigner, Stefan Sonderegger, Brigitta Dampier, Susanne Oehler, Martin Schreiber, Geert Berx, Amparo Cano, Hartmut Beug, and Roland Foisner. DeltaEF1 is a transcriptional repressor of E-cadherin and regulates epithelial plasticity in breast cancer cells. *Oncogene*, 24(14):2375–85, 2005.

S Emmons, H Phan, J Calley, W Chen, B James, and L Manseau. Cappuccino, a Drosophila maternal effect gene required for polarity of the egg and embryo, is related to the vertebrate limb deformity locus. *Genes Dev*, 9(20):2482–94, 1995.

J W Erickson, C j Zhang, R A Kahn, T Evans, and R A Cerione. Mammalian Cdc42 is a brefeldin A-sensitive component of the Golgi apparatus. *J Biol Chem*, 271(43):26850–4, 1996.

Guo-Huang Fan, Lynne A Lapierre, James R Goldenring, Jiqing Sai, and Ann Richmond. Rab11-family interacting protein 2 and myosin Vb are required for CXCR2 recycling and receptor-mediated chemotaxis. *Mol Biol Cell*, 15(5):2456–69, 2004.

V Faundez, JT Horng, and RB Kelly. A function for the AP3 coat complex in synaptic vesicle formation from endosomes. *Cell*, 93(3):423–32, 1998.

M Franco, P Chardin, M Chabre, and S Paris. Myristoylation is not required for GTP-dependent binding of ADP-ribosylation factor ARF1 to phospholipids. *J Biol Chem*, 268 (33):24531–4, 1993.

M Franco, P Chardin, M Chabre, and S Paris. Myristoylation of ADP-ribosylation factor 1 facilitates nucleotide exchange at physiological Mg2+ levels. *J Biol Chem*, 270(3):1337–41, 1995.

Z Freyberg, D Sweeney, A Siddhanta, S Bourgoin, M Frohman, and D Shields. Intracellular localization of phospholipase D1 in mammalian cells. *Mol Biol Cell*, 12(4):943–55, 2001.

UH Frixen, J Behrens, M Sachs, G Eberle, B Voss, A Warda, D Loechner, and W Birchmeier. E-cadherin-mediated cell-cell adhesion prevents invasiveness of human carcinoma cells. *J Cell Biol*, 113(1):173–85, 1991.

MA Frohman, Y Kanaho, Y Zhang, and AJ Morris. Regulation of phospholipase D1 activity by Rho GTPases. *Methods Enzymol*, 325:177–89, 2000.

Raymond V Fucini, Ji-Long Chen, Catherine Sharma, Michael M Kessels, and Mark Stamnes. Golgi vesicle proteins are linked to the assembly of an actin complex defined by mAbp1. *Mol Biol Cell*, 13(2):621–31, 2002.

T Fujii, AH Iwane, T Yanagida, and K Namba. Direct visualization of secondary structures of F-actin by electron cryomicroscopy. *Nature*, 467(7316):724–8, 2010.

Mitsunori Fukuda. Versatile role of Rab27 in membrane trafficking: focus on the Rab27 effector families. *J Biochem*, 137(1):9–16, 2005.

IG Ganley, K Carroll, L Bittova, and S Pfeffer. Rab9 GTPase regulates late endosome size and requires effector interaction for its stability. *Mol Biol Cell*, 15(12):5420–30, 2004.

S Gasca, D P Hill, J Klingensmith, and J Rossant. Characterization of a gene trap insertion into a novel gene, cordon-bleu, expressed in axial structures of the gastrulating mouse embryo. *Dev Genet*, 17(2):141–54, 1995.

J M Gaullier, A Simonsen, A D'Arrigo, B Bremnes, H Stenmark, and R Aasland. FYVE fingers bind PtdIns(3)P. *Nature*, 394(6692):432–3, 1998.

R N Ghosh, W G Mallet, T T Soe, T E McGraw, and F R Maxfield. An endocytosed TGN38 chimeric protein is delivered to the TGN after trafficking through the endocytic recycling compartment in CHO cells. *J Cell Biol*, 142(4):923–36, 1998.

PA Gleeson, JG Lock, MR Luke, and JL Stow. Domains of the TGN: coats, tethers and G proteins. *Traffic*, 5(5):315–26, 2004.

A Godi, P Pertile, R Meyers, P Marra, G Di Tullio, C Iurisci, A Luini, D Corda, and M A De Matteis. ARF mediates recruitment of PtdIns-4-OH kinase-beta and stimulates synthesis of PtdIns(4,5)P2 on the Golgi complex. *Nat Cell Biol*, 1(5):280–7, 1999.

Anna Godi, Antonella Di Campli, Athanasios Konstantakopoulos, Giuseppe Di Tullio, Dario R Alessi, Gursant S Kular, Tiziana Daniele, Pierfrancesco Marra, John M Lucocq, and M Antonietta De Matteis. FAPPs control Golgi-to-cell-surface membrane traffic by binding to ARF and PtdIns(4)P. *Nat Cell Biol*, 6(5):393–404, 2004.

J Goldberg. Structural basis for activation of ARF GTPase: mechanisms of guanine nucleotide exchange and GTP-myristoyl switching. *Cell*, 95(2):237–48, 1998.

J R Goldenring, K R Shen, H D Vaughan, and I M Modlin. Identification of a small GTP-binding protein, Rab25, expressed in the gastrointestinal mucosa, kidney, and lung. *J Biol Chem*, 268(25):18419–22, 1993.

J R Goldenring, J Smith, H D Vaughan, P Cameron, W Hawkins, and J Navarre. Rab11 is an apically located small GTP-binding protein in epithelial tissues. *Am J Physiol*, 270(3 Pt 1):G515–25, 1996.

Ilya Grigoriev, Daniel Splinter, Nanda Keijzer, Phebe S Wulf, Jeroen Demmers, Toshihisa Ohtsuka, Mauro Modesti, Ivan V Maly, Frank Grosveld, Casper C Hoogenraad, and Anna Akhmanova. Rab6 regulates transport and targeting of exocytotic carriers. *Dev Cell*, 13(2): 305–14, 2007.

C Griscelli and M Prunieras. Pigment dilution and immunodeficiency: a new syndrome. *Int J Dermatol*, 17(10):788–91, 1978.

F Gu and J Gruenberg. ARF1 regulates pH-dependent COP functions in the early endocytic pathway. *J Biol Chem*, 275(11):8154–60, 2000.

Karen M Hajra, David Y-S Chen, and Eric R Fearon. The SLUG zinc-finger protein represses E-cadherin in breast cancer. *Cancer Res*, 62(6):1613–8, 2002.

Chadwick M Hales, Jean-Pierre Vaerman, and James R Goldenring. Rab11 family interacting protein 2 associates with Myosin Vb and regulates plasma membrane recycling. *J Biol Chem*, 277(52):50415–21, 2002.

S M Hammond, Y M Altshuller, T C Sung, S A Rudge, K Rose, J Engebrecht, A J Morris, and M A Frohman. Human ADP-ribosylation factor-activated phosphatidylcholine-specific phospholipase D defines a new and highly conserved gene family. *J Biol Chem*, 270(50): 29640–3, 1995.

S M Hammond, J M Jenco, S Nakashima, K Cadwallader, Q Gu, S Cook, Y Nozawa, G D Prestwich, M A Frohman, and A J Morris. Characterization of two alternately spliced forms of phospholipase D1. Activation of the purified enzymes by phosphatidylinositol 4,5-bisphosphate, ADP-ribosylation factor, and Rho family monomeric GTP-binding proteins and protein kinase C-alpha. *J Biol Chem*, 272(6):3860–8, 1997.

Elizabeth S Harris, Fang Li, and Henry N Higgs. The mouse formin, FRLalpha, slows actin filament barbed end elongation, competes with capping protein, accelerates polymerization from monomers, and severs filaments. *J Biol Chem*, 279(19):20076–87, 2004.

Lee P Haynes, Geraint M H Thomas, and Robert D Burgoyne. Interaction of neuronal calcium sensor-1 and ADP-ribosylation factor 1 allows bidirectional control of phosphatidylinositol 4-kinase beta and trans-Golgi network-plasma membrane traffic. *J Biol Chem*, 280(7):6047–54, 2005.

LG Henage, JH Exton, and HA Brown. Kinetic analysis of a mammalian phospholipase D: allosteric modulation by monomeric GTPases, protein kinase C, and polyphosphoinositides. *J Biol Chem*, 281(6):3408–17, 2006.

M Hiroyama and JH Exton. Localization and regulation of phospholipase D2 by ARF6. *J Cell Biochem*, 95(1):149–64, 2005.

KC Holmes, D Popp, W Gebhard, and W Kabsch. Atomic model of the actin filament. *Nature*, 347(6288):44–9, 1990.

KC Holmes, I Angert, FJ Kull, W Jahn, and RR Schroeder. Electron cryo-microscopy shows how strong binding of myosin to actin releases nucleotide. *Nature*, 425(6956):423–7, 2003.

W E Hughes and P J Parker. Endosomal localization of phospholipase D 1a and 1b is defined by the C-termini of the proteins, and is independent of activity. *Biochem J*, 356(Pt 3): 727–36, 2001.

CL Jackson and JE Casanova. Turning on ARF: the Sec7 family of guanine-nucleotide-exchange factors. *Trends Cell Biol*, 10(2):60–7, 2000.

GM Jenkins and MA Frohman. Phospholipase D: a lipid centric review. *Cell Mol Life Sci*, 62 (19-20):2305–16, 2005.

Travis J Jewett, Elizabeth R Fischer, David J Mead, and Ted Hackstadt. Chlamydial TARP is a bacterial nucleator of actin. *Proc Natl Acad Sci U S A*, 103(42):15599–604, 2006.

Jian Jing, Jagath R Junutula, Christine Wu, Jemima Burden, Hugo Matern, Andrew A Peden, and Rytis Prekeris. FIP1/RCP binding to Golgin-97 regulates retrograde transport from recycling endosomes to the trans-Golgi network. *Mol Biol Cell*, 21(17):3041–53, 2010.

D H Jones, J B Morris, C P Morgan, H Kondo, R F Irvine, and S Cockcroft. Type I phosphatidylinositol 4-phosphate 5-kinase directly interacts with ADP-ribosylation factor 1 and

is responsible for phosphatidylinositol 4,5-bisphosphate synthesis in the golgi compartment. *J Biol Chem*, 275(18):13962–6, 2000a.

D R Jones, M A Sanjuan, and I Merida. Type Ialpha phosphatidylinositol 4-phosphate 5-kinase is a putative target for increased intracellular phosphatidic acid. *FEBS Lett*, 476(3): 160–5, 2000b.

W Kabsch, HG Mannherz, D Suck, EF Pai, and KC Holmes. Atomic structure of the actin:DNase I complex. *Nature*, 347(6288):37–44, 1990.

R A Kahn and A G Gilman. Purification of a protein cofactor required for ADP-ribosylation of the stimulatory regulatory component of adenylate cyclase by cholera toxin. *J Biol Chem*, 259(10):6228–34, 1984.

F Kartberg, L Asp, SY Dejgaard, M Smedh, J Fernandez-Rodriguez, T Nilsson, and JF Presley. ARFGAP2 and ARFGAP3 are essential for COPI coat assembly on the Golgi membrane of living cells. *J Biol Chem*, 285(47):36709–20, 2010.

E Kerkhoff. Cellular functions of the Spir actin-nucleation factors. *Trends Cell Biol*, 16(9): 477–83, 2006.

E Kerkhoff, J C Simpson, C B Leberfinger, I M Otto, T Doerks, P Bork, U R Rapp, T Raabe, and R Pepperkok. The Spir actin organizers are involved in vesicle transport processes. *Curr Biol*, 11(24):1963–8, 2001.

RD Klausner, JG Donaldson, and J Lippincott-Schwartz. Brefeldin A: insights into the control of membrane traffic and organelle structure. *J Cell Biol*, 116(5):1071–80, 1992.

A Kobielak, HA Pasolli, and E Fuchs. Mammalian formin-1 participates in adherens junctions and polymerization of linear actin cables. *Nat Cell Biol*, 6(1):21–30, 2004.

David R Kovar, Jeffrey R Kuhn, Andrea L Tichy, and Thomas D Pollard. The fission yeast cytokinesis formin Cdc12p is a barbed end actin filament capping protein gated by profilin. *J Cell Biol*, 161(5):875–87, 2003.

Michael Krauss, Jun-Yong Jia, Aurelien Roux, Rainer Beck, Felix T Wieland, Pietro De Camilli, and Volker Haucke. Arf1-GTP-induced tubule formation suggests a function of Arf

family proteins in curvature acquisition at sites of vesicle budding. *J Biol Chem*, 283(41): 27717–23, 2008.

T Kutateladze and M Overduin. Structural mechanism of endosome docking by the FYVE domain. *Science*, 291(5509):1793–6, 2001.

F Lai, L Stubbs, and K Artzt. Molecular analysis of mouse Rab11b: a new type of mammalian YPT/Rab protein. *Genomics*, 22(3):610–6, 1994.

Michael Lammers, Rolf Rose, Andrea Scrima, and Alfred Wittinghofer. The regulation of mDia1 by autoinhibition and its release by Rho*GTP. *EMBO J*, 24(23):4176–87, 2005.

L A Lapierre, R Kumar, C M Hales, J Navarre, S G Bhartur, J O Burnette, D W Jr Provance, J A Mercer, M Bahler, and J R Goldenring. Myosin vb is associated with plasma membrane recycling systems. *Mol Biol Cell*, 12(6):1843–57, 2001.

LA Lapierre, KM Avant, CM Caldwell, AJ Ham, S Hill, JA Williams, AJ Smolka, and JR Goldenring. Characterization of immunoisolated human gastric parietal cells tubulovesicles: identification of regulators of apical recycling. *Am J Physiol Gastrointest Liver Physiol*, 2007.

B Leader and P Leder. Formin-2, a novel formin homology protein of the cappuccino subfamily, is highly expressed in the developing and adult central nervous system. *Mech Dev*, 93(1-2): 221–31, 2000.

B Leader, H Lim, MJ Carabatsos, A Harrington, J Ecsedy, D Pellman, R Maas, and P Leder. Formin-2, polyploidy, hypofertility and positioning of the meiotic spindle in mouse oocytes. *Nat Cell Biol*, 4(12), 2002.

Mark A Lemmon. Phosphoinositide recognition domains. *Traffic*, 4(4):201–13, 2003.

Fang Li and Henry N Higgs. The mouse Formin mDia1 is a potent actin nucleation factor regulated by autoinhibition. *Curr Biol*, 13(15):1335–40, 2003.

Fang Li and Henry N Higgs. Dissecting requirements for auto-inhibition of actin nucleation by the formin, mDia1. *J Biol Chem*, 280(8):6986–92, 2005.

Hongbin Li, Fengli Guo, Boris Rubinstein, and Rong Li. Actin-driven chromosomal motility leads to symmetry breaking in mammalian meiotic oocytes. *Nat Cell Biol*, 10(11):1301–8, 2008.

Elena V Linardopoulou, Sean S Parghi, Cynthia Friedman, Gregory E Osborn, Susan M Parkhurst, and Barbara J Trask. Human subtelomeric WASH genes encode a new subclass of the WASP family. *PLoS Genet*, 3(12):e237, 2007.

Andrew J Lindsay and Mary W McCaffrey. Rab11-FIP2 functions in transferrin recycling and associates with endosomal membranes via its COOH-terminal domain. *J Biol Chem*, 277 (30):27193–9, 2002.

Andrew J Lindsay and Mary W McCaffrey. The C2 domains of the class I Rab11 family of interacting proteins target recycling vesicles to the plasma membrane. *J Cell Sci*, 117(Pt 19):4365–75, 2004.

Andrew J Lindsay, Alan G Hendrick, Giuseppina Cantalupo, Francesca Senic-Matuglia, Bruno Goud, Cecilia Bucci, and Mary W McCaffrey. Rab coupling protein (RCP), a novel Rab4 and Rab11 effector protein. *J Biol Chem*, 277(14):12190–9, 2002.

M Liscovitch, V Chalifa, P Pertile, C S Chen, and L C Cantley. Novel function of phosphatidylinositol 4,5-bisphosphate as a cofactor for brain membrane phospholipase D. *J Biol Chem*, 269(34):21403–6, 1994.

Y Liu, RA Kahn, and JH Prestegard. Structure and membrane interaction of myristoylated ARF1. *Structure*, 17(1):79–87, 2009.

Amy D B Liverman, Hui-Chun Cheng, Jennifer E Trosky, Daisy W Leung, Melanie L Yarbrough, Dara L Burdette, Michael K Rosen, and Kim Orth. Arp2/3-independent assembly of actin by Vibrio type III effector VopL. *Proc Natl Acad Sci U S A*, 104(43):17117–22, 2007.

John G Lock and Jennifer L Stow. Rab11 in recycling endosomes regulates the sorting and basolateral transport of E-cadherin. *Mol Biol Cell*, 16(4):1744–55, 2005.

John G Lock, Luke A Hammond, Fiona Houghton, Paul A Gleeson, and Jennifer L Stow. E-cadherin transport from the trans-Golgi network in tubulovesicular carriers is selectively regulated by golgin-97. *Traffic*, 6(12):1142–56, 2005.

D Lombardi, T Soldati, MA Riederer, Y Goda, M Zerial, and SR Pfeffer. Rab9 functions in transport between late endosomes and the trans Golgi network. *EMBO J*, 12(2):677–82, 1993.

J Lu, W Meng, F Poy, S Maiti, BL Goode, and MJ Eck. Structure of the FH2 domain of Daam1: implications for formin regulation of actin assembly. *J Mol Biol*, 369(5):1258–69, 2007.

L M Machesky, S J Atkinson, C Ampe, J Vandekerckhove, and T D Pollard. Purification of a cortical complex containing two unconventional actins from Acanthamoeba by affinity chromatography on profilin-agarose. *J Cell Biol*, 127(1):107–15, 1994.

I Majoul, M Straub, S W Hell, R Duden, and H D Soling. KDEL-cargo regulates interactions between proteins involved in COPI vesicle traffic: measurements in living cells using FRET. *Dev Cell*, 1(1):139–53, 2001.

F Mallard, C Antony, D Tenza, J Salamero, B Goud, and L Johannes. Direct pathway from early/recycling endosomes to the Golgi apparatus revealed through the study of shiga toxin B-fragment transport. *J Cell Biol*, 143(4):973–90, 1998.

L Manseau, J Calley, and H Phan. Profilin is required for posterior patterning of the Drosophila oocyte. *Development*, 122(7):2109–16, 1996.

L J Manseau and T Schupbach. cappuccino and spire: two unique maternal-effect loci required for both the anteroposterior and dorsoventral patterns of the Drosophila embryo. *Genes Dev*, 3(9):1437–52, 1989.

Maria Antonietta De Matteis, Antonella Di Campli, and Anna Godi. The role of the phosphoinositides at the Golgi complex. *Biochim Biophys Acta*, 1744(3):396–405, 2005.

AM McGough, CJ Staiger, JK Min, and KD Simonetti. The gelsolin family of actin regulatory proteins: modular structures, versatile functions. *FEBS Lett*, 552(2-3):75–81, 2003.

Jennifer M Meyers and Rytis Prekeris. Formation of mutually exclusive Rab11 complexes with members of the family of Rab11-interacting proteins regulates Rab11 endocytic targeting and function. *J Biol Chem*, 277(50):49003–10, 2002.

S Misra and J H Hurley. Crystal structure of a phosphatidylinositol 3-phosphate-specific membrane-targeting motif, the FYVE domain of Vps27p. *Cell*, 97(5):657–66, 1999.

Etienne Morel, Robert G Parton, and Jean Gruenberg. Annexin A2-dependent polymerization of actin mediates endosome biogenesis. *Dev Cell*, 16(3):445–57, 2009.

R D Mullins, J A Heuser, and T D Pollard. The interaction of Arp2/3 complex with actin: nucleation, high affinity pointed end capping, and formation of branching networks of filaments. *Proc Natl Acad Sci U S A*, 95(11):6181–6, 1998.

Kenneth R Myers and James E Casanova. Regulation of actin cytoskeleton dynamics by Arf-family GTPases. *Trends Cell Biol*, 18(4):184–92, 2008.

Waka Natsume, Kenji Tanabe, Shunsuke Kon, Naomi Yoshida, Toshio Watanabe, Tetsuo Torii, and Masanobu Satake. SMAP2, a novel ARF GTPase-activating protein, interacts with clathrin and clathrin assembly protein and functions on the AP-1-positive early endosome/trans-Golgi network. *Mol Biol Cell*, 17(6):2592–603, 2006.

Elaine Del Nery, Stephanie Miserey-Lenkei, Thomas Falguieres, Clement Nizak, Ludger Johannes, Franck Perez, and Bruno Goud. Rab6A and Rab6A' GTPases play non-overlapping roles in membrane trafficking. *Traffic*, 7(4):394–407, 2006.

Zhongzhen Nie and Paul A Randazzo. Arf GAPs and membrane traffic. *J Cell Sci*, 119(Pt 7):1203–11, 2006.

Zhongzhen Nie, Markus Boehm, Emily S Boja, William C Vass, Juan S Bonifacino, Henry M Fales, and Paul A Randazzo. Specific regulation of the adaptor protein complex AP-3 by the Arf GAP AGAP1. *Dev Cell*, 5(3):513–21, 2003.

Zhongzhen Nie, Jiajing Fei, Richard T Premont, and Paul A Randazzo. The Arf GAPs AGAP1 and AGAP2 distinguish between the adaptor protein complexes AP-1 and AP-3. *J Cell Sci*, 118(Pt 15):3555–66, 2005.

T Oda and Y Maeda. Multiple Conformations of F-actin. *Structure*, 18(7):761–7, 2010.

T Oda, M Iwasa, T Aihara, Y Maeda, and A Narita. The nature of the globular- to fibrous-actin transition. *Nature*, 457(7228):441–5, 2009.

Tamer T Onder, Piyush B Gupta, Sendurai A Mani, Jing Yang, Eric S Lander, and Robert A Weinberg. Loss of E-cadherin promotes metastasis via multiple downstream transcriptional pathways. *Cancer Res*, 68(10):3645–54, 2008.

CE Ooi, EC Dell'Angelica, and JS Bonifacino. ADP-Ribosylation factor 1 (ARF1) regulates recruitment of the AP-3 adaptor complex to membranes. *J Cell Biol*, 142(2):391–402, 1998.

C Ostermeier and A T Brunger. Structural basis of Rab effector specificity: crystal structure of the small G protein Rab3A complexed with the effector domain of rabphilin-3A. *Cell*, 96 (3):363–74, 1999.

T Otomo, DR Tomchick, C Otomo, SC Panchal, M Machius, and MK Rosen. Structural basis of actin filament nucleation and processive capping by a formin homology 2 domain. *Nature*, 433(7025):488–94, 2005a.

Takanori Otomo, Diana R Tomchick, Chinatsu Otomo, Sanjay C Panchal, Mischa Machius, and Michael K Rosen. Structural basis of actin filament nucleation and processive capping by a formin homology 2 domain. *Nature*, 433(7025):488–94, 2005b.

LR Otterbein, P Graceffa, and R Dominguez. The crystal structure of uncomplexed actin in the ADP state. *Science*, 293(5530):708–11, 2001.

D Pantaloni and MF Carlier. How profilin promotes actin filament assembly in the presence of thymosin beta 4. *Cell*, 75(5):1007–14, 1993.

Gilbert Di Paolo and Pietro De Camilli. Phosphoinositides in cell regulation and membrane dynamics. *Nature*, 443(7112):651–7, 2006.

V Patki, D C Lawe, S Corvera, J V Virbasius, and A Chawla. A functional PtdIns(3)P-binding motif. *Nature*, 394(6692):433–4, 1998.

Eija Paunola, Pieta K Mattila, and Pekka Lappalainen. WH2 domain: a small, versatile adapter for actin monomers. *FEBS Lett*, 513(1):92–7, 2002.

Markos Pechlivanis, Annette Samol, and Eugen Kerkhoff. Identification of a short Spir interaction sequence at the C-terminal end of formin subgroup proteins. *J Biol Chem*, 284(37): 25324–33, 2009.

AK Perl, P Wilgenbus, U Dahl, H Semb, and G Christofori. A causal role for E-cadherin in the transition from adenoma to carcinoma. *Nature*, 392(6672):190–3, 1998.

P Pertile, M Liscovitch, V Chalifa, and L C Cantley. Phosphatidylinositol 4,5-bisphosphate synthesis is required for activation of phospholipase D in U937 cells. *J Biol Chem*, 270(10): 5130–5, 1995.

P J Peters, V W Hsu, C E Ooi, D Finazzi, S B Teal, V Oorschot, J G Donaldson, and R D Klausner. Overexpression of wild-type and mutant ARF1 and ARF6: distinct perturbations of nonoverlapping membrane compartments. *J Cell Biol*, 128(6):1003–17, 1995.

A Peyroche, S Paris, and C L Jackson. Nucleotide exchange on ARF mediated by yeast Gea1 protein. *Nature*, 384(6608):479–81, 1996.

SR Pfeffer. Multiple routes of protein transport from endosomes to the trans Golgi network. *FEBS Lett*, 583(23):3811–6, 2009.

SR Pfeffer, AB Dirac-Svejstrup, and T Soldati. Rab GDP dissociation inhibitor: putting rab GTPases in the right place. *J Biol Chem*, 270(29):17057–9, 1995.

S Pleiser, R Rock, J Wellmann, M Gessler, and E Kerkhoff. Expression patterns of the mouse Spir-2 actin nucleator. *Gene Expr Patterns*, 10(7-8):345–50, 2010.

T D Pollard, L Blanchoin, and R D Mullins. Molecular mechanisms controlling actin filament dynamics in nonmuscle cells. *Annu Rev Biophys Biomol Struct*, 29(NIL):545–76, 2000.

TD Pollard and GG Borisy. Cellular motility driven by assembly and disassembly of actin filaments. *Cell*, 112(4):453–65, 2003.

TD Pollard and JA Cooper. Quantitative analysis of the effect of Acanthamoeba profilin on actin filament nucleation and elongation. *Biochemistry*, 23(26):6631–41, 1984.

Thomas D Pollard. Regulation of actin filament assembly by Arp2/3 complex and formins. *Annu Rev Biophys Biomol Struct*, 36(NIL):451–77, 2007.

Vincent Popoff, Gonzalo A Mardones, Daniele Tenza, Raul Rojas, Christophe Lamaze, Juan S Bonifacino, Graca Raposo, and Ludger Johannes. The retromer complex and clathrin define an early endosomal retrograde exit site. *J Cell Sci*, 120(Pt 12):2022–31, 2007.

R Prekeris, J Klumperman, and R H Scheller. A Rab11/Rip11 protein complex regulates apical membrane trafficking via recycling endosomes. *Mol Cell*, 6(6):1437–48, 2000.

John F Presley, Theresa H Ward, Andrea C Pfeifer, Eric D Siggia, Robert D Phair, and Jennifer Lippincott-Schwartz. Dissection of COPI and Arf1 dynamics in vivo and role in Golgi membrane transport. *Nature*, 417(6885):187–93, 2002.

M Pring, A Weber, and MR Bubb. Profilin-actin complexes directly elongate actin filaments at the barbed end. *Biochemistry*, 31(6):1827–36, 1992.

E Psachoulia and MS Sansom. PX- and FYVE-mediated interactions with membranes: simulation studies. *Biochemistry*, 48(23):5090–5, 2009.

Margot E Quinlan, John E Heuser, Eugen Kerkhoff, and R Dyche Mullins. Drosophila Spire is an actin nucleation factor. *Nature*, 433(7024):382–8, 2005.

Margot E Quinlan, Susanne Hilgert, Anaid Bedrossian, R Dyche Mullins, and Eugen Kerkhoff. Regulatory interactions between two actin nucleators, Spire and Cappuccino. *J Cell Biol*, 179(1):117–28, 2007.

Paul A Randazzo and Dianne S Hirsch. Arf GAPs: multifunctional proteins that regulate membrane traffic and actin remodelling. *Cell Signal*, 16(4):401–13, 2004.

M Ren, G Xu, J Zeng, C De Lemos-Chiarandini, M Adesnik, and DD Sabatini. Hydrolysis of GTP on rab11 is required for the direct delivery of transferrin from the pericentriolar recycling compartment to the cell surface but not from sorting endosomes. *Proc Natl Acad Sci U S A*, 95(11), 1998.

L Renault, B Guibert, and J Cherfils. Structural snapshots of the mechanism and inhibition of a guanine nucleotide exchange factor. *Nature*, 426(6966):525–30, 2003.

CH Robert, J Cherfils, L Mouawad, and D Perahia. Integrating three views of Arf1 activation dynamics. *J Mol Biol*, 337(4):969–83, 2004.

M Roberts, S Barry, A Woods, P van der Sluijs, and J Norman. PDGF-regulated rab4-dependent recycling of alphavbeta3 integrin from early endosomes is necessary for cell adhesion and spreading. *Curr Biol*, 11(18):1392–402, 2001.

RC Robinson, K Turbedsky, DA Kaiser, JB Marchand, HN Higgs, S Choe, and TD Pollard. Crystal structure of Arp2/3 complex. *Science*, 294(5547):1679–84, 2001.

S Romero, C Le Clainche, D Didry, C Egile, D Pantaloni, and MF Carlier. Formin is a processive motor that requires profilin to accelerate actin assembly and associated ATP hydrolysis. *Cell*, 119(3):419–29, 2004.

S Romero, D Didry, E Larquet, N Boisset, D Pantaloni, and MF Carlier. How ATP hydrolysis controls filament assembly from profilin-actin: implication for formin processivity. *J Biol Chem*, 282(11):8435–45, 2007.

Alicia E Rosales-Nieves, James E Johndrow, Lani C Keller, Craig R Magie, Delia M Pinto-Santini, and Susan M Parkhurst. Coordination of microtubule and microfilament dynamics by Drosophila Rho1, Spire and Cappuccino. *Nat Cell Biol*, 8(4):367–76, 2006.

MG Roth. Molecular mechanisms of PLD function in membrane traffic. *Traffic*, 9(8):1233–9, 2008.

Isabelle Sagot, Avital A Rodal, James Moseley, Bruce L Goode, and David Pellman. An actin nucleation mechanism mediated by Bni1 and profilin. *Nat Cell Biol*, 4(8):626–31, 2002.

O Schmalhofer, S Brabletz, and T Brabletz. E-cadherin, beta-catenin, and ZEB1 in malignant progression of cancer. *Cancer Metastasis Rev*, 28(1-2):151–66, 2009.

Andre Schonichen and Matthias Geyer. Fifteen formins for an actin filament: a molecular view on the regulation of human formins. *Biochim Biophys Acta*, 1803(2):152–63, 2010.

Melina Schuh and Jan Ellenberg. A new model for asymmetric spindle positioning in mouse oocytes. *Curr Biol*, 18(24):1986–92, 2008.

Nina Schumacher, Johanna M Borawski, Cornelia B Leberfinger, Manfred Gessler, and Eugen Kerkhoff. Overlapping expression pattern of the actin organizers Spir-1 and formin-2 in the

developing mouse nervous system and the adult brain. *Gene Expr Patterns*, 4(3):249–55, 2004.

MC Seabra. Nucleotide dependence of Rab geranylgeranylation. Rab escort protein interacts preferentially with GDP-bound Rab. *J Biol Chem*, 271(24):14398–404, 1996.

D Sept and JA McCammon. Thermodynamics and kinetics of actin filament nucleation. *Biophys J*, 81(2):667–74, 2001.

T Serafini, L Orci, M Amherdt, M Brunner, RA Kahn, and JE Rothman. ADP-ribosylation factor is a subunit of the coat of Golgi-derived COP-coated vesicles: a novel role for a GTP-binding protein. *Cell*, 67(2):239–53, 1991.

Xiaoyan Shen, Kai-Feng Xu, Qingyuan Fan, Gustavo Pacheco-Rodriguez, Joel Moss, and Martha Vaughan. Association of brefeldin A-inhibited guanine nucleotide-exchange protein 2 (BIG2) with recycling endosomes during transferrin uptake. *Proc Natl Acad Sci U S A*, 103(8):2635–40, 2006.

T Shiba, M Kawasaki, H Takatsu, T Nogi, N Matsugaki, N Igarashi, M Suzuki, R Kato, K Nakayama, and S Wakatsuki. Molecular mechanism of membrane recruitment of GGA by ARF in lysosomal protein transport. *Nat Struct Biol*, 10(5):386–93, 2003.

T Shiba, H Koga, HW Shin, M Kawasaki, R Kato, K Nakayama, and S Wakatsuki. Structural basis for Rab11-dependent membrane recruitment of a family of Rab11-interacting protein 3 (FIP3)/Arfophilin-1. *Proc Natl Acad Sci U S A*, 103(42), 2006.

Yoko Shiba, Winfried Romer, Gonzalo A Mardones, Patricia V Burgos, Christophe Lamaze, and Ludger Johannes. AGAP2 regulates retrograde transport between early endosomes and the TGN. *J Cell Sci*, 123(Pt 14):2381–90, 2010.

A Shimada, M Nyitrai, IR Vetter, D Kuehlmann, B Bugyi, S Narumiya, MA Geeves, and A Wittinghofer. The core FH2 domain of diaphanous-related formins is an elongated actin binding protein that inhibits polymerization. *Mol Cell*, 13(4):511–22, 2004.

Hye-Won Shin, Naoko Morinaga, Masatoshi Noda, and Kazuhisa Nakayama. BIG2, a guanine nucleotide exchange factor for ADP-ribosylation factors: its localization to recycling endosomes and implication in the endosome integrity. *Mol Biol Cell*, 15(12):5283–94, 2004.

OH Shin, AH Ross, I Mihai, and JH Exton. Identification of arfophilin, a target protein for GTP-bound class II ADP-ribosylation factors. *J Biol Chem*, 274(51):36609–15, 1999.

OH Shin, AD Couvillon, and JH Exton. Arfophilin is a common target of both class II and class III ADP-ribosylation factors. *Biochemistry*, 40(36):10846–52, 2001.

A Siddhanta and D Shields. Secretory vesicle budding from the trans-Golgi network is mediated by phosphatidic acid levels. *J Biol Chem*, 273(29):17995–8, 1998.

A Siddhanta, J M Backer, and D Shields. Inhibition of phosphatidic acid synthesis alters the structure of the Golgi apparatus and inhibits secretion in endocrine cells. *J Biol Chem*, 275 (16):12023–31, 2000.

U Sivars, D Aivazian, and S Pfeffer. Purification and properties of Yip3/PRA1 as a Rab GDI displacement factor. *Methods Enzymol*, 403:348–56, 2005.

T Soldati, A D Shapiro, A B Svejstrup, and S R Pfeffer. Membrane targeting of the small GTPase Rab9 is accompanied by nucleotide exchange. *Nature*, 369(6475):76–8, 1994.

Mark Stamnes. Regulating the actin cytoskeleton during vesicular transport. *Curr Opin Cell Biol*, 14(4):428–33, 2002.

H Stenmark. Rab GTPases as coordinators of vesicle traffic. *Nat Rev Mol Cell Biol*, 10(8): 513–25, 2009.

H Stenmark, R Aasland, BH Toh, and A D'Arrigo. Endosomal localization of the autoantigen EEA1 is mediated by a zinc-binding FYVE finger. *J Biol Chem*, 271(39):24048–54, 1996.

TC Sung, YM Altshuller, AJ Morris, and MA Frohman. Molecular analysis of mammalian phospholipase D2. *J Biol Chem*, 274(1):494–502, 1999.

Agnieszka Swiatecka-Urban, Laleh Talebian, Eiko Kanno, Sophie Moreau-Marquis, Bonita Coutermarsh, Karyn Hansen, Katherine H Karlson, Roxanna Barnaby, Richard E Cheney, George M Langford, Mitsunori Fukuda, and Bruce A Stanton. Myosin Vb is required for trafficking of the cystic fibrosis transmembrane conductance regulator in Rab11a-specific apical recycling endosomes in polarized human airway epithelial cells. *J Biol Chem*, 282 (32):23725–36, 2007.

Vincent C Tam, Davide Serruto, Michelle Dziejman, William Brieher, and John J Mekalanos. A type III secretion system in Vibrio cholerae translocates a formin/spire hybrid-like actin nucleator to promote intestinal colonization. *Cell Host Microbe*, 1(2):95–107, 2007.

W E Theurkauf. Premature microtubule-dependent cytoplasmic streaming in cappuccino and spire mutant oocytes. *Science*, 265(5181):2093–6, 1994.

O Ullrich, H Stenmark, K Alexandrov, L A Huber, K Kaibuchi, T Sasaki, Y Takai, and M Zerial. Rab GDP dissociation inhibitor as a general regulator for the membrane association of rab proteins. *J Biol Chem*, 268(24):18143–50, 1993.

O Ullrich, S Reinsch, S Urbe, M Zerial, and R G Parton. Rab11 regulates recycling through the pericentriolar recycling endosome. *J Cell Biol*, 135(4):913–24, 1996.

Edit Urban, Sonja Jacob, Maria Nemethova, Guenter P Resch, and J Victor Small. Electron tomography reveals unbranched networks of actin filaments in lamellipodia. *Nat Cell Biol*, 12(5):429–35, 2010.

S Urbe, LA Huber, M Zerial, SA Tooze, and RG Parton. Rab11, a small GTPase associated with both constitutive and regulated secretory pathways in PC12 cells. *FEBS Lett*, 334(2): 175–82, 1993.

DM Veltman and RH Insall. WASP family proteins: their evolution and its physiological implications. *Mol Biol Cell*, 21(16):2880–93, 2010.

Laura A Volpicelli, James J Lah, Guofu Fang, James R Goldenring, and Allan I Levey. Rab11a and myosin Vb regulate recycling of the M4 muscarinic acetylcholine receptor. *J Neurosci*, 22(22):9776–84, 2002.

Laura A Volpicelli-Daley, Yawei Li, Chun-Jiang Zhang, and Richard A Kahn. Isoform-selective effects of the depletion of ADP-ribosylation factors 1-5 on membrane traffic. *Mol Biol Cell*, 16(10):4495–508, 2005.

Deborah M Wallace, Andrew J Lindsay, Alan G Hendrick, and Mary W McCaffrey. The novel Rab11-FIP/Rip/RCP family of proteins displays extensive homo- and hetero-interacting abilities. *Biochem Biophys Res Commun*, 292(4):909–15, 2002.

Bradley J Wallar and Arthur S Alberts. The formins: active scaffolds that remodel the cytoskeleton. *Trends Cell Biol*, 13(8):435–46, 2003.

Z Wang, JG Edwards, N Riley, Jr Provance DW, R Karcher, XD Li, IG Davison, M Ikebe, JA Mercer, JA Kauer, and MD Ehlers. Myosin Vb mobilizes recycling endosomes and AMPA receptors for postsynaptic plasticity. *Cell*, 135(3):535–48, 2008.

Matthew D Welch and R Dyche Mullins. Cellular control of actin nucleation. *Annu Rev Cell Dev Biol*, 18(NIL):247–88, 2002.

M Wilcke, L Johannes, T Galli, V Mayau, B Goud, and J Salamero. Rab11 regulates the compartmentalization of early endosomes required for efficient transport from early endosomes to the trans-golgi network. *J Cell Biol*, 151(6):1207–20, 2000.

X Wu, K Rao, M B Bowers, N G Copeland, N A Jenkins, and J A 3rd Hammer. Rab27a enables myosin Va-dependent melanosome capture by recruiting the myosin to the organelle. *J Cell Sci*, 114(Pt 6):1091–100, 2001.

Yingwu Xu, James B Moseley, Isabelle Sagot, Florence Poy, David Pellman, Bruce L Goode, and Michael J Eck. Crystal structures of a Formin Homology-2 domain reveal a tethered dimer architecture. *Cell*, 116(5):711–23, 2004.

M Yamashita, T Higashi, S Suetsugu, Y Sato, T Ikeda, R Shirakawa, T Kita, T Takenawa, H Horiuchi, S Fukai, and O Nureki. Crystal structure of human DAAM1 formin homology 2 domain. *Genes Cells*, 12(11):1255–65, 2007.

Jing Yang and Robert A Weinberg. Epithelial-mesenchymal transition: at the crossroads of development and tumor metastasis. *Dev Cell*, 14(6):818–29, 2008.

S Yeoh, B Pope, HG Mannherz, and A Weeds. Determining the differences in actin binding by human ADF and cofilin. *J Mol Biol*, 315(4):911–25, 2002.

C Zhao, G Du, K Skowronek, MA Frohman, and D Bar-Sagi. Phospholipase D2-generated phosphatidic acid couples EGFR stimulation to Ras activation by Sos. *Nat Cell Biol*, 9(6): 706–12, 2007.

LP Zhao, JS Koslovsky, J Reinhard, M BÃ€hler, AE Witt, Jr Provance DW, and JA Mercer. Cloning and characterization of myr 6, an unconventional myosin of the dilute/myosin-V family. *Proc Natl Acad Sci U S A*, 93(20):10826–31, 1996.

F Zhou, P Leder, and SS Martin. Formin-1 protein associates with microtubules through a peptide domain encoded by exon-2. *Exp Cell Res*, 312(7):1119–26, 2006.

J Bradley Zuchero, Amanda S Coutts, Margot E Quinlan, Nicholas B La Thangue, and R Dyche Mullins. p53-cofactor JMY is a multifunctional actin nucleation factor. *Nat Cell Biol*, 11(4):451–9, 2009.